



THE HONG KONG
POLYTECHNIC UNIVERSITY

香港理工大學

Pao Yue-kong Library

包玉剛圖書館

Copyright Undertaking

This thesis is protected by copyright, with all rights reserved.

By reading and using the thesis, the reader understands and agrees to the following terms:

1. The reader will abide by the rules and legal ordinances governing copyright regarding the use of the thesis.
2. The reader will use the thesis for the purpose of research or private study only and not for distribution or further reproduction or any other purpose.
3. The reader agrees to indemnify and hold the University harmless from and against any loss, damage, cost, liability or expenses arising from copyright infringement or unauthorized usage.

IMPORTANT

If you have reasons to believe that any materials in this thesis are deemed not suitable to be distributed in this form, or a copyright owner having difficulty with the material being included in our database, please contact lbsys@polyu.edu.hk providing details. The Library will look into your claim and consider taking remedial action upon receipt of the written requests.

**COORDINATED OPTIMAL DESIGN OF
ZERO/LOW ENERGY BUILDINGS IN
HIGH-DENSITY CITIES CONSIDERING
THEIR INTERACTION WITH LOCAL
MICROCLIMATE**

ZHAO ZEMING

PhD

The Hong Kong Polytechnic University

2024

The Hong Kong Polytechnic University

Department of Building Environment and Energy Engineering

**Coordinated Optimal Design of Zero/Low
Energy Buildings in High-density Cities
Considering Their Interaction with Local
Microclimate**

ZHAO ZEMING

**A thesis submitted in partial fulfillment of the requirements for the
degree of Doctor of Philosophy**

May 2024

CERTIFICATE OF ORIGINALITY

I hereby declare that this thesis is my own work and that, to the best of my knowledge and belief, it reproduces no material previously published or written, nor material that has been accepted for the award of any other degree or diploma, except where due acknowledgement has been made in the text.

_____ (Signed)

Zeming Zhao (Name of student)

ABSTRACT

Abstract of thesis entitled: Coordinated Optimal Design of Zero/Low Energy Buildings in High-density Cities Considering Their Interaction with Local Microclimate

Submitted by: Zeming Zhao

For the degree of: Doctor of Philosophy

at The Hong Kong Polytechnic University in October 2024

Load reduction is a fundamental means for achieving the goal of zero/low-energy buildings and for accomplishing carbon-neutrality. Zero/low energy buildings with low energy demand and high utilization of renewable energy are therefore recognized as effective means to facilitate carbon neutrality, and are receiving increasing attention from government, society and professionals. As the world undergoing an intense process of urbanization, the development of high-density cities becomes rapid. In high-density areas, buildings can modify the surrounding microclimate and are recognized as one of the main contributors to the urban local microclimate. Meanwhile, the microclimate also has a considerable impact on the building energy performance. However, there is still lack of an effective design optimization method to identify global optimal solutions enhancing both building energy performance and pedestrian thermal comfort while considering the interaction between buildings and the local

microclimate. The mutual impacts between them are ignored in current optimal design practices for zero/low energy buildings due to a lack of comprehensive understanding. In addition, the accurate prediction of the local microclimate surrounding the building with low computing cost is currently absent, which is the foundation for effective optimization.

This study therefore aims to develop an effective and comprehensive optimal design method based on multi-objective optimization for zero/low energy buildings and local microclimate, considering their interactions in high-density cities. Machine learning-based surrogate models are also developed for fast evaluation of the local microclimate.

The most influential design parameters of high-rise and low-rise buildings in different climate zones are identified by sensitivity analysis, and the impacts of climate and building height are studied and compared. A total of thirty-five design parameters under five categories are considered. Five Chinese climate zones covering three typical climates worldwide are researched. The key design parameters affecting winter thermal discomfort in climate zones typically without heating provision are also identified. The impact of thermal bridge on building energy performance is further investigated. Remarkable finding is that overhangs are among the most important elements for high-rise buildings in all climate zones concerned, while skylights are among the most influential elements for low-rise buildings concerning building load.

A comprehensive and systematic analysis is conducted to investigate the mutual impacts between new individual building design and the local microclimate, and to identify the major

influential building parameters on both local microclimate and building energy performance in subtropical urban area. A large number of high-resolution microclimate and building simulations based on advanced GIS spatial analysis technique are performed under different building designs for the mutual impact assessment. A global sensitivity analysis is conducted to identify the major influential building parameters. The results show that different building designs lead to significant variation of local wind velocity (i.e., $-0.95\sim+4.51$ m/s) and air temperature (i.e., $-0.60\sim+1.17$ K), while the local microclimate results in a change in the building energy consumption from -41.75kJ/m^2 to 291.54kJ/m^2 .

Machine learning-based surrogate models are developed to predict the impacts of local microclimate (i.e., local air temperature and wind velocity) due to the addition of a new individual building in high-density urban area. Two complementary machine learning-based surrogate models are identified and recommended for their high accuracy and high efficiency, including an SVR-based local air temperature model and a LightGBM-based local wind velocity model. They are identified by evaluating and comparing eight alternative machine learning models, four for each model development. 200 sets of CFD simulation data corresponding to different building designs are used for the model training and validation. The results show that the developed surrogate models can dramatically reduce computation time (from over 5 hours to less than a second for a single prediction) while keeping the same order of accuracy of CFD simulations for local microclimate prediction of individual buildings. It therefore facilitates the fast, comprehensive and accurate prediction of the impacts on the local

microclimate at the early design stage of new construction and renovation of individual buildings, for designers to deliver preferred local microclimate and/or avoid unacceptable microclimate changes.

A coordinated design optimization method is proposed, allowing the design optimization of a zero/low energy building and its microclimate to be achieved within practically affordable time by adopting an effective quantification method. Local microclimate surrogate models and automated building simulation are integrated with the optimizer to enhance the optimization efficiency and generalizability. The essential design variables can, therefore, be optimized comprehensively with affordable computation efforts using multi-objective optimization. The global optimal solutions (i.e., Pareto front) identified by NSGA-II are further evaluated using the entropy-TOPSIS method to determine the best solution. The proposed method is tested and validated by implementing it in a development case of integrated building in Hong Kong. The results show that, when using the coordinated optimal design method, the total building energy consumption can be saved up to 63.6% and the pedestrian thermal discomfort degree can be reduced up to 1.9 K. The computation time of a design optimization is reduced by 99.98% (i.e., from 42684.44 to 8.89 hours) compared with that using conventional simulation methods.

PUBLICATIONS ARISING FROM THE THESIS

Journal Papers

- [1] **Zeming Zhao**, Hangxin Li* and Shengwei Wang*. 2022. Identification of the key design parameters of Zero/low energy buildings and the impacts of climate and building morphology. *Applied Energy*, 328, 120185.
- [2] **Zeming Zhao**, Hangxin Li* and Shengwei Wang*. 2024. The mutual impacts of individual building design and local microclimate in high-density cities and the major influential parameters. *Building Simulation*.
- [3] **Zeming Zhao**, Hangxin Li* and Shengwei Wang. 2024. Machine learning-based surrogate models for fast impact assessment of a new building on urban local microclimate at design stage. *Building and Environment*, 112142.
- [4] **Zeming Zhao**, Hangxin Li* and Shengwei Wang*. 2024. Surrogate-assisted coordinated design optimization of building and its microclimate considering their mutual impacts. *Applied Energy*, under review.

Conference papers

- [1] **Zeming Zhao***, Hangxin Li and Shengwei Wang. Identification and comparison of key design parameters of high-rise and low-rise zero/low energy buildings in subtropical regions. *Proceedings of the International Conference on Applied Energy*, 2021. In: CUE 2021. Matsue, Japan; Sep. 4-8th, 2021.

- [2] **Zeming Zhao***, Hangxin Li and Shengwei Wang. Data-driven model for building energy performance prediction considering the impact of local microclimate. *Proceedings of the 11th International Conference on Sustainable Development in Building and Environment, 2023*. In: SuDBE 2023. Espoo, Finland; Aug. 14-18th, 2023.

ACKNOWLEDGEMENTS

First and foremost, I would like to express my sincerest appreciation to my supervisor, Professor Shengwei Wang, and co-supervisor, Doctor Hangxin Li, for their patient supervision, inspiring guidance, valuable suggestions, and continuous support during my Ph.D. study. I am very fortunate to have them as not only my supervisors but also my sincere friends. They are the forerunners who have illuminated my academic research and personal life.

Additionally, I would like to thank Professor Fu Xiao and Doctor Kui Shan. Their valuable suggestions and sincere encouragement have broadened my horizons and motivated me to strive for excellence.

My sincere gratitude also goes to all the teammates in the Building Energy and Automation Research Laboratory. Their kind assistance has uplifted my spirits and helped me progress. I will always cherish the memorable years I have spent with them.

Lastly, I would like to express my deep appreciation to my family and friends. Their love, support, and understanding have enabled me to pursue my studies wholeheartedly, free from worries. Without them, my life would not be as vibrant and fulfilling.

TABLE OF CONTENTS

COORDINATED OPTIMAL DESIGN OF ZERO/LOW ENERGY BUILDINGS IN HIGH-DENSITY CITIES CONSIDERING THEIR INTERACTION WITH LOCAL MICROCLIMATE.....	I
CERTIFICATE OF ORIGINALITY	I
ABSTRACT.....	II
PUBLICATIONS ARISING FROM THE THESIS.....	VI
ACKNOWLEDGEMENTS	VIII
TABLE OF CONTENTS	IX
LIST OF FIGURES.....	XIV
LIST OF TABLES	XVIII
NOMENCLATURE	XXI
CHAPTER 1 INTRODUCTION	1
1.1 Background and motivation.....	1
1.2 Aim and objectives	4
1.3 Organization of thesis	6
CHAPTER 2 LITERATURE REVIEW	11

2.1 Overview of zero/low energy buildings technologies and parametric studies.....	11
2.2 Mutual impacts between buildings and local microclimate.....	18
2.3 Modelling and simulation of local microclimate	27
2.4 Design optimization of zero/low energy buildings and local microclimate	36
2.5 Summary of research gaps	45
CHAPTER 3 OVERVIEW OF THE RESEARCH SCENARIO AND BUILDING PERFORMANCE	
SIMULATION 47	
3.1 Description of the research scenario	47
3.2 Building performance simulation	48
3.3 Summary	54
CHAPTER 4 IDENTIFICATION OF THE KEY DESIGN PARAMETERS OF ZERO/LOW ENERGY	
BUILDINGS UNDER DIFFERENT CLIMATES AND BUILDING MORPHOLOGIES	56
4.1 Overview of building models and climate conditions concerned	56
4.2 Initial selection of parameters affecting building performance	60
4.3 Methodology and procedure for identifying the key design parameters.....	63
4.4 Results of sensitivity analysis	68
4.5 Analysis on impact of thermal bridge on building energy performance.....	81

4.6 Recommendations on key building design parameters to be optimized	85
4.7 Summary	90
CHAPTER 5 INVESTIGATION ON THE MUTUAL IMPACTS OF ZERO/LOW ENERGY BUILDING DESIGN AND LOCAL MICROCLIMATE	92
5.1 Main building parameters concerned.....	92
5.2 Overall assessment procedure and methods	94
5.3 High-resolution 3D microclimate simulation and building simulation using advanced GIS- based spatial analysis techniques	96
5.4 Analysis on impacts of building design on local microclimate	103
5.5 Analysis on impacts of local microclimate on building energy performance.....	112
5.6 Identification of the major influential building parameters on both local microclimate and building performance	114
5.7 Summary	123
CHAPTER 6 DEVELOPMENT OF A GENERIC DATA-DRIVEN LOCAL MICROCLIMATE MODEL CONSIDERING THE IMPACTS OF BUILDING DESIGN	125
6.1 Methodology of the machine learning-based surrogate models development.....	125
6.2 Development of alternative data-driven models	132

6.3 Results of local microclimate prediction	136
6.4 Performance validation of alternative data-driven models	143
6.5 Discussion on the model efficiency and accuracy	148
6.6 Recommendation on the data-driven model for microclimate simulation.....	151
6.7 Summary	152
CHAPTER 7 DEVELOPMENT OF A COORDINATED DESIGN OPTIMIZATION METHOD OF	
ZERO/LOW ENERGY BUILDINGS CONSIDERING THEIR INTERACTION WITH LOCAL	
MICROCLIMATE 154	
7.1 Procedure of coordinated design optimization and optimization problem formulation.....	154
7.2 Building design variables and optimization objectives.....	158
7.3 Preprocessing of design optimization	161
7.4 Results and analysis of optimization case study	164
7.5 Summary	176
CHAPTER 8 CONCLUSION AND FUTURE WORK	179
8.1 Main contribution of this study	179
8.2 Conclusions.....	180
8.3 Recommendations for future work	184

REFERENCE.....184

LIST OF FIGURES

Figure 1.1 Organization of main chapters.....	10
Figure 3.1 Aerial view of the study area and the location of the new building	48
Figure 3.2 An example of the building geometry model for coordinated design optimization	50
Figure 3.3 Logic of coordinated natural ventilation, heating and air-conditioning controls in simulation.....	52
Figure 3.4 Daylight dimming control logic	53
Figure 4.1 Geometry model of high-rise and low-rise building	57
Figure 4.2 Typical cities of the 5 climate zones	59
Figure 4.3 Procedures of sensitivity analysis.....	65
Figure 4.4 Highly sensitive (top 20) parameters of the high-rise buildings in 5 climate zones—Building energy performance	73
Figure 4.5 Highly sensitive (top 20) parameters of the high-rise buildings in climate zones without heating provision — Winter thermal discomfort.....	73
Figure 4.6 Highly sensitive (top 20) parameters of the low-rise buildings in 5 climate zones— Building energy performance	78
Figure 4.7 Highly sensitive (top 20) parameters of the low-rise buildings in climate zones without heating provision — Winter thermal discomfort.....	78
Figure 5.1 Outline of the overall research methodology and procedure.....	96

Figure 5.2 3D geometry model of the target district in SketchUp.....	98
Figure 5.3 3D computational domain in SpaceClaim.....	99
Figure 5.4 Local air temperature differences between with and without the new building under different scenarios.....	105
Figure 5.5 Air temperature distributions at z=1.5m of magnified view of study area	106
Figure 5.6 Local wind velocity differences between with and without the new building under different scenarios.....	108
Figure 5.7 Wind velocity distributions at z=1.5m of magnified view of study area ..	109
Figure 5.8 Pedestrian thermal discomfort degrees under different scenarios.....	109
Figure 5.9 Pedestrian thermal discomfort degrees of the district with the new building under different scenarios.....	112
Figure 5.10 Building energy consumption, outdoor air temperature and wind velocity differences between local microclimate and TMY under different scenarios	113
Figure 5.11 SPEA correlation coefficient between building parameters and the performance indexes concerned.....	117
Figure 5.12 Windward-side local microclimate differences at different distances under different settings of air-conditioner heat rejection.....	120
Figure 6.1 Outline of the overall research methodology and procedure.....	128
Figure 6.2 Neural network for predicting the changes of local microclimate	129
Figure 6.3 Predicted local air temperature difference given by different machine learning models.....	137

Figure 6.4 Pedestrian-level local air temperature distribution of the reference case calculated by CFD simulations	138
Figure 6.5 Pedestrian-level local air temperature distribution of the Case 8 calculated by CFD simulations	138
Figure 6.6 Predicted local air temperature vs actual local air temperature	139
Figure 6.7 Predicted local wind velocity difference given by different machine learning models	141
Figure 6.8 Pedestrian-level local wind velocity distribution of the reference case calculated by CFD simulations	142
Figure 6.9 Pedestrian-level local air temperature distribution of the Case 33 calculated by CFD simulations	142
Figure 6.10 Predicted local wind velocity vs actual wind velocity.....	143
Figure 6.11 Prediction errors of different machine learning models in predicting local air temperature difference	145
Figure 6.12 Prediction errors of different machine learning models in predicting local wind velocity difference	147
Figure 7.1 Outline of the overall research methodology and procedure.....	147
Figure 7.2 The relationship between design variables and objectives of the energy performance-driven design and the environmental performance-driven design.	162
Figure 7.3 Historical design samples (1st to 80th generation) and Pareto optimal set in the coordinated optimal design	166

Figure 7.4 Searching range, and mean value, median value and distribution of the Pareto front
of the building design variables 168

Figure 7.5 Rankings and scores of the Pareto optimal solutions evaluated by entropy-TOPSIS
method..... 173

Figure 7.6 The best solution on the Pareto front..... 173

Figure 7.7 Comparison of time consumption for traditional method and proposed method176

LIST OF TABLES

Table 2.1 Representative studies on parametric analysis of buildings	17
Table 2.2 Representative studies on the impacts of building design on local microclimate	20
Table 2.3 Representative studies on the impacts of local microclimate on building performance	23
Table 2.4 Representative studies on local microclimate prediction model development adopting machine learning methods	32
Table 2.5 Representative studies on design optimization of local microclimate based on data- driven methods.....	41
Table 3.1 Daily schedule of occupancy rate	53
Table 3.2 Daily schedule of electric light utilization rate	54
Table 3.3 Daily schedule of electric equipment utilization rate	54
Table 4.1 The internal load settings of the building	57
Table 4.2 Settings of occupancy rate and the lights and equipment utilization rate.....	58
Table 4.3 The climate zones in China and the climate zones of the world of the typical cities	59
Table 4.4 Parameters affecting building performance concerned for sensitivity analysis	62
Table 4.5 Performance objectives concerned for sensitivity analysis in different climate zones	66
Table 4.6 Settings of the factors and efficiencies in Eqs. (4.2)	67

Table 4.7 The 15 (out of the 35 or 34) parameters of the least impact on building energy performance in 5 climate zones — High-rise buildings	84
Table 4.8 The 15 (out of the 35 or 34) parameters of the least impact on building energy performance in 5 climate zones — Low-rise buildings	84
Table 4.9 The 15 (out of the 35 and 31) parameters of the least impact on building energy performance in severe cold zone.....	85
Table 4.10 (a) Parameters need to be optimization for climate zones with heating provision	87
Table 4.10 (b) Parameters need to be optimization for mild zone without heating provision	88
Table 4.10 (c) Parameters need to be optimization for hot summer & warm winter zone without heating provision	88
Table 5.1 Building parameters concerned in this study.....	94
Table 5.2 The internal settings and the settings of the parameters not under investigation in the simulation model.....	102
Table 5.3 Ranking of major building parameters affecting local microclimate	122
Table 5.4 Ranking of major building parameters affecting pedestrian thermal discomfort degree and building energy consumption considering microclimate impacts	122
Table 6.1 Hyperparameter optimization for the prediction model of local microclimate impacts	135
Table 6.2 Performance of different machine learning models for local air temperature difference prediction	145

Table 6.3 Performance of different machine learning models for local wind velocity	
difference prediction	147
Table 7.1 Design variables of coordinated optimal design of building and local microclimate	
.....	158
Table 7.2 Pareto optimal solutions of the coordinated optimal design of building and local	
microclimate	169

NOMENCLATURE

Abbreviations

<i>ACO</i>	<i>Ant colony optimization algorithm</i>
<i>ANN</i>	<i>Artificial neural network</i>
<i>CFD</i>	<i>Computational fluid dynamics</i>
<i>CNN</i>	<i>Convolutional neural network</i>
<i>COP</i>	<i>Coefficient of performance</i>
<i>GAN</i>	<i>Generative adversarial network</i>
<i>GIS</i>	<i>Geographic information system</i>
<i>HypE</i>	<i>Hypervolume estimation algorithm</i>
<i>LightGBM</i>	<i>Light gradient boosting machine</i>
<i>LSTM</i>	<i>Long short-term memory</i>
<i>MAD</i>	<i>Median absolute deviation</i>
<i>MAE</i>	<i>Mean absolute error</i>
<i>MAPE</i>	<i>Mean absolute percentage error</i>
<i>NSGA-II</i>	<i>Non-dominated sorting genetic algorithms</i>
<i>PET</i>	<i>Physiologically equivalent temperature</i>
<i>PMV</i>	<i>Predicted mean vote</i>
<i>PSO</i>	<i>Particle swarm optimization algorithm</i>
<i>RANS</i>	<i>Reynolds-averaged Navier–Stokes equations</i>
<i>RF</i>	<i>Random forest</i>
<i>RMSE</i>	<i>Root mean squared error</i>
<i>RNN</i>	<i>Recurrent neural network</i>
<i>RSM</i>	<i>Response surface method</i>
<i>SA</i>	<i>Simulated annealing</i>
<i>SPEA</i>	<i>Spearman correlation coefficient</i>
<i>SVR</i>	<i>Support vector regression</i>
<i>TMY</i>	<i>Typical meteorological year</i>
<i>TOPSIS</i>	<i>The technique for order preference by similarity to ideal solution</i>
<i>UHI</i>	<i>urban heat island</i>

UTCI *Universal thermal climate index*

Symbols

U_T	<i>Total assembly wall U-value ($W/(m^2 \cdot K)$)</i>
U_0	<i>Wall U value ($W/(m^2 \cdot K)$)</i>
A_{tot}	<i>Total opaque wall area (m^2)</i>
E_{tot}	<i>Annual total building consumption (kWh)</i>
f_{ele}	<i>Conversion factor</i>
E_{LE}	<i>Annual lighting electricity consumption (kWh)</i>
E_{EE}	<i>Annual electricity consumption of other electric equipment (kWh)</i>
E_{HE}	<i>Equivalent annual electricity consumption for heating (kWh)</i>
Q_{HL}	<i>Annual heating demand of building (kWh)</i>
η_s	<i>Efficiency of district heating system with gas-fired boiler</i>
q_{gas}	<i>Heating value of natural gas</i>
q_{ccop}	<i>Coal consumption of power generation</i>
φ_{cftc}	<i>Conversion factor converting gas to standard coal</i>
E_{CE}	<i>Annual consumption of cooling (kWh)</i>
Q_{CL}	<i>Annual cooling demand of building (kWh)</i>
$SCOP_s$	<i>Overall coefficient of performance of air-conditioning system</i>
D_{dis}	<i>Thermal discomfort index</i>
PMV_i	<i>Hourly average value of PMV</i>
φ_T	<i>Combined linear thermal bridge transmittance ($W/(m \cdot K)$)</i>
D_{discom}	<i>Pedestrian thermal discomfort degree ($^{\circ}C$)</i>
PET_{ave}	<i>Average PET of male and female ($^{\circ}C$)</i>
PET_{male}	<i>PET of male (PET_{male}) and female (PET_{female}) ($^{\circ}C$)</i>
PET_{female}	<i>PET of female ($^{\circ}C$)</i>
PET_n	<i>Neutral physiological equivalent temperature ($^{\circ}C$)</i>
U_z	<i>Vertical velocity profile (m/s)</i>
U_s	<i>Velocity at the reference height (m/s)</i>
z_s	<i>Reference height (m)</i>
I_z	<i>Turbulent intensity</i>
l_z	<i>Turbulence integral length.</i>

C_μ	<i>Model constant</i>
\hat{y}_i	<i>Predicted value</i>
y_i	<i>True value</i>
$p_{i,j}$	<i>Normalized value of the design variable</i>
E_j	<i>Information entropy</i>
w_j	<i>Weight given to each evaluation criteria</i>
p_j^+	<i>Positive ideal solution</i>
p_j^-	<i>Negative ideal solution</i>
d_i^+	<i>Euclidean Distance of each Pareto optimal solution to positive ideal solution</i>
d_i^-	<i>Euclidean Distance of each Pareto optimal solution to negative ideal solution</i>
C_i	<i>Relative closeness of each Pareto optimal solution to ideal solution</i>

Greek letters

φ	<i>Linear thermal transmittance (W/(m·K))</i>
χ	<i>Point thermal transmittance (W/K)</i>
α	<i>Power-law exponent</i>
k	<i>Turbulent kinetic energy</i>
\mathcal{E}	<i>Dissipation</i>

Subscripts

L	<i>Length of a linear thermal transmittance (m)</i>
z	<i>Vertical coordinate of the calculation point (m/s)</i>
n	<i>Total number of samples</i>
F	<i>Design optimization objective</i>
X	<i>Design variable</i>
bui	<i>Building</i>
mic	<i>Local microclimate</i>
C	<i>Design constraint</i>
d	<i>Width of the building (m)</i>
P	<i>Normalized decision matrix</i>

CHAPTER 1 INTRODUCTION

1.1 Background and motivation

Carbon neutrality is increasingly recognized as the world's most urgent mission to limit global warming. Around 137 countries have committed to achieving carbon neutrality [1]. The government of the Hong Kong SAR has also pledged to achieve net zero carbon emissions by 2050 [2]. Reducing energy demand and increasing renewable energy generation are the fundamental means to achieve this challenging goal. Zero/low energy buildings with low energy demand and high utilization of renewable energy are therefore considered as effective means to facilitate the achievement of carbon neutrality, and are receiving increasing attention from government, society and professionals [3-8]. The zero/low energy buildings are typically associated with significantly reduced energy needs through energy efficiency technologies and passive design methods. This approach allows for the maintenance of indoor environmental quality and the achievement of energy reduction goals. Currently, most of the research related to zero/low energy buildings focuses on low-rise buildings, which are relatively easy to achieve zero/low energy standards because certain energy-efficient technologies, such as ground cooling and green roofs, have limitations when applied in high-rise buildings due to roof area, site coverage, and structural load limitations [9]. However, most countries are undergoing a fast urbanization process today, and most newly-constructed urban blocks are composed of high-rise buildings to increase land use efficiency in high-density urban cities [10]. Therefore, the design of zero/low energy buildings in high-density cities becomes an important objective

for building energy efficiency, as achieving the goal of low energy consumption can lead to significant energy conservation.

As the world experiences rapid urbanization, the population in urban cities has been increasing intensely over the past decades. Currently, around 56% of the global population lives in urban areas, and this percentage will continue to increase to 61% by 2030 according to the United Nations [11]. In order to cope with the increase in population and improve the quality of the living environment, new building development or building renewal becomes common in high-density cities. The new development can modify the local microclimate, such as by blocking wind flow and affecting heat removal in summer. One major phenomenon is the urban heat island (UHI) effect. A UHI refers to an urban area with a higher temperature than its rural surroundings. The UHI can contribute to thermal discomfort among urban residents and even lead to heat-related illnesses such as respiratory difficulties, heat cramps, heat exhaustion, and non-fatal heat stroke.

As buildings are recognized as major contributors to the urban local microclimate, attention must be paid to how zero/low energy building design affects the local microclimate. Both building morphology and thermal characteristics can have significant impacts on the local microclimate [12]. Different building morphologies can result in a variation in local air temperature by up to 2.5°C in Zürich, Switzerland [13]. The application of cooling material with high albedo on building envelope design can lead to a decrease of local air temperature up to 0.7 °C in Thessaloniki, Greece [14]. On the other hand, the microclimate also affects the

building energy performance considerably [15]. In Rome, the variation of the local air temperature can cause a reduction in heating load by up to 21% and an increase in cooling load by up to 74% in residential buildings [16]. As urbanization accelerates the development of high-density urban areas, the impact of changes to a building on the surrounding microclimate becomes more pronounced due to limited space. Therefore, it is necessary to consider the mutual impacts when optimizing the design of zero/low energy buildings to improve both building energy performance and outdoor thermal comfort. However, there are still several challenges to address in the design optimization of zero/low energy buildings, considering their interaction with the local microclimate in high-density cities:

Firstly, the mutual impacts between zero/low energy building design and the local microclimate have been ignored in the design optimization of zero/low energy buildings in current design practices due to a lack of comprehensive understanding and particularly effective assessment methods. Existing investigations on the local microclimate are always at the district scale for district/urban planning and are insufficient to support the design of zero/low energy buildings. There is still a lack of comprehensive understanding of the major influential building parameters affecting both building energy performance and the local microclimate to support zero/low energy building design while considering mutual impacts.

Secondly, there is still a lack of accurate prediction methods for the local microclimate surrounding buildings that have low computing costs to assist in the design optimization of zero/low energy buildings while considering their interaction with the local microclimate. Due

to the complexity of both the geometric model of the urban neighborhood/district and the variations in the local microclimate, there is significant bias in estimating the local microclimate. Existing predictions of high-resolution temporal and spatial local microclimate information mostly rely on CFD simulations, which face significant challenges in practical applications for the design optimization of zero/low energy buildings due to the complexity of setting up simulations and high computing loads. The development of a fast and accurate prediction method for the local microclimate is necessary and serves as the foundation for the design optimization of zero/low energy buildings while considering their interaction with the local microclimate.

Thirdly, the trade-offs between building energy performance and the local microclimate have not been addressed in the design of zero/low energy buildings due to complexity. Existing studies on the design optimization of zero/low energy buildings have not considered outdoor thermal comfort, while the impact of the local microclimate on building energy performance is also ignored in the design optimization. The mutual impacts between zero/low energy and microclimate are ignored when making the design optimization. It is necessary to propose compromise design solutions that strike a balance to maximize the benefits of building energy efficiency and pedestrian thermal comfort.

1.2 Aim and objectives

The aim of this PhD study is to develop an effective and comprehensive optimal design method based on multi-objective optimization for zero/low energy buildings and local microclimate

considering their interactions in high-density cities. Additionally, machine learning-based surrogate models are developed for the fast prediction of the local microclimate. It is accomplished by addressing the following objectives:

1. Develop an automated building performance simulation model considering the interaction with local microclimate. The building performance model is utilized for testing and validating the proposed coordinated design optimization method efficiently, generically, and automatically when applied to new design scenarios.

2. Develop a global sensitivity analysis method and conduct systematic and comparative sensitivity analyses to investigate the impacts of building design parameters on the energy performance of zero/low energy buildings in different climate zones, taking into consideration the impacts of climate and building height. The intention is to identify the most influential design parameters of zero/low energy buildings in different climate zones and at different building heights for testing and validation of the proposed coordinated design optimization method.

3. Investigate the mutual impacts between zero/low energy building design and the local microclimate, considering their interaction, and conduct a global sensitivity analysis to investigate the impacts of design parameters on building energy performance and the local microclimate. The intention is to identify the major influential building parameters affecting both the local microclimate and building energy performance in a subtropical urban area. Perform a large number of high-resolution microclimate and building simulations based on

advanced GIS spatial analysis techniques under different building designs for mutual impact assessment.

4. Develop surrogate models of local microclimate (i.e., local air temperature surrogate model and local wind velocity surrogate model) with high efficiency and high accuracy. The surrogate models of local microclimate are utilized for the fast and accurate prediction of local microclimate changes under different building designs, which is the foundation of the test and validation of the proposed coordinated design optimization method.

5. Develop a coordinated optimal design method for zero/low energy buildings and their local microclimate considering the interactions between them. This method is expected to achieve simultaneous design optimization of buildings and local microclimate effectively and identify the global optimal design solutions maximizing the benefits of energy efficiency in zero/low energy building and pedestrian thermal comfort.

1.3 Organization of thesis

This thesis consists of 8 chapters as shown in Figure 1.1, which are organized as follows.

Chapter 1 presents the background and motivations for developing zero/low energy buildings considering the interaction with the local microclimate. The technical challenges faced in developing zero/low energy buildings considering their interaction with the local microclimate are discussed. Then, the aims and objectives of this study are presented as well as the organization of this thesis.

Chapter 2 presents a comprehensive literature review on the mutual impacts between zero/low energy buildings and the local microclimate, as well as the modelling and optimal design of zero/low energy buildings and the local microclimate. The zero/low energy building studies are reviewed in terms of the definition, technologies and the parametric studies of zero/low energy buildings. The mutual impacts between buildings and the local microclimate are reviewed in terms of the impacts of building design on the local microclimate, the impacts of the local microclimate on building performance, and the studies on mutual impacts between buildings and the local microclimate. The modelling and simulation of local microclimate are reviewed in terms of the conventional methods and the emerging data-driven methods. The optimal design of zero/low energy buildings and local microclimate is reviewed in terms of the design optimization of zero/low energy buildings, the design optimization of local microclimate and the multi-objective design optimizations. The research gaps in the above subject areas are summarized.

Chapter 3 presents an overview of the research scenario used in this study and the automated building simulation model. A new building to be developed in an existing district in Hong Kong, which is a typical design scenario of high-density urban area, is determined as the research scenario for the test and validation of the proposed surrogate models of local microclimate and the proposed coordinated design method. The automated building simulation model is of efficiency and generalizability when applying to new design scenarios.

Chapter 4 presents the identification of the most influential design parameters of high-rise and low-rise zero/low energy buildings in different climate zones. The global sensitivity analysis method is performed and a total of thirty-five design parameters under five categories are considered to identify the key envelope design parameters that significantly affect the building energy performance. The key design parameters affecting winter thermal discomfort in climate zones typically lacking heating provision are also identified. The impact of thermal bridge on building energy performance is further investigated.

Chapter 5 presents the investigation on the mutual impacts between new individual building design and local microclimate considering the interaction and the identification of the major influential parameters of zero/low energy buildings on both local microclimate and building energy performance in the subtropical urban area. A large number of high-resolution microclimate and building simulations based on advanced GIS spatial analysis techniques are performed under different building designs for mutual impact assessment. A global sensitivity analysis is conducted to identify the major influential building parameters.

Chapter 6 presents the procedures and methods for developing local microclimate surrogate models. Machine learning-based surrogate models are developed to predict the impacts on local microclimate (i.e., local air temperature and wind velocity) due to the addition of new individual zero/low energy buildings. 200 sets of CFD simulation data corresponding to different building designs are used for the training and validation of the model. Four machine learning algorithms are evaluated and compared for the model development, including ANN,

SVR, RF and LightGBM. A case study is conducted to validate the local microclimate surrogate models.

Chapter 7 presents the procedure and methods of the proposed coordinated design optimization method for zero/low energy buildings and the local microclimate, considering the interactions between them. Comprehensive design variables are optimized using multi-objective optimization. The automated building simulation and local microclimate surrogate models are combined with the optimizer to enhance efficiency and generalizability. The obtained Pareto optimal solutions are evaluated using the entropy-TOPSIS method, and the best solution is recommended. A case study in Hong Kong is utilized to test and validate the proposed method.

Chapter 8 summarizes the main contributions and conclusions of the work conducted in this PhD project and provides recommendations for future research on the subjects covered in this study.

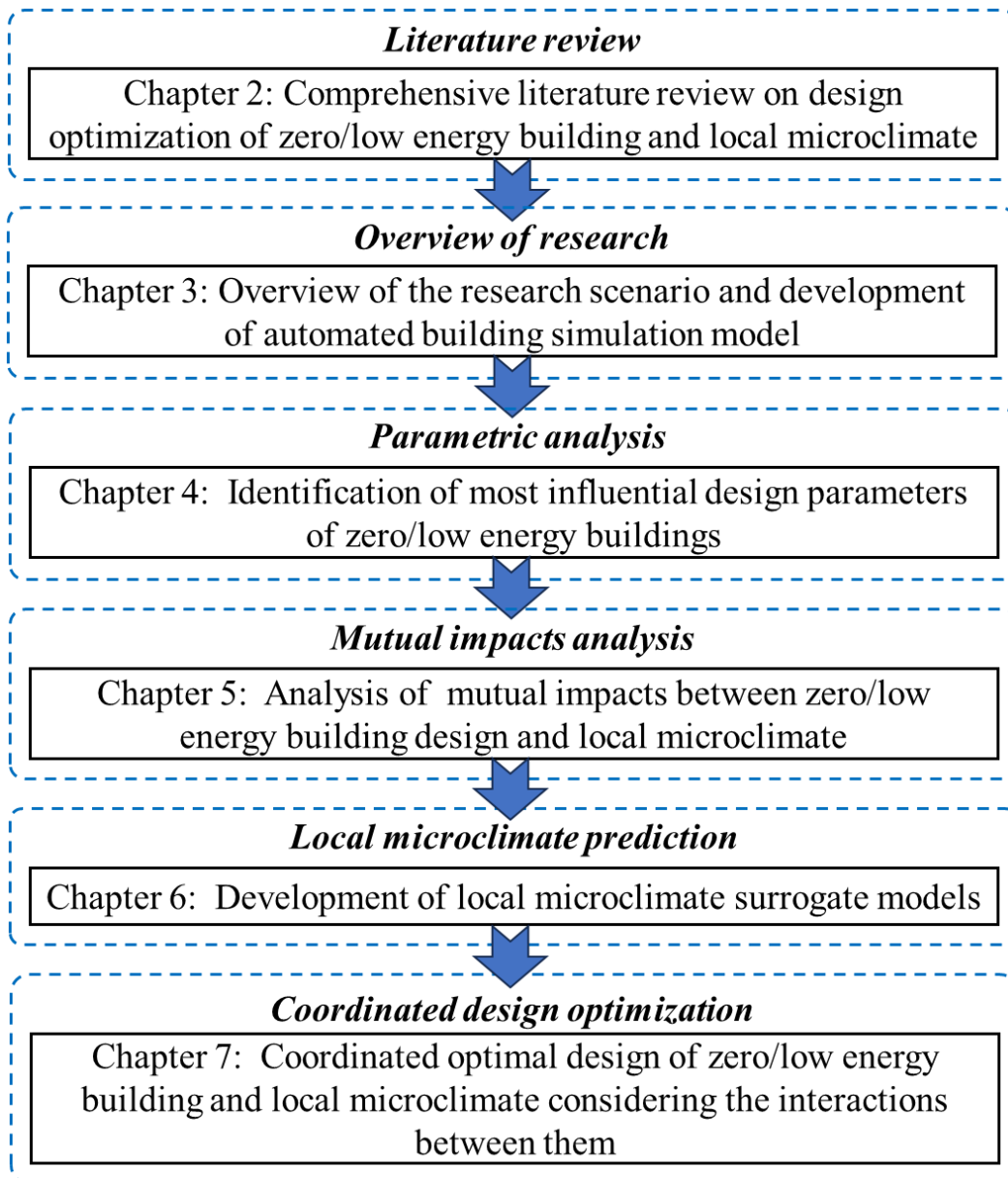


Figure 1.1 Organization of main chapters

CHAPTER 2 LITERATURE REVIEW

A comprehensive literature review on the optimal design of zero/low energy buildings and local microclimate is conducted to provide the research background and a clear picture of what has been done and what needs to be done (i.e., the research gaps) in this research domain.

Section 2.1 presents an overview of the studies on zero/low energy buildings, including the definition and zero/low energy technologies, and the parametric studies of zero/low energy buildings. Section 2.2 presents a review on the mutual impacts between buildings and the local microclimate, including the impacts of building design on the local microclimate, the impacts of the local microclimate on building performance, and the studies on mutual impacts between buildings and the local microclimate. Section 2.3 presents the modelling and simulation of local microclimate, including the conventional methods and the emerging data-driven methods. Section 2.4 presents a review of the optimal design of zero/low energy buildings and the local microclimate, including the design optimization of zero/low energy buildings, the design optimization of the local microclimate, and the multi-objective design optimizations. Section 2.5 presents a summary of the research gaps in the above research areas.

2.1 Overview of zero/low energy buildings technologies and parametric studies

2.1.1 Definition and technologies of zero/low energy buildings

Zero/low energy buildings have received widespread attention in recent years due to their low energy demand and high utilization of renewable energy, which have been seen as effective

solutions to reduce carbon emissions and facilitate the achievement of carbon neutrality. In concept, zero/low energy buildings have greatly reduced energy demand through energy efficiency measures so that the remaining energy demand can be supplied by renewable energy technologies [3,8]. The term “zero energy” refers to the balance between building energy demand and the building energy supply. At the strictest level, zero energy buildings generate enough renewable energy on-site to equal or exceed their energy use. Therefore, two major tasks must be addressed in the development of zero/low energy buildings. One task is to minimize the energy demand of buildings through energy efficiency measures. The other task is to generate energy for buildings through renewable energy technologies and other means.

As for the energy-efficient measures for zero/low energy buildings, there are three aspects concerned in previous studies: building envelope, building energy systems and internal conditions [7]. Buildings in different climate zones have different requirements for building envelopes that aim to reduce heat gain in summer and heat loss in winter. The strategies are mainly related to wall, window, roof, floor, and skylight. For instance, Akbari et al. investigated the energy saving potential of reflective roofs for residential and commercial buildings in the eleven United States metropolitan statistical areas in a variety of climates. In the hottest and sunniest cities, such as Phoenix, the largest savings are of 51 dollars per year per 1000 ft² roof area of air-conditioned buildings. However, as the climate gets cooler, the savings decrease. In Miami, the savings are of 30 dollars [17]. As for the building energy systems, HVAC systems, and electric lighting systems are the two major energy-consuming systems in buildings, which

account for 40~60% and 20~30% of total building energy consumption [7]. Zhu et al. proposed an advanced model predictive control method for chillers that are integrated with cold water storage technology in data centers. The coefficient of performance (COP) was increased by 1.96, the cooling system energy consumption was reduced by 5.8%, and the power usage effectiveness was reduced by 0.013 when utilizing the proposed method compared with the baseline strategy [18]. Internal conditions, including the indoor design conditions and internal heat load, have significant energy-saving potential. For instance, Sadineni et al. concluded that raising the thermostat temperature from 23.9 °C to 26.1 °C from 4:00 PM to 7:00 PM resulted in the decreased average demand by 69% during the peak period [19].

The renewable energy technologies are utilized to supply the remaining energy for zero/low energy buildings. The strategies mainly include the utilization of photovoltaics, wind turbines, solar water heaters, heat pumps and district heating and cooling [7]. Li et al. adopted semi-transparent photovoltaic panels together with the dimming controls in office buildings, through which the annual building electricity was saved by 1203 MWh and the peak cooling load was reduced by 450 kW. In the meantime, the utilization of semi-transparent photovoltaics is also environmentally friendly due to the reduction of annual emissions of CO₂, SO₂, NO_x, and particulates by the amounts of 852, 2.62, 1.45, and 0.11 tons [20]. The hybrid PV-wind power generation systems have developed rapidly in recent years as the solar availability and the wind availability can compensate for each other at different times of the year. TAZAY et al. proposed a grid-connected large-scale PV/wind hybrid power system in the Gabel El-Zeit region located

along the coast of the Red Sea, Egypt. The developed PV/wind hybrid power system can achieve a total annual electricity generation of about 1509.85 GWh/year, including the generation from the PV station of 118.15 GWh/year (7.83 %) and generation from the wind farm 1391.7 GWh/year (92.17%) [21].

2.1.2 Parametric studies of zero/low energy buildings

In recent years, many efforts have been made to identify the key design parameters affecting building performance [22-69]. These parameters are critical to the optimal design of building envelopes in order to achieve zero/low energy buildings. Some representative studies are summarized and listed in Table 2.1. For instance, Li et al. investigated the impacts of the main design parameters and conducted a multi-stage sensitivity analysis to identify the key influential design parameters in the subtropical climate for zero/low energy buildings among a total of 29 parameters. The zero carbon low-rise building in Hong Kong is selected as the reference building [43]. Chen et al. utilized the multiple linear regression to conduct sensitivity analysis for a standard floor of a typical high-rise residential building in hot and humid climates [42]. The window transmittance property and window-to-ground ratio were determined as the most influential parameters affecting daylight, natural ventilation, and thermal comfort performance in hot and humid climates. Li et al. investigated the impacts of nine building envelope parameters and spatial factors on the energy demand of a multi-story ultra-low-energy building in hot summer and cold winter zones, and recommended that increasing the standard floor area and reducing the floor height are critical to building energy efficiency [48].

It can be observed from the reviewed 48 papers that most of the current studies (i.e. 36 out of 48) related to the identification of the key design parameters concern the low-rise buildings, while a small part (i.e. 12 out of 48) concerning the high-rise buildings. This means that the highly sensitive parameters for building envelope design are mainly identified from low-rise buildings in previous studies, while the key design parameters for high-rise buildings have not been sufficiently investigated. However, the significant difference between low-rise and high-rise buildings cannot be ignored, and has to be considered seriously [46]. As for the existing studies on high-rise buildings, there are two limitations, which are summarized in the following. Firstly, a typical floor of high-rise buildings is usually selected and used in performance evaluation to save simulation time [9,22,40,42,44], while it cannot represent performance of the entire building as building performance on different floors may vary [33]. Secondly, current studies have considered only part of the main design parameters, so that some key design issues (e.g., the overhang and skylight) of high-rise buildings may be ignored [9,22,23,31,33,40,42,44,46,50,51,62]. There is also a lack of comparison between key design parameters of high-rise and low-rise buildings.

Currently, the key design parameters of the building envelope in different climate zones around the world have been studied [22-69]. Zhao et al. investigated the impacts of seven building design parameters on the heating and cooling energy demand of the standard floor in a high-rise residential building in five climate zones of China. The results showed that optimizing the three most sensitive design parameters led to the reduction of total energy demand by 75

kWh/(m²·a) in the severe cold zone, 40 kWh/(m²·a) in the cold and the hot summer and cold winter zones, 50 kWh/(m²·a) in the hot summer and warm winter zone, and 35 kWh/(m²·a) in the mild zone [22]. Guo et al. conducted a sensitivity analysis to assess the impacts of six building design parameters on the building energy demands and thermal comfort of a seven-storey office building in five climate zones in China. The results indicated that the energy saving potential of different climate zones was different when optimizing the design parameters. The severe cold zone achieved the greatest energy saving by 18–24%, the hot summer and cold winter zone achieved the energy saving of 16–19%, and the cold zone and mild zone achieved energy savings of 12–15%. However, the hot summer and warm winter zone achieved the lowest energy savings, at only 5–7% [27].

It can be observed that the highly-sensitive design parameters for building performance in different climate zones vary. The indoor temperature set-point and parameters associated to air tightness are commonly the highly sensitive parameters in all kinds of climate zones. In the climate zone with severe cold winter, the U-value of external wall and the thickness of insulation are the key parameters affecting building energy performance [22]. As for the climate zone with hot summer, the parameters related to skylight and solar protection are the most influential [43]. The parameters related to window thermal characteristics are the crucial ones to the zones with mild climate [9,22]. However, the parameters considered in different studies vary, which are not comprehensive enough to quantify the impact on building performance in different climate zones. Although there are some studies comparing key design

parameters of the building envelope in different climate zones, only part of the main design parameters are taken into account. Therefore, the outputs of existing studies are insufficient to compare the major design concerns in different climate zones. Furthermore, in existing studies, the diversity of local design conditions in different climate zones, which leads to the diversity of building performance objectives, has almost been ignored when setting the simulation models. Therefore, the parameters identified by sensitivity analysis may not be representative for certain climate zones because building performance may not be quantified according to local energy demand in reality.

Table 2.1 Representative studies on parametric analysis of buildings

Reference	Climate zones	Building performance objectives	Number of parameters considered	Type of building
Guo et al. [27]	5 climate zones of China	Cooling, heating and total energy demands, thermal comfort index	6	Office building (7 storeys)
Zhao et al. [22]	5 climate zones of China	Cooling, heating and total energy demands	7	Standard floor in high-rise residential building
Lee et al. [41]	Korea	Heating demand	15	Rural house (1 storey)
Li et al. [43]	Hot and humid subtropical climate zone (HK)	Comprehensive objective (building energy consumption and winter thermal discomfort)	29	Low-rise building
Chen et al. [42]	Hot and humid subtropical climatic zone (HK)	Indoor environment index (illuminance level, air change rate and ASHRAE55 comfort time)	9	Standard floor in high-rise residential building (30–40 storeys)
Yıldız et al. [33]	Hot-humid climate zone (Izmir, Turkey)	Heating and cooling energy loads	35	High-rise apartment building (10 storeys)
Lam [31]	Hot and humid subtropical climate zone (HK)	Annual building energy consumption and peak design load	12	High-rise office building (40 storeys)
Delgarm [47]	4 climate zones of Iran (cold, mild, warm–dry, and	Total building energy demands (cooling, heating and lighting)	12	Multi-story building (4 storeys)

	warm-humid)			
Heiselberg [28]	Denmark	Heating, ventilation, cooling and lighting energy use	21	Office building (7 storeys)
Li [48]	Hot summer and cold winter zone of China	Heating and cooling load	9	Multi-story office building (5 storeys)
Yu [23]	Hot summer and cold winter zone of China	Cooling, heating and yearly energy use	8	Multi-story building (6 storeys)
Feng [30]	Severe cold zone of China	Heating, cooling and total building energy	4	Low-rise residential building (2 storeys)
Lu [24]	Hot and humid subtropical climate zone (HK)	Combination of total annualized cost, CO2 emissions and grid interaction index	4	Low-rise building
Tavares [26]	Portugal	Annual cooling, heating and electric energy	10	Multi-story office building (5 storeys)
Andarini [29]	Indonesia	Decrease of cooling energy demand	9	Office building (3 storeys)
Samuelson [60]	2 ASHRAE climate zones	Energy Use Intensity, peak loads and passive survivability	9	High-rise residential building
CORRADO [36]	Italy	Heating and cooling energy demand	13	Single-family house (2 storeys)
Raji [59]	Temperate maritime climate	Annual heating, cooling and lighting demand	14	High-rise office building
Menberg [52]	England	Annual heating demand	11	Office building (2 storeys)

2.2 Mutual impacts between buildings and local microclimate

2.2.1 Impacts of building design on local microclimate

In the past decade, increasing efforts have been made to investigate the impacts of building design on the local microclimate [12-15,70-89]. The representative studies are summarized in Table 2.2. The methods used to quantify the impacts can be classified into two categories, i.e., on-site monitoring and simulation. When the on-site monitoring method is adopted, monitoring stations are used to collect local weather data, such as dry-bulb temperature, relative humidity, global solar radiation, wind direction, and wind speed. When the simulation method is adopted,

the impacts of buildings in the neighborhood or district on the local microclimate were mainly investigated using software such as FLUENT, STEVE, UWG, SOLENE, OpenFOAM and CitySim. The study period varies from a selected hour to one year. The factors concerned include the district density and district geometry parameters (e.g., plan density, street height/width ratio and sky view factor), building morphology parameters (e.g., building aspect ratio and building height) and thermal characteristics parameters (e.g., albedo and emissivity).

According to the analysis results, the design of the district can have significant impacts on the surrounding local microclimate under different climate conditions. For instance, Bourbia et al. monitored the local air temperature for one month in Constantine, Algeria to investigate the impacts of district morphology parameters on the local microclimate. The results showed that variations in district morphology parameters, including street height-to-width ratio, sky view factor, and street orientation, led to an increase in local air temperature of up to 6 K in the Mediterranean climate [81]. Allegrini et al. simulated the local microclimate in one typical hour affected by the six different district height topologies utilizing the coupled Computational Fluid Dynamics (CFD) and building energy simulations in the software OpenFOAM and CitySim. The local air temperature increased by 1.5–2.5 K due to variations in district height topologies in Zürich, Switzerland, with a temperate maritime climate [13]. Merlier et al. investigated the impacts of building configurations of the district on local air temperature on two selected days utilizing the SOLENE-microclimat models, which led to an increase in local

air temperature in the range of 1.7~2.8 K in Lyon, France, with a Continental temperate marine climate [82].

Not only do building morphology but also building thermal characteristics have an effect on the surrounding local microclimate. Ali-Toudert et al. combined urban microclimate and building energy modelling in TEB and TRNSYS to simulate the local air temperature at the neighborhood scale in Mannheim, Germany. It was concluded that variations in thermal insulation, thermal inertia, albedo, and emissivity of the building envelope, street aspect ratio, and plan density led to variations in local air temperature in the range of in the range of -1.21~+0.34 K in the Temperate continental climate[70]. Tsoka et al. investigated the application of cooling material with high albedo on building envelope design in Thessaloniki, Greece, using the ENVI-met model, which led to a decrease in local air temperature of up to 0.7 °C in the Mediterranean climate [14].

Table 2.2 Representative studies on the impacts of building design on local microclimate

Reference	Location and climate	Building-related factors concerned	Research scale	Quantification method	Period	Impacts on microclimate
[12]	Reading, UK; Temperate maritime	Building form	Neighborhood	On-site monitoring	1 year	T: -0.27~+0.7 K
[89]	Singapore; Tropical rainforest	Floor area ratio, gross site coverage, open space ratio, number of stories, sky view factor	District	Simulation (STEVE)	-	T: -1.3 K
[70]	Mannheim, German; Temperate continental	Thermal insulation, thermal inertia, albedo and	Neighborhood	Simulation (TRNSYS)	1 year	T: -1.21~+0.34 K

		emissivity of building envelope, street aspect ratio, plan density				
[75]	Basel, Switzerland ; Toulouse, France; Temperate maritime	Thermal properties of construction materials	City	Simulation (UWG)	1 year	T: +2.4~+3.6 K
[13]	Zürich, Switzerland ; Temperate maritime	Building height topologies of district	District	Simulation (OpenFOAM & CitySim)	A selected hour	T: +1.5~+2.5 K
[81]	Constantine, Algeria; Mediterranean	Street height/width ratio, sky view factor	District	On-site monitoring	1 month	T: +3~+6 K
[82]	Lyon, France; Continental temperate marine	Building configuration of district	District	Simulation (SOLENE-microclimat)	Two selected days	T: +1.7~+2.8 K
[83]	Serres, Greece; Mediterranean	District geometry and street configuration	District	On-site monitoring	1 month	WS: -67%~-75%; T: +5~+5.5 K in afternoon and night, -7 K in morning
[84]	Zürich, Switzerland	District geometry and albedo	District	Simulation (CFD & CitySym)	A summer afternoon	T: +1 K
[14]	Thessaloniki, Greece	Cooling materials of building (emissivity and albedo), district aspect ratio	District	Simulation (ENVI-met)	A typical summer day under clear sky condition	T: -0.5~-0.7 K

Note: T and WS refer to air temperature and wind speed respectively.

2.2.2 Impacts of local microclimate on building performance

Meanwhile, the impacts of the local microclimate can influence building performance across different climate conditions [12,15,16,82,88-99]. The representative studies are summarized in Table 2.3. The climate conditions vary from temperate to tropical, and from continental to maritime. Typical reference buildings were selected as examples to investigate the impacts of the local microclimate on building performance in previous studies. Building cooling and heating loads are the major building performance metrics of concern. A few studies also investigated the impacts of cooling/heating degree days, indoor air temperature, dehumidification load, and night ventilation cooling potential [12,15,92]. The simulation method is usually adopted to quantify these impacts. The simulation software includes IES-VE, TRNSYS, EnergyPlus, DeST, City Energy Analyst, WUFI Plus, and SOLENE-microclimat. The simulation period varies from a typical day to several years.

Table 2.3 shows that the local microclimate significantly impacts building performance in different climate conditions and for different building types. For instance, when the local air temperature increased by around 1.1-1.2 K, the building cooling load increased by 5% in Zürich, Switzerland, with a temperate maritime climate [88], but by up to 41% in Milan, Italy, with a Mediterranean climate [92]. Zinzi et al. monitored the UHI effect in Rome, Italy, which led to an increase in air temperature of about 0.7 K in summer and 1 K in winter compared with a rural reference. The monitored data were used to simulate building energy consumption, and the results showed that the UHI effect resulted in a reduction in heating energy consumption

by up to 21% in residential buildings and 18% in office buildings, while the urban heat island effect resulted in an increase in cooling energy consumption by up to 74% in residential buildings and 53% in office buildings in the Mediterranean climate [16]. Palme et al. estimated the cooling demand of various types of residential buildings in four South American Pacific coastal cities, considering the UHI effect to investigate its impact on building energy performance. The results indicated that the UHI effect led to an increase in building cooling demand in the range of 15~200% in the tropical rainforest and desert climates [91]. Cui et al. analyzed the UHI effect in Beijing, China, utilizing the long-term measured weather dataset from 1961 to 2014 for ten rural stations and seven urban stations. When taking the UHI effect into consideration, the cooling load increased by 11%, while the heating load decreased by 16% in the temperate monsoon climate [94]. Merlier et al. investigated the energy demand of a monozonal building, considering the urban microclimate in Lyon, France. It is concluded that an increase of air temperature in the range of 1.7~2.8 K resulted in a decrease in heating demand in the range of 5~7%, while it resulted in an increase in cooling demand in the range of 23~100% in the continental temperate marine climate [82].

Table 2.3 Representative studies on the impacts of local microclimate on building performance

Reference	Location and climate	Variation of microclimate	Building type	Quantification method	Period	Impacts on building performance
[12]	Reading, UK; Temperate maritime	T: -0.27~+0.73 K	A five-storey faculty building	Simulation (IES-VE)	1 year	HL: -10.8%; night ventilation cooling potential: +26~+31%

[88]	Zürich, Switzerland; Temperate maritime	T: -0.7~+1.2 K; WS: -1.7~-0.1m/s	Real buildings in a district	Simulation (City Energy Analyst)	An extreme hot day	CL: +5%
[15]	Shenzhen, China; Subtropical monsoon	T: +5.9 K; RH: -26.3%	4 DOE reference buildings	Classical equations	1 week	Cooling degree days: +12.60%, heating degree days: -11.92%
[16]	Rome, Italy; Mediterranean	T: +2.8 K in summer, +1 K in winter	A residential building & an office building	Simulation (TRNSYS)	3 years	CL: +53~+74%; HL: -18~-21%
[91]	4 South American Pacific coastal cities; Tropical rainforest & desert	T: -1.15 ~ +0.59 K at night, +0.15 ~ +4.87 K in daytime	Single building	Simulation (UWG and TRNSYS)	A summer week	CL: +15~+200%
[92]	Milan, Italy; Mediterranean	T: +1.1 K; H: -0.67g/kg	A residential building	Simulation (WUFI Plus)	6 years	HL: -12~-16%; CL: +39~+41%; dehumidification load: -74~-78%; T: +1.4+1.5 K
[93]	Barcelona, Spain; Mediterranean	T: +1.7 K in summer, +2.8 K in winter	A residential building	Simulation (EnergyPlus)	Two summer days	Sensible CL: +18%~+28%
[94]	Beijing, China; Temperate monsoon	T: +2.5 K in summer daytime, +8 K in winter nighttime	A seven-storey office building	Simulation (DeST)	1 year	CL: +11%; HL: -16%
[96]	Hong Kong, China; Subtropical monsoon	T: +2.4 K; H: +0.68g/kg	A high-rise residential building	Simulation (DeST)	9 years	Sensible CL: +100%; latent CL: +96%
[82]	Lyon,	T:	A	Simulation	Two	HL: -5%~-7%;

	France; Continental temperate marine	+1.7~+2.8 K	monozo ne building	(SOLENE- microclimat)	selecte d days	CL: +23~+100%
--	---	----------------	--------------------------	------------------------------	-------------------	------------------

Note: T, RH, H and WS refer to air temperature, relative humidity, absolute humidity and wind speed respectively; HL and CL refer to heating load and cooling load respectively.

2.2.3 Studies on mutual impacts between buildings and local microclimate

It can be observed that considerable work has been done to investigate the impacts of building design on the local microclimate and the effects of the local microclimate on building performance [12-16,70-99]. The mutual impacts between them are rarely addressed and should not be ignored. Due to limited space in developed, high-density cities, the development or renewal of individual buildings in existing districts is common compared to developing entire districts. The compact layout may result in more significant mutual impacts of building variations on the surrounding microclimate. Therefore, a new design perspective is needed for developing individual buildings in existing high-density districts.

According to existing studies investigating the impacts of the local microclimate on building performance, most primarily use meteorological data considering the local microclimate to simulate building performance, while the impact of building design on the local microclimate is often ignored [16,82,90-99]. Among the large number of studies, only a few (4 [12,15,88,89] of the reviewed 37 [12-16,70-99]) study the mutual impacts between them. For instance, Xie et al. performed a one-year measurement of the microclimate surrounding four typical types of built forms, including a street canyon, a courtyard, a semi-closed courtyard, and a relatively larger open area in Reading, UK. A five-storey faculty building was selected as the reference

building to simulate the building energy demand, and the results showed that different building forms resulted in variations of local air temperature in the range of $-0.27\sim+0.73$ K compared with typical meteorological year (TMY) data, which led to a decrease of annual heating demand up to 10.8% and a variation in night ventilation cooling potential in the range of $+26\sim+31\%$ in the Temperate maritime climate [12]. Mosteiro-Romero et al. coupled the microclimate simulation model ENVI-met with the district-scale energy simulation tool City Energy Analyst to evaluate district energy demand, considering the urban microclimate effect. The results indicated that the district microclimate, with variations in local air temperature in the range of $-0.7\sim+1.2$ K and wind speed in the range of $-1.7\sim-0.1$ m/s, led to a 5% increase in space cooling demand on the selected day and more than an 8% increase in peak cooling load for each building in the district with a temperate maritime climate [88].

However, several research gaps can still be observed from the literature, particularly regarding the design of new individual buildings. Firstly, existing studies mainly investigate the impacts of district design rather than those of individual building design on the local microclimate [15,88,89]. These district design parameters related to district density and geometry (e.g., plan density, street height/width ratio, and sky view factor) are less applicable to individual building design due to existing surroundings. Though these research outcomes can be adopted in district/urban planning, they are insufficient to support the design of buildings. Secondly, several existing studies investigate the impacts of building design on the local microclimate by monitoring the local microclimate surrounding the limited existing buildings [12]. However,

there is still a lack of comprehensive understanding of the major influential building parameters on both building performance and the local microclimate to support building design, considering mutual impacts. Thirdly, a simplified geometric model of the neighborhood/district is usually used in previous research, which ignores the real terrain [12-16,70-99]. This may increase the bias in estimating the impacts between buildings and local microclimate [100].

2.3 Modelling and simulation of local microclimate

2.3.1 Conventional methods

Currently, predictions of urban climate mostly rely on simulation. Numerous urban climate simulations have been performed at different scales, including mesoscale, local scale, and microscale [101]. *At the mesoscale*, the whole city and its surrounding suburban or rural area are investigated. The dimension range is typically more than several kilometers. The MESO-NH model integrated with the Town Energy Balance (TEB) model and the Weather Research and Forecast (WRF) model integrated with the Building Effect Parameterization (BEP) model are generally used for simulation [16,102]. At this scale, local characteristics cannot be explicitly represented due to low horizontal resolution. *At the local scale*, the microclimate in a district is typically modeled. Two major categories of models are used for the simulation, i.e., parametric models and explicit models. The parametric models do not represent the explicit 3D (three-dimensional) geometry, but use parameters to translate the impacts. Its dimension range is typically a hundred meters to several kilometers. Typical parametric models include the Urban Weather Generator (UWG) model, the Canyon Air Temperature (CAT) model, and the

Canopy Interface Model (CIM) [75,103]. The explicit models represent the 3D geometry and allow for a detailed representation of the microclimate surrounding buildings. Its dimension range is typically several meters to a hundred meters. Typical explicit models include ENVI-met and SOLENE-Microclimat, the simulation of which is based on CFD simulations [82,88]. *At the microscale*, the microclimate of a street is simulated. The dimension range is typically several meters to a hundred meters. At this scale, the microclimate can be modeled in more detail [70]. Therefore, CFD models are widely developed for local microclimate predictions with high 3D resolution.

CFD simulations can provide a feasible way to make predictions of high-resolution temporal and spatial local microclimate information with detailed flow fields by numerically solving sets of non-linear governing equations [104]. Considerable work has been done on detailed analysis of airflow motion, heat transfer, and contaminant transport, as well as wind flow and pollution dispersion around buildings in urban environments through CFD simulations [105]. Chen et al. conducted CFD simulations to investigate the influence of building height variations and building packing densities on the city breathability and flow adjustment [78]. The results showed that with variations in building heights, taller buildings had larger drag forces and greater city breathability than shorter buildings. Allegrini et al. performed CFD simulations in OpenFOAM to compare the local microclimate created by different district designs. Twelve CFD simulation models were developed concerning two designs of district geometries, two wind directions, two wind speeds, and two different albedos of building envelopes in Zürich,

Switzerland, and the best design was selected for achieving the most comfortable local microclimate at pedestrian level (2m above ground) [71]. Yassin investigated the flow and dispersion of gaseous emissions from vehicle exhaust in a street canyon with variations in the district aspect ratio and wind direction.. The three-dimensional flow and dispersion of gaseous pollutants were simulated utilizing a CFD simulation model numerically solved by Reynolds-averaged Navier–Stokes (RANS) equations. The results indicated that when the wind direction and district aspect ratio increased, the pollutant concentration levels decreased [77]. Chow et al. conducted a numerical analysis of the airflow and heat dissipation at the condensing units of a low-rise residential building in Hong Kong, China. The condenser heat dissipation was influenced by the plant room location and the building layout, which affected the surrounding local microclimate. The CFD simulations were conducted for five design options in order to avoid the adverse effects on the local microclimate [86]. Although CFD simulations are effective in providing accurate high-resolution local microclimate predictions, they face great challenges in their wide and practical application in new building design optimization due to their complexity in setting up simulations and the high computing load.

2.3.2 Emerging data-driven methods

The technology advancements and increasing availability of machine learning techniques make fast and even real-time predictions of the local microclimate practical. In recent years, a few attempts have been made to develop machine learning models for predicting the local microclimate [72,106-116]. The representative studies are summarized in Table 2.4. It can be

seen that various machine learning methods have been used, e.g., multivariate linear regression, gaussian process regression, long short-term memory (LSTM) network, gradient boosting regression, artificial neural network (ANN), random forests (RF), support vector regression (SVR), recurrent neural network (RNN) and generative adversarial network (GAN). Different models have been developed to predict local microclimate (e.g., wind velocity, air temperature, relative humidity, and solar radiation) at building, district, and city scales. The urban morphological parameters and the meteorological parameters are usually used as the model inputs. CFD simulation data are mostly used for the model development, while very few studies utilize monitoring data.

Wu et al. constructed surrogate models to predict the wind velocity ratio and wind velocity Gini index of a residential district based on 400 CFD simulation results, in which eleven urban morphological parameters are determined as the model inputs. Overall, six machine learning algorithms, including multivariate linear regression, multivariate polynomial regression, support vector regression, random forest regression, bagging regression, and gradient boosted regression trees regression, are compared to determine the best fit surrogate model for assisting mathematical urban microclimate design optimization [106].

Wu et al. used Gaussian process regression to train the prediction model of pedestrian-level wind velocity to assist the optimization of wind comfort utilizing 90 CFD simulation results. The building factors included building width, building depth, building height, and building orientation angle, which were determined as the model inputs, while the wind velocity at 57

measuring positions in the district was determined as the model output. The model achieved good performance and its mean absolute error (MAE) was in the range of 0~0.2 m/s [107].

Kastner et al. developed a surrogate model for prediction of wind velocity distributions in an urban district utilizing the GAN algorithm, which was able to process arbitrary building geometries. Structural Similarity Index Measure was selected as the performance index of the model accuracy, the value of which ranged from 75% to 97% based on the CFD simulation results of 564 different urban geometries [108].

Huang et al. developed a GAN-based surrogate model to accelerate the environmental performance-driven urban design optimization, through which pedestrian level wind, annual cumulative solar radiation, and Universal Thermal Climate Index (UTCI) in urban districts could be predicted in real time. 300 CFD simulation results, radiation simulation results, and UTCI simulation results for obtaining the distributions of pedestrian-level wind, annual cumulative solar radiation, and UTCI under varied morphologies of urban blocks were used to generate the dataset for training. The results showed that the GAN-based surrogate model can speed up 120–240 times compared to conventional numerical simulations. [109].

Zhang et al. developed a long short-term memory network model based on on-site monitoring data to predict the local microclimate of the target building for the next hour [114]. The model had a rather low root mean squared error (RMSE) of 0.75 °C for air temperature and 0.65 m/s for wind velocity, indicating high accuracy in prediction, indicating a rather high accuracy for prediction.

Kong et al. simulated the microclimate in a district in the U.S. based on CFD and Geographic Information System (GIS), and used the simulation data to train the ANN-based microclimate model for predicting local wind velocity and temperature under variations in wind direction [115]. Five sets of CFD simulation results of the whole computational domain were utilized to obtain the dataset for model development.

Table 2.4 Representative studies on local microclimate prediction model development adopting machine learning methods

Reference	Inputs	Outputs	Machine learning methods	Microclimate scale	Data source and volume
[106]	11 urban morphological parameters	Wind velocity ratio, wind velocity Gini index	Multivariate linear regression, multivariate polynomial regression, SVR, RF, bagging regression, gradient boosted regression	District	400 CFD simulation data
[107]	Building width, building depth, building height, building orientation angle	Wind velocity at of 57 measuring positions	Gaussian process regression	District of target building	90 CFD simulation data
[108]	Wind velocity distribution under varied morphologies of urban block	Wind velocity distribution	GAN	District	564 CFD simulation data

[109]	Pedestrian level wind, annual cumulative solar radiation, Universal Thermal Climate Index (UTCI) distribution under varied morphologies of urban block	Pedestrian level wind, annual cumulative solar radiation and Universal Thermal Climate Index (UTCI) distribution	GAN	District	300 CFD, Radiation, UTCI simulation data
[110]	Wind velocity distribution under varied morphologies of urban block	Wind velocity distribution	GAN	District	1025 CFD simulation data
[111]	Height, width of main structure, height, width, depth, shape of central core, orientation of building	Percentage of wind comfort, percentage of thermal comfort	ANN	Lift-up building	150 CFD simulation data
[112]	Wind velocities at different locations around the building	Wind velocities at unmeasured locations around the building	GAN, multiple imputations by chained equations (MICE), neighbored distanced imputation (NDI)	Target building	Measurement data of wind velocity at 555 locations
[113]	Wind velocity distribution under varied morphologies of urban block	Wind velocity distribution	Convolutional neural network (CNN)	District	3500 CFD simulation data

[114]	24 hours data of temperature, relative humidity, dew point, solar radiation, wind direction, wind speed	Following one hour data of temperature, relative humidity, dew point, solar radiation, wind direction, and wind speed	LSTM	Target building	4 years measurement data from 2016 to 2019
[104]	Urban density, target building heights, buildings' height variation, opening size, wind direction, orientation of urban canyons	CIOI index reflecting cross ventilation potential	Multivariate linear regression, gradient boosting regression	Target building	3,840 CFD simulation data
[72]	Urban morphology factor, solar exposure factor, albedo coefficient	Average monthly temperature	Multiple linear regression	City	Weather data from weather stations in Turin, satellite data and urban variables data from the Technical Map of the Metropolitan
[115]	3 orthogonal coordinates (x,y,z) and the wind direction	3 wind velocity components (v_x, v_y, v_z) and the air temperature	ANN	District	5 sets of CFD simulation data of the whole computational domain
[116]	Wind velocity distribution under varied layout and configurations of 4 buildings	Wind velocity distribution	CNN	District	3600 CFD simulation data

However, several research gaps can still be observed from the literature. Firstly, the dataset collection of some existing studies is relying on monitoring the existing buildings, district or city, which cannot meet the need of investigating the effect of building variations on local microclimate to help with the building optimal design [72,112,114]. Secondly, many existing machine learning models are developed to predict the local microclimate under the variations of urban morphologies rather than building morphologies [106,115]. The models can be applied for district and urban planning, but not applicable to the new individual building design in high-density cities. As for the models concentrating on the building design, the input variables are not comprehensive enough and ignored some key design parameters such as thermal characteristics [107]. The influence of building on local microclimate has been underestimated. There is still lack of the prediction model of local microclimate assisting the systematic and comprehensive analysis for building design. Thirdly, many deep learning models (i.e., CNN, GAN) developed to predict the spatial distribution of local microclimate parameters have limitations regarding the model complexity and high requirement for the data volume and data quality, which increases the computational cost [108-113,116]. The accuracy of these models significantly relies on the dataset volume for model training [109], which is not friendly to the research whose data generation depends on the time-consuming CFD simulations. The larger the data volume is required, the more computational cost increases. Fourthly, the current predictions are mostly concerning about the wind flow, very few papers concentrate on the air temperature which is essential to the outdoor thermal comfort [72,114].

2.4 Design optimization of zero/low energy buildings and local microclimate

2.4.1 Design optimization of zero/low energy buildings

As buildings are considered as the key factor affecting total global energy consumption, the design optimization of zero/low energy buildings are investigated with growing interests in recent years. Previous studies related to design optimization of buildings mainly focus on the building envelope design and energy systems design [117-133].

The optimized variables of building envelope design can be summarized into categories of building layout and shape parameters, envelope thermal characteristics parameters, construction quality parameters and energy efficient strategy parameters [117-133]. The parameters related to building layout and shape include building orientation, footprint, building aspect ratio, number of storeys, building-height-to-street-width ratio, window-to-wall ratio, etc. The parameters related to envelope thermal characteristics include the U-value, thermal absorptance, solar absorptance, solar heat gain coefficient, visible light transmittance of wall, roof and window, etc. The parameters related to construction quality include air-tightness of façade, linear coefficient of thermal bridges, etc. The parameters related to energy efficient strategy, such as shading strategy parameters, include shading material type, overhang projection ratio, overhang depth, overhang installation angle, etc.

The variables related to energy systems mainly include HVAC system parameters, power generation system parameters, and energy storage system parameters. The cooling/heating setpoint temperature, supply air temperature setpoints, supply/return water temperature

setpoints, heat exchanger efficiency, ventilation supply airflow rate, capacity and number of wind turbines and chillers, capacity of battery, photovoltaic surface area and photovoltaic tilt angle on façades are widely used for design optimization of building energy systems [117-133].

The objectives concerned in building design optimization are mainly minimizing the building energy demand (e.g. energy demand of cooling, heating and lighting), minimizing the building life cycle cost and life cycle environmental impact; while maximizing the power generation of renewable energy, maximizing the indoor thermal comfort and visual comfort [117-133]. The optimization methods used include genetic algorithm (GA), ant colony optimization algorithm (ACO), particle swarm optimization algorithm (PSO), response surface method (RSM), firefly algorithm, Manta-Ray foraging optimization algorithm and hypervolume estimation algorithm (HypE).

For instance, Li et al. made the coordinated optimal design of building envelope and energy systems using GA for stand-alone and grid-connected zero/low energy buildings. The multi-stage design optimization was conducted considering the interactions between building envelope and energy system. The Hong Kong zero carbon building was utilized as the reference building, and the results showed that the proposed method could efficiently save 4% of the total cost comparing with the uncoordinated design and reduce the accumulated unmet cooling loads by over 22% [117]. Bui et al. used modified firefly algorithm to optimize the design of the adaptive façade system in buildings, in which the thermal and visible transmittance was adaptive to the dynamically varying climatic conditions. Two case studies including a typical

single office room and a medium office building were conducted for validating the performance of the adaptive façade system, and the results indicated that 14.2–29.0% building energy consumption could be reduced compared to the static façades [124].

However, the mutual impacts between building design and local microclimate are not concerned in the process of building design optimization [117-133]. Based on the literature review [106,107,109,111,116-138], it can be observed that there has been no current research finding the compromise design solution to making balance of building energy performance and outdoor thermal comfort. It means there is a lack of consideration of mutual impacts between building design and microclimate when making the design optimization. Among the large numbers of studies on building design optimization, the objective related to ensuring outdoor thermal comfort has not been addressed [117-133]. In the meanwhile, the impact of the local microclimate on building energy demand has been largely ignored [106,107,109,111,116,134-138]. It may lead to significant bias of energy performance estimation affecting the results of building design optimization [100].

2.4.2 Design optimization of local microclimate

With growing interest in the outdoor wind and thermal comfort in recent years, several studies have investigated the urban microclimate and addressed the environmental performance optimization based on data-driven models. The representative studies are summarized in Table 2.5 [106,107,109,111,116,134-138]. It can be seen that the microclimate optimization is mostly proceeded at the district scale. The optimization variables mainly include urban morphological

design parameters (e.g. building coverage ratio, plan area density, buildings geometry configuration) and building morphological design parameters (e.g., building width, depth, height, orientation). The design variables are generally optimized under typical meteorological weather condition to minimize building energy demand, life cycle cost or environmental impact (e.g., carbon emissions and pollutant emissions), while maximizing renewable power generation, indoor thermal comfort, and visual comfort. Detailed evaluation indexes related to wind and thermal comfort are used as the optimization objectives, such as the wind velocity ratio, the wind velocity Gini index, the Universal Thermal Climate Index (UTCI), and the Physiologically Equivalent Temperature (PET). Optimization methods such as genetic algorithm (GA), ant colony optimization algorithm (ACO), particle swarm optimization algorithm (PSO), response surface method (RSM), firefly algorithm, Manta Ray foraging optimization algorithm and hypervolume estimation algorithm (HypE) are widely adopted.

For instance, Wu et al. adopted Non-dominated Sorting Genetic Algorithms (NSGA-II) to address the urban morphological design problems in order to maximize economic benefits while ensuring the outdoor wind comfort for a residential district. In this way, a near-optimal site plan with a wind velocity ratio of 0.36, a wind velocity Gini index of 0.31, and a gross profit of 4.05×10^8 RMB was obtained [106]. Huang et al. combined GAN-based surrogate model with NSGA-II algorithm to achieve real-time optimization of urban morphology in order to increase urban block ventilation and reduce thermal discomfort, which offers a time advantage over simulations when the number of optimized samples exceeds 174 [109].

Weerasuriya et al. utilized NSGA-II to make design optimization for lift-up buildings in order to improve both the wind and thermal comfort in pedestrian level. Through optimizing the lift-up building parameters, including the height and width of the main structure, the height, width, and depth of the central core, and the orientation, the surrounding area of the lift-up building with pedestrian thermal comfort was enlarged by 18% in hot climates with calm wind conditions and by 10% in cold climates with windy conditions, while the surrounding area with pedestrian wind comfort was enlarged by 46% in hot climates with calm wind conditions and by 37% in cold climates with windy conditions [111].

However, currently, these studies mainly focus on the urban/district design optimization [106,107,109,111,116,134-138]. Only a few papers address individual building design [32]. The optimization of individual buildings is significant in high-density urban areas, because the development or renewal of individual buildings in existing districts is common practice compared to the full development of entire districts due to limited available space. A trade-off between building performance and local microclimate in design optimization is beneficial when considering their interaction (i.e., the impact of building design on local microclimate and the impact of local microclimate on building performance). Some key building design variables, such as the variables related to envelope thermal characteristics, are ignored [107,111,137], which leads to the incomplete optimization. The wind environment is generally considered, while the impacts on local air temperature, which is also a primary factor affecting

building performance and outdoor thermal comfort, are often ignored [106,107,109,111,116,135-138].

Table 2.5 Representative studies on design optimization of local microclimate based on data-driven methods

Reference	Variables	Objectives	Optimization methods	Optimization scale	Goals
[106]	Building width; building depth; floors number of high-rise building, mid-rise building and low-rise building	Wind velocity ratio; wind velocity Gini index; gross profit	NSGA-II	District	Maximize economic benefits; maximize outdoor wind comfort
[107]	Building width; building depth; building height; building orientation	Positions meeting wind comfort level	NSGA-II	Target building	Maximize summer and winter outdoor wind comfort
[109]	Building coverage ratio; floor area ratio; average building height; standard deviation of building height; building shape factor; frontal area ratio	Pedestrian level wind; radiation; UTCI	NSGA-II	District	Maximize urban block ventilation; minimize heat and discomfort
[111]	Height and width of main structure; height, width, depth of central core; orientation of building	Percentage area of wind comfort; percentage area of thermal comfort	NSGA-II	Lift-up building	Maximize pedestrian wind comfort and thermal comfort

[116]	Aspect ratio; ratio of long side to short side; horizontal rotation angle of building; corner cutting dimensions at corners of building	Building height; along-wind force coefficient; wind velocity	GA; SA; sequential quadratic programming method	District	Minimize wind forces; minimize local strong winds around buildings; maximize heights of buildings in development area
[134]	Angle of central street segment, bridge location, building volumes.	Minimize squared difference from target temperature, maximize comfortable area and minimize dangerous areas, maximize visitor potential, minimize average travel time	GA	City	Maximize outdoor wind comfort and thermal comfort
[135]	Buildings heights configuration; plan area densities	Aerodynamic index of urban area	GA; PSO	District	Improve pedestrian-level wind conditions; minimize low-wind-speed regions; maximize outdoor urban ventilation; maximize outdoor wind comfort

[136]	Building densities; building plot ratios; building height; number of buildings in the plot; number of buildings in the columns; building spacing	Sunshine hours; wind speed; solar radiation heat gain	GA	District	Maximize outdoor wind comfort and thermal comfort
[137]	Face-to-face gaps between buildings; height of upper building; height of lift-up core, width of lift-up core	Area weighted mean wind velocity ratio; area weighted PET	NSGA-II	Lift-up building	Maximize pedestrian level wind comfort and thermal comfort
[138]	Buildings' layout in the block	Daylight factor; sky view ratio; window sunlight hours; site sunlight hours; UTCI	NSGA-II	District	Maximize indoor visual comfort and outdoor thermal comfort

2.4.3 Multi-objective design optimizations

The mutual impacts between buildings and the local microclimate have not been addressed in design optimization due to the complexity of attaining design objectives related not only to building performance but also to microclimate improvement. When different design objectives need to be attained, decision-makers can only agree on compromise design solutions to achieve a balance and maximize the benefits of multiple conflicting objectives [107]. With the increasing application of multi-objective optimization methods, different objectives can be optimized simultaneously and the global optimum solutions can be found. Evolutionary

algorithms are popular methods used for solving the problem of multi-objective optimization as they can address computational complexity, spread, and convergence of Pareto solutions [139]. The non-dominated sorting approach NSGA-II is the most widely used method in tackling microclimate optimization due to its good performance and fast convergence speed, as shown in Table 2.5.

For instance, Wu et al. reached compromise design solutions of building morphology considering different wind comfort requirements in winter and summer using the evolutionary search algorithm. The building morphology variables, including building width, depth, height, and orientation, were optimized for the positions meeting the wind comfort level based on NSGA-II [107].

Du et al. investigated the design optimization for lift-up buildings utilizing NSGA-II in order to maximize both the wind and thermal comfort. The Pareto optimal solutions were identified for both weighted wind velocity parameter and outdoor thermal comfort parameter PET, in which the face-to-face gaps between buildings, the height of the upper building, the height of the lift-up core, and the width of the lift-up core were optimized [137].

Wang et al. used NSGA-II to optimize the layout of high-rise residential buildings in the district in order to find integrated solutions ensuring both indoor visual comfort and outdoor thermal comfort. The results showed that almost 21% of the building layout options had better performance than the baseline case due to the identified top 30 options out of 150 options, in

which the objectives related to daylighting were maximized while the objectives related to thermal discomfort were minimized [138].

2.5 Summary of research gaps

This chapter provides a comprehensive review of the mutual impacts between zero/low energy buildings and the local microclimate, as well as their optimal design. Based on the above review, the research gaps can be summarized as follows:

- The key design parameters for high-rise buildings have not been sufficiently investigated. Current studies on key design parameters mainly focused on low-rise buildings, but the significant difference between low-rise and high-rise buildings cannot be ignored. There is a lack of comparison between the key design parameters of high-rise and low-rise buildings. Existing studies investigating the key design parameters in different climate zones are insufficient for making a comprehensive comparison due to the limited parameters considered.
- The mutual impacts between zero/low energy buildings and the local microclimate are seldom studied in existing studies. The existing studies mainly investigate the impacts of district design rather than individual building design on the local microclimate, which is insufficient to support the zero/low energy building design. The simplified geometry model of the neighborhood/district is usually used in previous research, which may introduce bias when estimating the impacts between buildings and the local microclimate.

- There is still a lack of fast and accurate prediction models for the local microclimate that assist in the systematic and comprehensive analysis of zero/low energy building design. Existing machine learning models have been developed to predict the local microclimate under variations of district morphologies rather than building morphologies. They are not applicable for assisting zero/low energy building design. The input variables are not comprehensive enough, and some key design parameters are ignored, which may lead to underestimating the building's impact on the local microclimate.
- The mutual impacts between buildings and the local microclimate have not been addressed in design optimization due to the complexity of identifying compromise design solutions that balance building energy performance and outdoor thermal comfort. Most of the current studies focus on district design optimization rather than building design optimization. Some key building design variables, such as variables related to envelope thermal characteristics, are ignored, resulting in incomplete optimization.

CHAPTER 3 OVERVIEW OF THE RESEARCH SCENARIO AND BUILDING PERFORMANCE SIMULATION

This chapter presents an overview of the research scenario and the automated building simulation model used in this study. A typical design scenario in a high-density urban area, in which a new zero/low energy building is to be developed in an existing district in Hong Kong, is determined as the research scenario for the test and validation of the proposed method. The automated building simulation with efficiency and generalizability is utilized to simulate the building energy performance for the analysis of mutual impacts and the test and validation of the proposed surrogate models of local microclimate and the proposed coordinated design method in this PhD study.

3.1 Description of the research scenario

A new zero/low energy building to be developed in Kowloon, Hong Kong is used as the case to investigate the mutual impacts between individual zero/low energy building design and local microclimate in high-density city in this study. This will also test and validate the proposed surrogate models of local microclimate and the proposed coordinated design method in a high-density city. Due to the limited available space in developed and high-density cities, the development or renewal of individual buildings within existing districts is a common practice compared to the full development of entire districts. Figure 3.1 shows an aerial view of the study area and the location of the new zero/low energy building.

The zero/low energy building will be located on a hillside near Tat Hong Avenue, Kowloon, which is a dense and central urban area in Hong Kong. The maximum land area available for the new building is 170m×125m. Hong Kong is characterized by high-density and high-rise development. The climate in Hong Kong is subtropical monsoon. In summer, the average air temperature is approximately 28°C and the average relative humidity is more than 80% [140], while in winter, an ambient temperature below 10°C is uncommon in urban areas [43]. The prevailing wind direction is from the east.

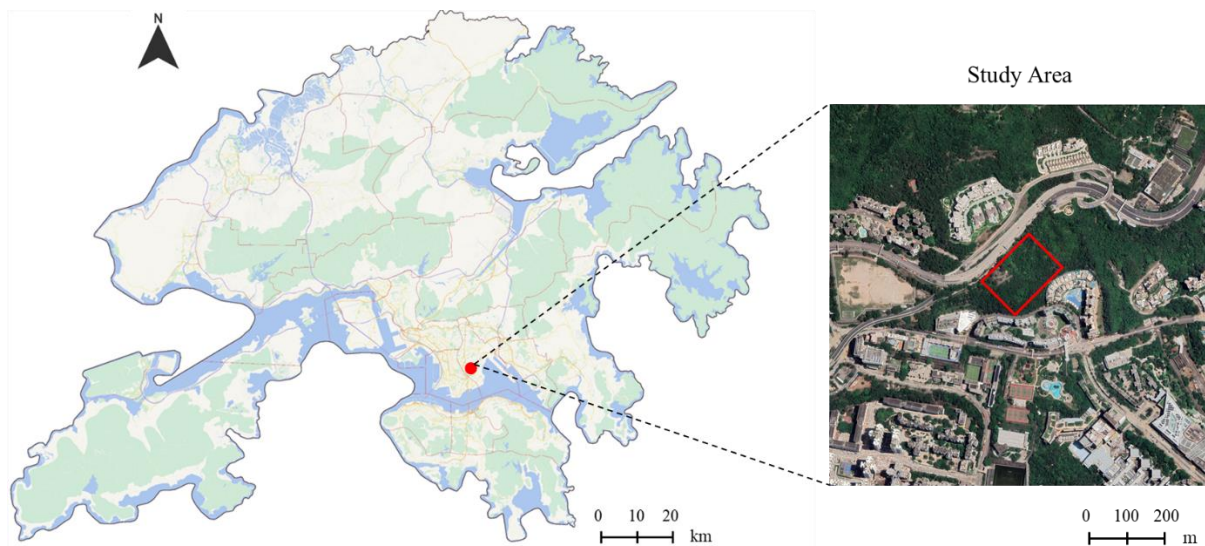


Figure 3.1 Aerial view of the study area and the location of the new building

3.2 Building performance simulation

The impacts of the local microclimate on the building energy performance considering the interaction between them are quantified by: the building energy consumption per area of the building in subtropical region on summer typical design day including 24 hours. The weather

data which considers the impacts of local microclimate is used for the building energy performance simulation.

The automated building performance simulation model is utilized to quantify building energy consumption. In climate zones without heating provision, the building energy consumption consists of the energy consumption for cooling, lighting, and other equipment in the building. In the climate zones with heating provision, the building energy consumption consists of the energy consumption for cooling, heating, lighting and other equipment in the building. In Chapter 4, in order to make a comprehensive analysis and comparison of the design parameters of zero/low energy buildings in different climate zones, a total of five typical cities in five different climate zones are investigated in the sensitivity analysis. In Chapter 5, Chapter 6, and Chapter 7, in order to test and validate the proposed methods, only the research scenario in Hong Kong with the subtropical monsoon is utilized as the case study.

The building is assumed to function as a public building that integrates teaching, offices, events, and accommodation for a campus. It is designed to serve as versatile spaces accommodating various activities and needs and to provide users with a multifunctional environment that facilitates communication, learning, work, and living activities. The building performance model is developed using the software EnergyPlus, which is combined with the optimization technique through Eppy toolkit in Python. The simulation process is efficient and takes only about four seconds for a single simulation. The model also has high generalizability and automation due to its easy operation when applied to a new design scenario. The building

performance simulation can proceed automatically by only modifying the settings of the simulation model in Python.

In order to take the mutual impacts between building design and local microclimate into consideration, the local microclimate data obtained from surrogate models are used as meteorological data in the automated building performance simulation to calculate building energy consumption. Figure 3.2 shows an example of the building geometry model used for building performance simulation.

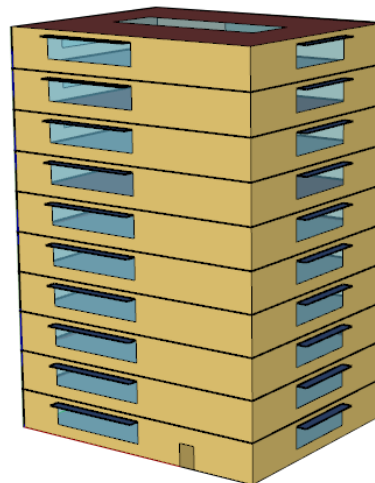


Figure 3.2 An example of the building geometry model for coordinated design optimization

A coordinated control of natural ventilation, air conditioning and heating, along with a daylighting control system, is adopted, as natural ventilation and daylighting are generally utilized to minimize building energy consumption in zero/low energy buildings. The logic of the coordinated control of natural ventilation, air conditioning, and heating is illustrated in Figure 3.3. When the indoor temperature is between the heating set point and cooling setpoint, natural ventilation is utilized to minimize the energy consumption of cooling and mechanical

ventilation while maintaining indoor thermal comfort. However, when the indoor temperature reaches the heating or cooling set point during the building and system operating time, natural ventilation is shut off, and mechanical ventilation is switched on. Outside the operating time, mechanical ventilation, air conditioning and heating systems are switched off. When mechanical ventilation is on, the heating or cooling system is switched on if heating or cooling is required. In the absence of heating provision, the Predicted Mean Vote (PMV) is used to calculate the discomfort index if the indoor air temperature is equal to or lower than the indoor heating set point for winter thermal discomfort assessment.

In winter, to prevent buildings in severe cold zones and cold zones from suffering from severe cold, a constant temperature set point for heating is set at 5°C outside the building's operating period, according to standards [141].

Humidity control is also considered to be part of the simulation model. The set point for relative humidity during summer operating time is set at 60% for dehumidification. Humidification is not considered in the simulation model because the energy consumption for humidification is not included in the calculation of building energy consumption, according to standards [142].

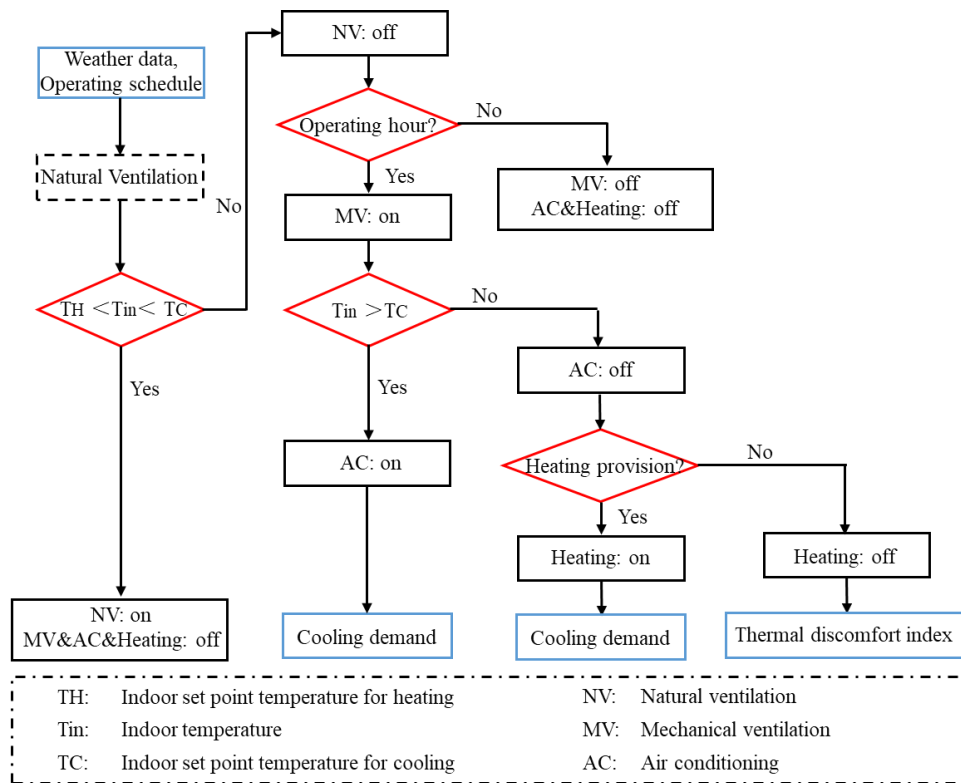


Figure 3.3 Logic of coordinated natural ventilation, heating and air-conditioning controls in simulation

The electric lighting is adjusted based on daylight illumination. Daylight illumination at the center of the room, at a height of 2.0 m, is selected as the reference point. The control logic of electric lighting is illustrated in Figure 3.4. The lower and upper limits for daylighting illuminance are set as 0 and 500 lux, respectively. When daylight illuminance increases between the lower limit and upper limit, the electric lighting power input decreases linearly from the full lighting load to 10% of the load. When daylight illuminance exceeds 500 lux, the electric lighting is switched off, and its power input becomes zero.

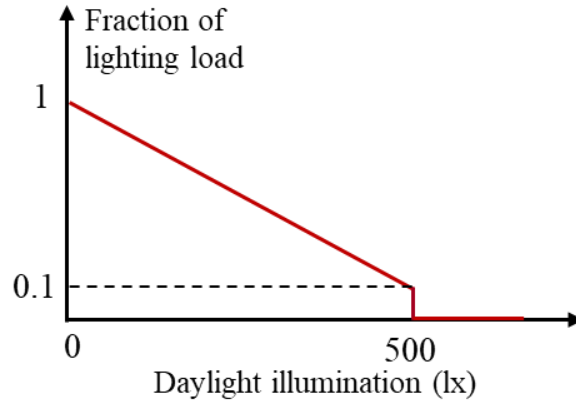


Figure 3.4 Daylight dimming control logic

The operating time of the building and the air-conditioning system is from 0:00 to 24:00 on all days. The water-cooled electric chillers are adopted for the cooling system. The overall coefficient of performance of air-conditioning system is determined as 4. The control logics of the air-conditioning and lighting systems in the model are set to maximize the use of natural ventilation and daylight. The schedules of the occupancy rate and the utilization rates of electric lights, equipment and HVAC system are set according to Table 4-6. As a large number of building performance simulations are required for a comprehensive analysis of the mutual impact between the new building and the local microclimate, JEPlus is adopted to automate the process of conducting numerous building performance simulations. JEPlus can automatically modify the parameter values (i.e., the six parameters listed in Table 3) in the building simulation model according to the generated scenarios and invoke EnergyPlus to perform the simulation.

Table 3.1 Daily schedule of occupancy rate

Operating Time	Occupancy rate
0:00~8:00	0.95
8:00~9:00	0.90

9:00~17:00	0.30
17:00~19:00	0.50
19:00~24:00	0.95

Table 3.2 Daily schedule of electric light utilization rate

Operating Time	Electric light utilization rate
0:00~1:00	0.3
1:00~2:00	0.2
2:00~6:00	0.1
6:00~7:00	0.7
7:00~8:00	0.4
8:00~10:00	0.6
10:00~17:00	0.36
17:00~19:00	0.5
19:00~24:00	0.8

Table 3.3 Daily schedule of electric equipment utilization rate

Operating Time	Electric equipment utilization rate
0:00~1:00	0.3
1:00~2:00	0.2
2:00~5:00	0.1
5:00~6:00	0.2
6:00~7:00	0.4
7:00~8:00	0.5
8:00~10:00	0.4
10:00~17:00	0.25
17:00~19:00	0.6
19:00~20:00	0.8
20:00~23:00	0.9
23:00~24:00	0.5

3.3 Summary

This chapter presents an overview of the research scenario and the automated building simulation model used in this study. A typical design scenario in a high-density urban area is determined as the research scenario for testing and validating the proposed method. The

scenario involves a new zero/low energy building to be developed in an existing district in Hong Kong. The automated building simulation is utilized to quantify the building energy performance, considering the interaction with the local microclimate, in order to reduce computation time and enhance generalizability. The automated building simulation serves as the basis for analyzing mutual impacts and for testing and validating the proposed local microclimate surrogate models and coordinated design method in this PhD study.

CHAPTER 4 IDENTIFICATION OF THE KEY DESIGN PARAMETERS OF ZERO/LOW ENERGY BUILDINGS UNDER DIFFERENT CLIMATES AND BUILDING MORPHOLOGIES

This chapter presents a systematic and comparative study of the key design parameters of building envelopes under different climate conditions and building morphologies. The most influential design parameters of high-rise and low-rise zero/low energy buildings in five climate zones, which cover three typical climates worldwide, are identified. The global sensitivity analysis method, Morris, is used, considering a total of thirty-five design parameters under five categories, to identify the key envelope design parameters that significantly affect the building energy performance. The key design parameters affecting winter thermal discomfort in climate zones typically without heating provision are also identified. The impacts of climate and building height are studied and compared. The impact of thermal bridge on building energy performance is further investigated.

4.1 Overview of building models and climate conditions concerned

4.1.1 Description of high-rise and low-rise building models

The typical geometry models of the high-rise and low-rise buildings are determined in this chapter in order to make comparison of the key design parameters at fair bases, as shown in Figure 4.1. The building geometry models are built in the software OpenStudio Sketchup [64]. The low-rise building is determined as a one-story building, and the high-rise building is

determined as a ten-story building, considering the height requirement [65] while ensuring that height difference between the buildings is significant enough to differentiate them for investigating the impacts of building morphology. The building shape is determined as a rectangle, and the standard floor of the high-rise and low-rise building is set to be the same for cross-comparison analysis between them. The floor area of a typical floor is determined as 500m^2 ($25\text{m}\times 20\text{m}$) and the typical floor height is determined as 3.6m . The aspect ratio is $1.25:1$ and the shape coefficient is 0.458 .

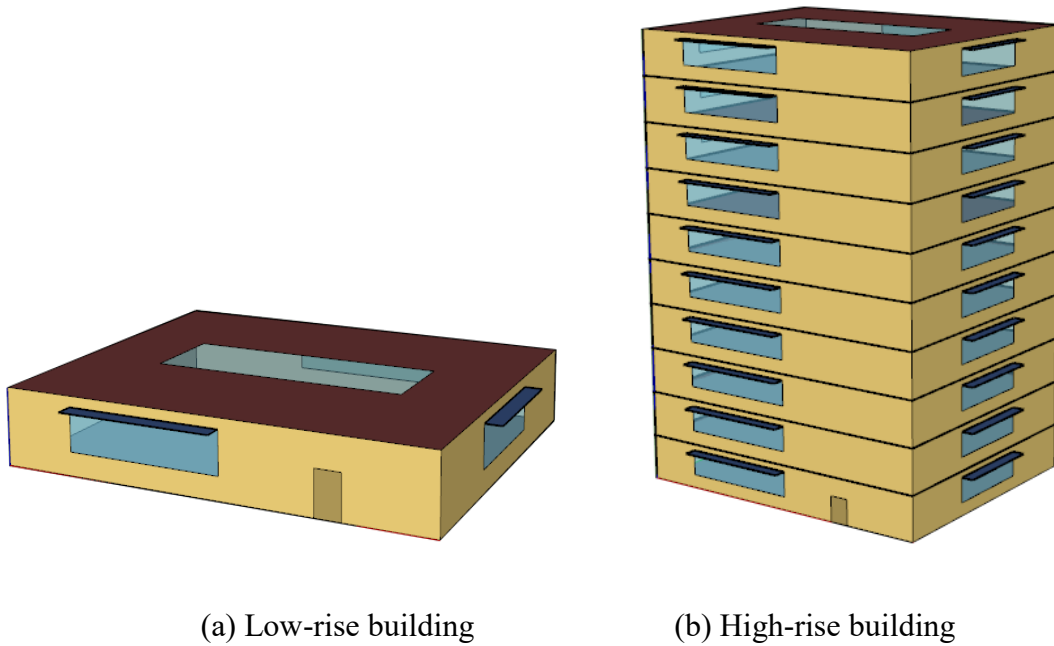


Figure 4.1 Geometry model of high-rise and low-rise building

Table 4.1 The internal load settings of the building

Item	Design Value
Occupancy	$4\text{ m}^2/\text{person}$
People load	$108\text{ W}/\text{person}$
Lighting load	$10\text{ W}/\text{m}^2$
Electric equipment load	$7.6\text{ W}/\text{m}^2$

Table 4.2 Settings of occupancy rate and the lights and equipment utilization rate

Operating Time	Rate
8:00~9:00, Weekdays	0.2
9:00~12:00, Weekdays	0.95
12:00~14:00, Weekdays	0.5
14:00~18:00, Weekdays	0.95
18:00~20:00, Weekdays	0.3
8:00~18:00, Saturdays	0.3

The function of the building is assumed to be an office building for both the high-rise and low-rise buildings. And the internal setting of the simulation model is shown as Table 4.1. The operating time of the building and system is 8:00~20:00 on weekdays and 8:00~18:00 on Saturdays. The occupancy rate and the lights and equipment utilization rate are set as Table 4.2.

4.1.2 Selection of cities in different climate zones

In this study, all 5 climate zones of different climate conditions in China are studied in order to make a comprehensive comparison of the main building design parameters in different climate conditions. These 5 climate zones include: severe cold zone, cold zone, hot summer & cold winter zone, mild zone and hot summer & warm winter zone, which cover three typical climates out of six usually considered in the world. One typical city is selected in each of the five climate zones, as shown in Figure 4.2, including: Harbin, Beijing, Shanghai, Hong Kong and Kunming. Their categorization of each typical city in the China's climate zones and the World's climates are shown in Table 4.3.

Table 4.3 The climate zones in China and the climate zones of the world of the typical cities

Typical cities	Climate zones in China	Climates in the world
Harbin	Severe cold zone	Temperate monsoon climate
Beijing	Cold zone	Temperate monsoon climate
Shanghai	Hot summer & cold winter zone	Subtropical monsoon and monsoon humid climate
Kunming	Mild zone	Subtropical monsoon and monsoon humid climate
Hong Kong	Hot summer & warm winter zone	Tropical monsoon climate



Figure 4.2 Typical cities of the 5 climate zones

The typical meteorological year (TMY) weather data [55] is used for simulation tests. The cities in severe cold zone (Harbin), cold zone (Beijing), and in hot summer and cold winter zone (Shanghai) are designed with both cooling and heating provisions due to the presence of hot summer and cold winter. However, cities in mild zone (Kunming) and in hot summer and warm winter zone (Hong Kong) are designed with only cooling provision, in accordance with the local requirements in standards and the normal design practice, despite the occurrence of certain cold days beyond the thermal comfort range in winter.

4.2 Initial selection of parameters affecting building performance

A comprehensive and collective consideration of the parameters deemed influential on building performance in previous studies is undertaken in this study. A total of 35 parameters affecting building performance are considered in the sensitivity analysis. They are divided into 5 categories including: building layout and shape, envelope thermal characteristics, construction quality, system design and energy efficiency measures. The preset ranges of these parameters are determined based on the design codes [61-63,65] and previous research [22-69], which are summarized in Table 4.4. The ranges are set the same for different climate zones in order to make a fair comparison of the key design parameters in different climate zones. Thus wide parameter ranges are adopted in this study as the requirements for zero/low energy building design are different in different climate zones, while the wide range settings will not lead to inaccuracy of the sensitivity analysis results for zero/low energy buildings. Furthermore, the parameters are set as continuous variables with a uniform distribution over their preset ranges.

Among these parameters, some are related to building nomenclature design or the building envelope design, such as layout and shape, envelope thermal characteristics, construction quality, and the overhang under energy efficient measures. The others are not related to building nomenclature design or building envelope design, such as system design parameters and heat recovery parameters under energy-efficient measures. However, they are also included in the sensitivity analysis in order to make a comprehensive comparison of the relative

significance of each parameter and further identify the key design parameters related to building envelope.

In this study, sensitivity analysis is based on a comprehensive consideration of the building envelope parameters, including the parameters related to wall, window, roof and ground, and systematic comparison of their impacts in different climate zones. Among these parameters, the parameters related to skylight and overhang are mostly ignored and not studied sufficiently in previous research. The parameters related to thermal bridge are usually considered as influential factors of building energy performance in climate zones with cold winter [41,67]. In fact, thermal bridge is identified as a key influential factor in some previous studies [41]. But, in those studies, only a few influential factors, rather than all the factors, are considered and compared. In this study, a comprehensive study considering all the influential parameters is conducted. At the same time, to avoid the underestimation on the impact of thermal bridge, the overall wall U-value integrating multiple transmittance types associated to thermal bridge is determined in the building performance simulation, as shown in Eq. (4.1) [60].

$$U_T = \frac{\sum(\varphi \cdot L) + \sum(\chi)}{A_{tot}} + U_0 \quad (4.1)$$

where, U_T is the total assembly wall U-value (W/(m²·K)), which represents the overall effect of thermal bridge. U_0 is the wall U value (W/(m²·K)). A_{tot} is the total opaque wall area (m²). φ is the linear thermal transmittance (W/(m·K)) representing the added heat flow associated with a linear thermal bridge that is not included in the U_0 . L is the length of a linear thermal

transmittance (m). χ is the point thermal transmittance (W/K) representing the added heat flow associated with a point thermal bridge that is not included in U_0 .

Table 4.4 Parameters affecting building performance concerned for sensitivity analysis

Category	Parameter (Unit)	Abbreviation	Value Range	Units
Layout and Shape	Building orientation	BO	0~360	°
	Window to wall ratio	WWR	0.1~0.9	-
	Skylight to roof ratio	SRR	0~0.9	-
Envelope Thermal Characteristics	Wall U-value	WU	0.09~ 11.1	W/(m ² ·K)
	Wall specific heat	WSH	800~2000	J/(kg·K)
	Wall thermal absorptance	WTA	0.1~0.9	-
	Wall solar absorptance	WSA	0.1~0.9	-
	Wall visible absorptance	WVA	0.1~0.9	-
	Roof U-value	RU	0.09~ 4.8	W/(m ² ·K)
	Roof specific heat	RSH	450~1400	J/(kg·K)
	Roof thermal absorptance	RTA	0.1~0.9	-
	Roof solar absorptance	RSA	0.1~0.9	-
	Roof visible absorptance	RVA	0.1~0.9	-
	Ground slab U-value	GU	0.15~2.27	W/(m ² ·K)
	Ground slab specific heat	GSH	800~2000	J/(kg·K)
	Ground thermal absorptance	GTH	0.1~0.9	-
	Window U-value	WIU	0.2~7.0	W/(m ² ·K)
	Window SHGC	WSHGC	0.1~0.9	W/(m ² ·K)
	Window visible light transmittance	WVLT	0.06, 0.1~0.9	-
	Skylight U-value	SU	0.2~7.0	W/(m ² ·K)
	Skylight SHGC	SSHGC	0.1~0.9	W/(m ² ·K)
	Skylight visible light transmittance	SVLT	0.06, 0.1~0.9	-
Construction Quality	Infiltration air mass flowrate coefficient	IAMF	1~1.5	1/h
	Floor slab linear thermal transmittance	FSLTT	0.007~1.842	W/(m·K)
	Glazing transition linear thermal transmittance	GTLTT	0.030~1.058	W/(m·K)
	Parapet linear thermal transmittance	PLTT	0.056~1.060	W/(m·K)
	Corner linear thermal transmittance	CLTT	0.036~0.684	W/(m·K)
	Interior wall intersection linear thermal transmittance	IWILTT	0.039~1.150	W/(m·K)
System Design	Outdoor airflow rate	OAR	0~0.02	m ³ /(person·s)
	Indoor setpoint temperature for cooling	STC	22~28	°C

	Indoor setpoint temperature for heating	STH	16~22	°C
Energy Efficient Measures	Overhang tilt angle	OTA	0~180	°
	Overhang depth as fraction of window/door height	ODF	0~3	-
	Sensible heat recovery effectiveness	SHRE	0~0.9	-
	Latent heat recovery effectiveness	LHRE	0~0.9	-

4.3 Methodology and procedure for identifying the key design parameters

Sensitivity analysis is conducted to identify the key design parameters for high-rise and low-rise buildings in different climate zones. First, an efficient method, Morris, is selected to identify the highly sensitive parameters in each climate zone. Then the key parameters, essential for the optimal design for high-rise and low-rise buildings in different climate zones, are selected. The parameters selected as the inputs in sensitivity analysis are the same for both high-rise and low-rise buildings in each climate zone, while the objectives, used to evaluate the building performance, are not the same for different climate zones. As for climate zones with both cooling and heating provisions, the objective is the total annual energy consumption of a building. For zones without heating provision where the thermal comfort cannot be guaranteed in winter, the objectives are the building total annual energy and the “winter thermal discomfort” instead. Furthermore, the performance objective is quantified by building performance simulation and the settings in each model are selected according to the real local design conditions for different climate zones.

4.3.1 Procedure and methods of sensitivity analysis

In this study, the sensitivity analysis is conducted to identify the highly sensitive parameters which affect the building energy performance in each of the climate zones. As for climate zones with heating provision, the sensitivity analysis is conducted to identify the key parameters affecting the building energy consumption, while, for climate zones without heating provision, the key parameters affecting the building energy consumption and winter thermal discomfort are identified respectively.

The procedure of sensitivity analysis is illustrated in Figure 4.3. First, SimLab is used to generate the samples of scenarios as the '*joblist*', which will be provided to JEPlus. Then JEPlus is adopted to conduct the parametric study according to the *joblist* based on the building performance simulation in EnergyPlus. In this way, the performance objectives in each of the input scenarios will be obtained and then be returned to SimLab. Finally, the sensitivity analysis will be implemented in SimLab. The sensitivity analysis is performed by quantifying the impact of each parameter on the performance objective, such that each parameter will be sampled within its preset range. The parametric study is conducted by performing a large number of simulations. JEPlus, the parametric study software, is used to set the model parameters for building simulation automatically. EnergyPlus will do the building performance simulation for each sample. Simlab is the software used to make sensitivity analysis.

Morris is selected as the sensitivity analysis method, which is a global sensitivity analysis method to rank all of the input parameters. It is an efficient sensitivity analysis method with

low calculation expense, applicable for analyzing a large number of parameters. In this study, Morris sampling method is selected when using the Morris sensitivity analysis method. 2 indicators are used to measure the sensitivity of each parameter, including μ and σ . The value of μ represents the absolute value of elementary effects of a parameter, which reflects the importance of this parameter. The value of σ represents the non-linear effects of a parameter, which reflects the interactions with other parameters. In this study, only the absolute elementary effects are concerned, and thus μ is used to measure the relative importance of each parameter.

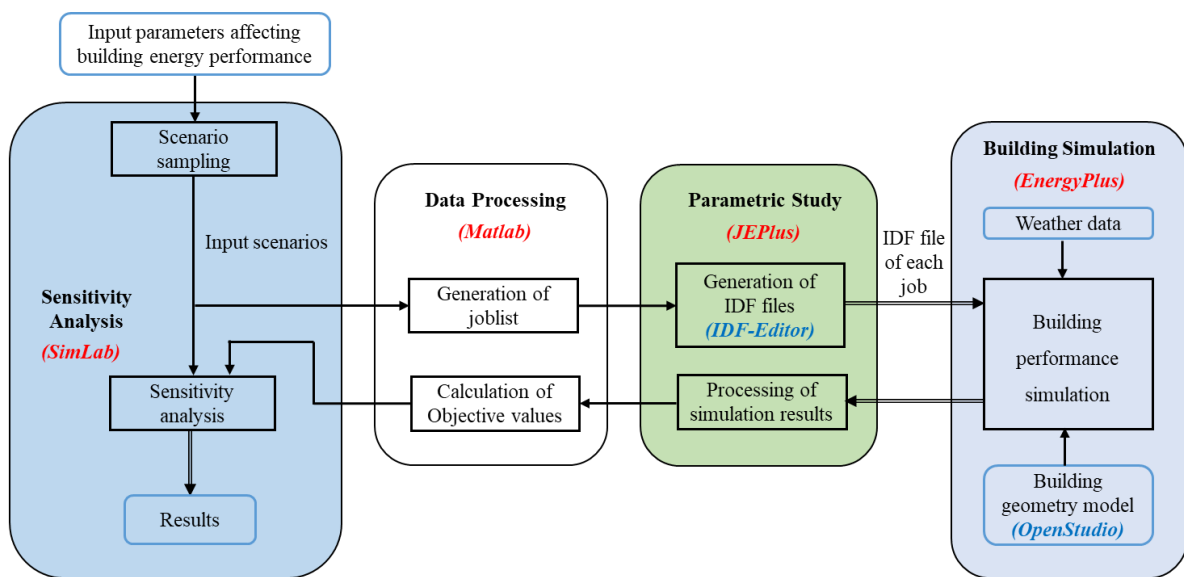


Figure 4.3 Procedures of sensitivity analysis

4.3.2 Performance objectives of sensitivity analysis

In this study, building performance is evaluated using not only the building energy demand but also the indoor thermal comfort. The performance objectives of buildings in different climate zones are not set the same (as shown in Table 4.5). Instead, they are determined according to

the local requirements in standards [62], actual demand of users and design conditions. Currently, nearly all of the office buildings in different climate zones are with cooling provision in hot summer so that the satisfactory indoor thermal comfort in summer is assumed in this study. The buildings in all climate zones adopt the cooling system using water-cooled electric chillers for fair comparison.

Table 4.5 Performance objectives concerned for sensitivity analysis in different climate zones

Climate zone	Performance objective
Severe cold zone	Building energy consumption
Cold zone	
Hot summer & cold winter zone	
Mild zone	Building energy consumption and winter thermal discomfort
Hot summer & warm winter zone	

In climate zones where the buildings are with heating provision, the satisfactory indoor thermal comfort can also be assumed in cold winter. The heating system is determined as district heating with gas-fired boiler for buildings in all climate zones with heating provision. The performance objective is to quantify building energy consumption only, including that for heating, cooling, lighting and other equipment, as shown in Eqs. (4.2) [61].

$$\begin{aligned}
 E_{tot} &= (E_{HE} + E_{CE} + E_{LE} + E_{EE}) \cdot f_{ele} \quad (4.2) \\
 &= (Q_{HL}/\eta_s/q_{gas}/q_{ccop} \cdot \varphi_{cfgtc} + Q_{CL}/SCOP_s + E_{LE} + E_{EE}) \cdot f_{ele}
 \end{aligned}$$

where, E_{tot} is the performance objective, i.e. the annual total building consumption (kWh), which is converted into primary energy. f_{ele} is the conversion factor [63]. E_{LE} is the annual lighting electricity consumption (kWh). E_{EE} is the annual electricity consumption (kWh) of other electric equipment. E_{HE} is the equivalent annual electricity consumption (kWh) for

heating. It is converted from Q_{HL} the annual heating demand of building (kWh) [61]. η_s is the efficiency of district heating system with gas-fired boiler. q_{gas} is the heating value of natural gas. q_{ccop} is the coal consumption of power generation. φ_{cftc} is the conversion factor converting gas to standard coal. E_{CE} is the annual consumption (kWh) of cooling, which is calculated from Q_{CL} the annual cooling demand of building (kWh). $SCOP_s$ is the overall coefficient of performance of air-conditioning system. The values of the factors involved in Eqs. (4.2) are set according to the requirements of zero/low energy building design specified in Ref. [63], as listed in Table 4.6.

Table 4.6 Settings of the factors and efficiencies in Eqs. (4.2)

ll	Value	Units
$f_{electricity}$	2.6	kWh/kWh
η_s	0.75	-
q_{gas}	9.87	kWh/m ³
q_{ccop}	0.36	kgce/kWh
φ_{cftc}	1.21	kgce/m ³
$SCOP_s$	4	-

However, in the climate zones without severe cold winter but there are a few cold days during which the indoor environment may be out of the thermal comfort range. Two building energy performance objectives are defined. The one is used to evaluate the building energy consumption. The other is used to evaluate the winter thermal discomfort. Building energy consumption includes that used for cooling, lighting and other equipment. A discomfort index, D_{dis} is defined to evaluate the winter thermal discomfort, which is calculated based on the hourly PMV according to Eqs. (4.4-4.5). A PMV value less than -0.5 represents discomfort due to too cold [62], which is then accumulated to form the discomfort index.

$$\begin{aligned}
E_{tot} &= E_{Cooling} + E_{Lighting} + E_{Equipment} \\
&= (E_{CE} + E_{LE} + E_{EE}) \cdot f_{electricity} \\
&= (Q_{CL}/SCOP_s + E_{LE} + E_{EE}) \cdot f_{electricity}
\end{aligned} \tag{4.3}$$

$$D_{dis} = \sum X_i \tag{4.4}$$

$$X_{,i} = \begin{cases} |PMV_i - (-0.5)| & PMV_i < -0.5 \\ 0 & PMV_i \geq -0.5 \end{cases} \tag{4.5}$$

where, D_{dis} is the thermal discomfort index, which is annual accumulation of hourly thermal discomfort in the operating period over the typical year. PMV_i is hourly average value of PMV.

4.4 Results of sensitivity analysis

4.4.1 High-rise buildings in different climate zones

Climate zones with heating provision in winter

The top 20 highly sensitive parameters for the building energy performance of the high-rise buildings in climate zones with both heating and cooling provisions are shown in Figure 4.4 (a-c). These parameters are ranked according to their μ value. It can be seen that the most sensitive parameters are the outdoor airflow rate, sensible heat recovery effectiveness, infiltration air mass flowrate coefficient, indoor setpoint temperature for heating and indoor setpoint temperature for cooling. All of them are the parameters not related to the building envelope. The top 3 parameters are the outdoor airflow rate, sensible heat recovery effectiveness and infiltration air mass flowrate coefficient. These are the parameters associated

to the fresh air heating/cooling loads. It is due to the significant difference between the indoor and outdoor temperature and humidity in these regions.

The other top 10 highly sensitive parameters are associated to overhang, window and wall for the high-rise buildings. In the “severe cold zone”, as shown in Figure 4.4 (a), the parameters associated to window and wall are the most important building envelope parameters. Where, the window U value and WWR are ranked 5th and 7th. The wall thermal absorptance and wall U value are ranked 8th and 10th. However, in the “cold zone” and “hot summer & cold winter zone” of higher outdoor air temperature, the parameters associated to overhang are the most important parameters for the high-rise buildings. Where, the overhang tilt angle and overhang depth as fraction are ranked 6th and 9th in “cold zone” and are ranked 6th and 7th in “hot summer & cold winter zone”.

Among the highly sensitive parameters associated to window, the window U-value is more sensitive for the zones with lower outdoor air temperature, Where, it is ranked 5th in “severe cold zone”, 8th in “cold zone” and 11th in “hot summer & cold winter zone”. With the increase of the outdoor air temperature, the window visible light transmittance becomes much more significant. It is ranked 10th in “hot summer & cold winter zone”, 11th in “cold zone”, 15th in “severe cold zone”. Among the parameters associated to the wall, the results show that the wall thermal absorptance is a key parameter influencing the building energy performance. It is ranked 8th in “severe cold zone”, 10th in “cold zone” and 12th in “hot summer & cold winter zone”. In fact, the wall thermal absorptance has been ignored and rarely been investigated

before. The wall U-value is another the highly sensitive one (ranked 10th in “severe cold zone”, 12th in “cold zone” and 13th in “hot summer & cold winter zone” in this study), which is consistent with the conclusion reported in previous studies [9,30]. The parameters associated to the overhang, i.e., the overhang tilt angle and overhang depth as fraction of height, are significant for the high-rise buildings (both of them are ranked the top ten in the regions with heating provision). However, they have seldom been studied before. In terms of the rankings, this study shows (see Figure 4.4 (a-c)) that the overhang tilt angle is always more significant than overhang depth as fraction of height in regions of concern.

Climate zones without heating provision in winter

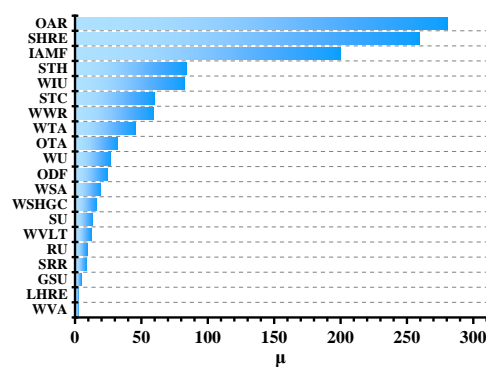
It can be seen from Fig.6 (d-e) that, in the climate zones without heating in winter, the building energy performance is mainly affected by the building envelope parameters. Although the most sensitive parameter is indoor setpoint temperature for cooling, nearly all of the other parameters of the top 10 are related to overhang, window and wall. In these areas without heating provision, overhang tilt angle is still more significant than the overhang depth as fraction of height. The overhang tilt angle and overhang depth as fraction are ranked 2nd and 3rd in “mild zone” and are ranked 4th and 5th in “hot summer & warm winter zone” respectively. As for the key parameters related to window, the window visible light transmittance, WWR and window SHGC are the most important ones. The rankings of them are 4th, 5th and 6th in “mild zone” and 6th, 9th and 8th in “hot summer & warm winter zone” respectively. Among the sensitive parameters related to wall, the wall solar absorptance is more significant than the wall thermal

absorptance. The wall solar absorptance is ranked 7th and 10th in “mild zone” and wall thermal absorptance is ranked 10th and 14th in “hot summer & warm winter zone”, respectively. The skylight is also a crucial element for the high-rise buildings. The SRR and skylight SHGC are the highly sensitive ones. They are ranked 8th and 9th in “mild zone” and 12th and 11th in “hot summer & warm winter zone”, respectively.

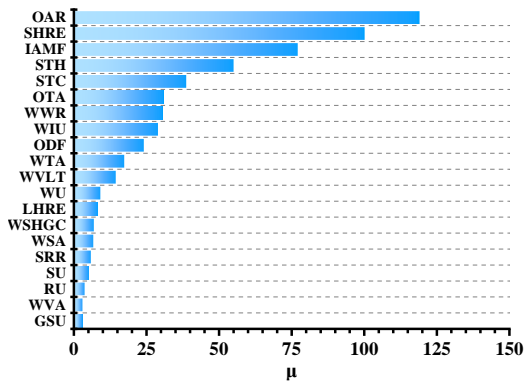
When compared with the “mild zone” where the summer is not severely hot and the winter is not very cold, the building performance in the “hot summer & warm winter zone” is affected much more by the outdoor fresh air, so that the outdoor airflow rate and infiltration air mass flowrate coefficient are more significant. The outdoor airflow rate and infiltration air mass flowrate coefficient are ranked 1st and 7th in “hot summer & warm winter zone, and 12th and 11th in “mild zone” respectively. The latent heat recovery effectiveness (ranked 3rd) is also a key parameter in “hot summer & warm winter zone”. But it is not significant in the “mild zone” (ranked 16th). Therefore, it is important to the zones where the outdoor air relative humidity is much higher such as “hot summer & cold winter zone” (ranked 9th) and “hot summer & warm winter zone”.

In the regions without heating provision in winter, the parameters significantly affecting winter thermal discomfort for the high-rise are shown in Figure 4.5 (a-b). It can be seen that the indoor thermal discomfort of the high-rise buildings is mainly affected by the outdoor fresh air and building envelope. The top 2 significant parameters are the outdoor airflow rate and infiltration air mass flowrate coefficient, which are in fact not envelope parameters. As for the building

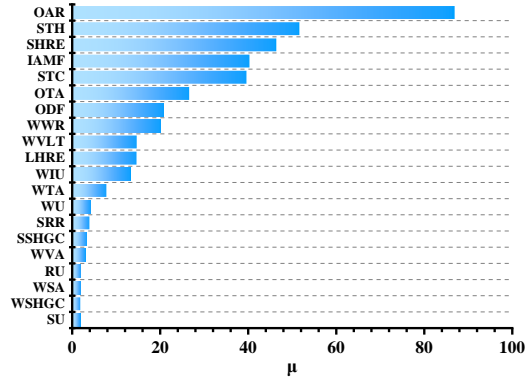
envelope, the wall, window and skylight are the most crucial elements. The wall thermal absorptance and solar absorptance, SHGC and area ratio of both window and skylight are the highly sensitive ones affecting both the winter thermal discomfort and building energy performance in this region. Note, nearly all of them are among the top 10, concerning both the winter thermal discomfort and building energy performance. However, the window U-value is the key parameter affecting the winter thermal discomfort (ranked 7th in “mild zone” and 6th in “hot summer & cold winter zone”) but not significant to energy performance (ranked 14th in “mild zone” and 16th in “hot summer & cold winter zone”) of high-rise buildings in zones without heating provision. Furthermore, the overhang tilt angle also has high impact on the winter thermal discomfort (ranked 11th in “mild zone” and 9th in “hot summer & cold winter zone”), although it is not as significant as its impact to the building energy performance (ranked 2nd in “mild zone” and 4th in “hot summer & cold winter zone”).



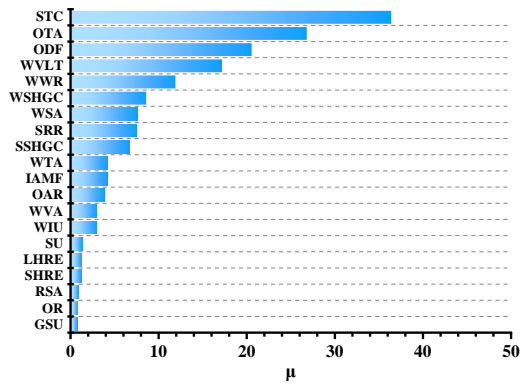
(a) Severe cold zone



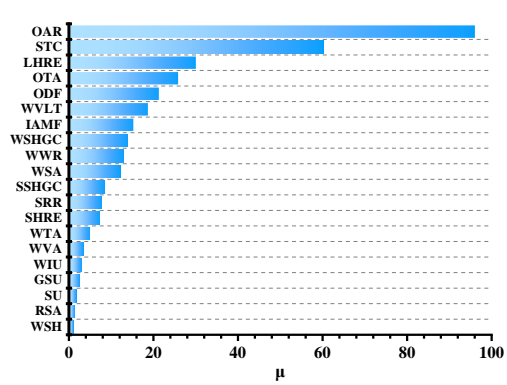
(b) Cold zone



(c) Hot summer and cold winter zone



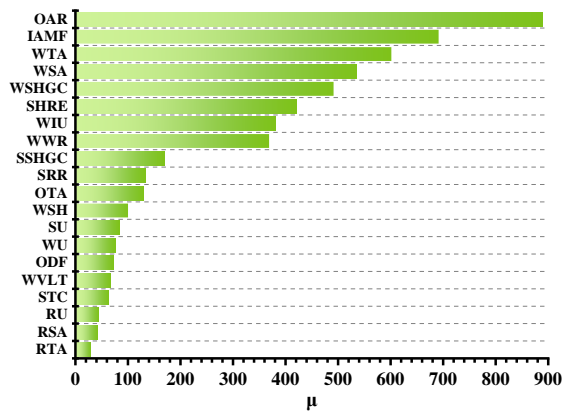
(d) Mild zone



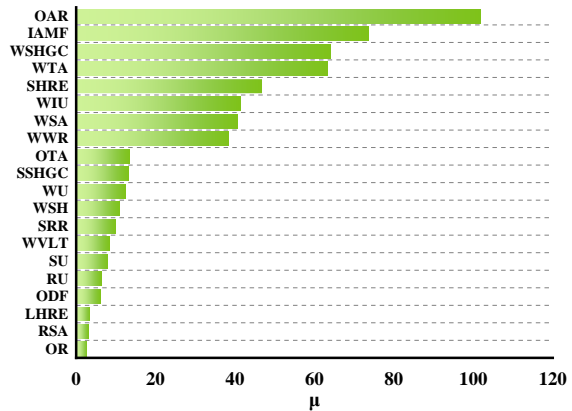
(e) Hot summer and warm winter zone

Figure 4.4 Highly sensitive (top 20) parameters of the high-rise buildings in 5 climate zones

— Building energy performance



(a) Mild zone



(b) Hot summer and warm winter zone

Figure 4.5 Highly sensitive (top 20) parameters of the high-rise buildings in climate zones

without heating provision — Winter thermal discomfort

4.4.2 Low-rise buildings in different climate zones

Climate zones with heating in winter

The top 20 highly sensitive parameters for the building energy performance of the low-rise buildings in climate zones with both heating and cooling provision are shown in Figure 4.6 (a-c). According to the μ value, the most sensitive parameters are not related to building envelope. But they are outdoor airflow rate, sensible heat recovery effectiveness, infiltration air mass flowrate coefficient and indoor setpoint temperature for cooling. It means that the low-rise buildings in these regions are also affected significantly by the fresh air loads because of the huge difference between the indoor and outdoor air temperature and humidity.

The other top 10 highly sensitive parameters of the low-rise buildings in “severe cold zone”, “cold zone” and “hot summer & cold winter zone” are associated to the skylight, roof and ground. Among the highly sensitive parameters related to skylight, SRR is the significant one in the zones with heating provision in winter (ranked 7th in “severe cold zone”, 5th in “cold zone” and 5th in “hot summer & cold winter zone”). Besides SRR, the skylight U-value becomes much more significant with the decrease of outdoor air temperature (ranked 4th in “severe cold zone”, 7th in “cold zone” and 11th in “hot summer & cold winter zone”). The skylight SHGC becomes much more significant with the increase of outdoor air temperature (ranked 3rd in “hot summer & cold winter zone”, 10th in “cold zone” and 16th in “severe cold zone”). Roof U-value and ground slab U-value are the key parameters (ranked 6th and 9th in “hot summer & cold winter zone”, 8th and 9th in “cold zone”, 9th and 8th in “severe cold zone”,

respectively). Therefore, the U-value of the top surface (e.g., roof and skylight) and the bottom surface (e.g., ground slab) of low-rise buildings are very important to the building energy performance. The latent heat recovery effectiveness (ranked 10th) is also a key parameter affecting the building energy performance in “hot summer & cold winter zone” where the outdoor air relative humidity is much higher.

Climate zones without heating provision in winter

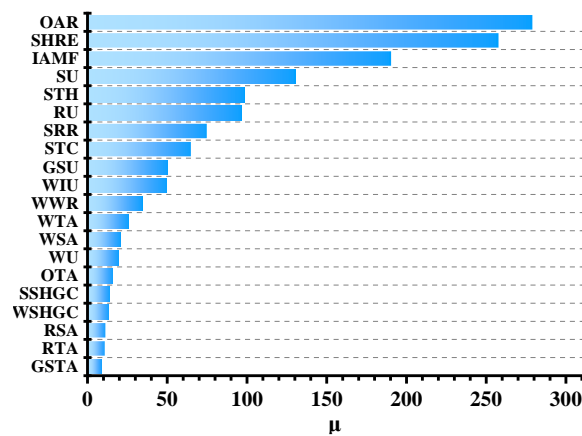
It can be seen from Figure 4.7 (d-e) that the key parameters affecting building energy performance of the low-rise in climate zones without heating provision in winter are significantly different with them in climate zones with heating provision. They are mainly related to the building envelope, although the setpoint temperature for cooling is the most significant parameter (ranked 1st in “mild zone” and 2nd in “hot summer & warm winter zone”). According to the rankings of these parameters, the most important elements affecting the building energy performance of the low-rise buildings are the skylight and ground. They are also the significant elements to the low-rise buildings in the regions with heating provision. The key parameters associated to skylight are skylight SHGC, SRR and skylight U-value. They are ranked 1st, 2nd and 5th in “mild zone”, 1st, 3rd and 8th in “hot summer & warm winter zone”, respectively. The key parameter related to ground slab is the ground slab U-value (ranked 4th in “mild zone” and 5th in “hot summer & warm winter zone”), the same as in climate zones with heating in winter. While the parameters related to solar protection and solar absorption are also important to the climate zones without heating in winter, such as overhang tilt angle

(ranked 5th in “mild zone” and “hot summer & warm winter zone”), wall solar absorptance (ranked 8th in “mild zone” and 10th in “hot summer & warm winter zone”) and roof solar absorptance (ranked 9th in “mild zone” and 11th in “hot summer & warm winter zone”).

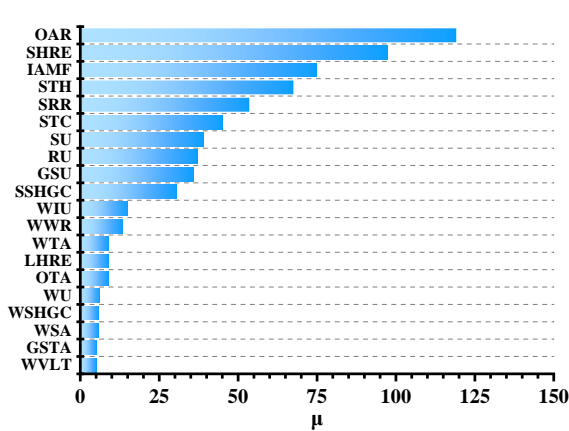
Comparing the key parameters in the “mild zones” and the “hot summer & cold winter zone”, the parameters related to outdoor fresh air, including outdoor airflow rate, latent heat recovery effectiveness and infiltration air mass flowrate coefficient, are more important to the building energy performance in the “hot summer & cold winter zone”. Where, they are ranked 2nd, 6th and 7th in “hot summer & warm winter zone” but they are out of the top 10 in “mild zone”. It is due to the significant difference of the indoor and outdoor temperature and humidity in the “hot summer & cold winter zone”. Besides the key parameters associated to building envelope mentioned above, WWR and ground slab specific heat are the highly sensitive parameters in the “mild zones” but not sensitive to the “hot summer & cold winter zone”. Where, they are ranked 7th and 10th in “mild zone” but they are out of the top 10 in “hot summer & warm winter zone”.

As shown in Figure 4.7 (a-b), the highly sensitive parameters affecting the indoor thermal discomfort of low-rise buildings in the zones without heating provision are all associated to the building envelope and outdoor fresh air. The most significant parameters are related to skylight, including skylight SHGC, skylight U-value and SRR (ranked 1st, 3rd and 5th in “mild zone” and 1st, 3rd and 8th in “hot summer & warm winter zone”, respectively), the same as the parameters affecting the building energy performance. The outdoor airflow rate, infiltration air mass

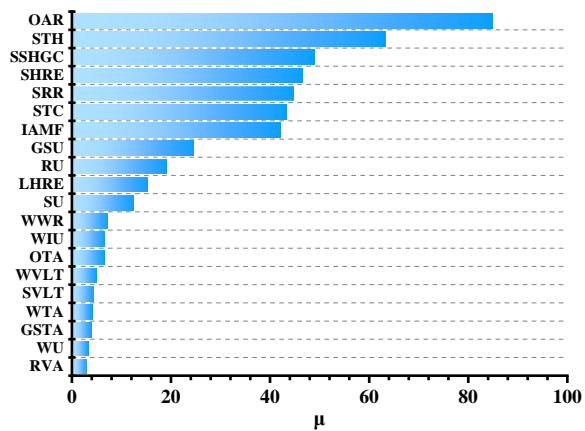
flowrate coefficient and sensible heat recovery, which are not envelope parameters but associated to outdoor fresh air, are also the top 10 sensitive parameters. According to the rankings, the wall and roof are also the crucial elements of the low-rise buildings besides the skylight. The key parameters associated to wall including wall thermal absorptance and wall solar absorptance (ranked 6th and 7th in “mild zone” and 7th and 11th in the “hot summer & warm winter zone”, respectively). The key parameters associated to roof include the roof U-value and roof solar absorptance (ranked 8th and 9th in “mild zone” and 5th and 10th in “hot summer & warm winter zone”, respectively).



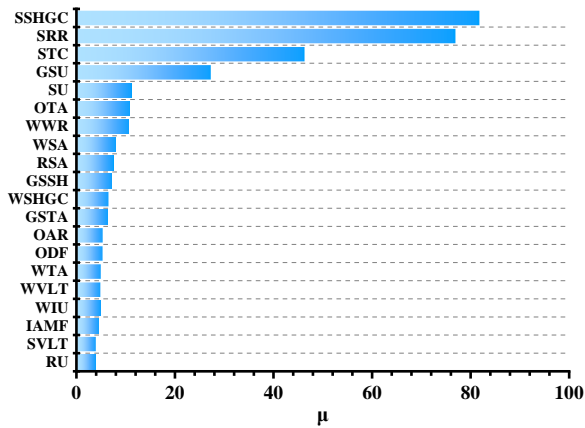
(a) Severe cold zone



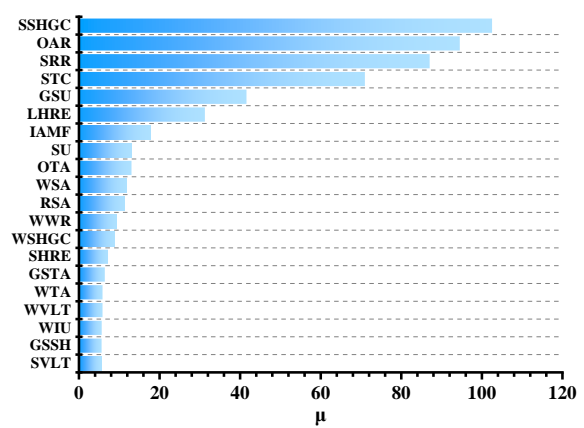
(b) Cold zone



(c) Hot summer & cold winter zone



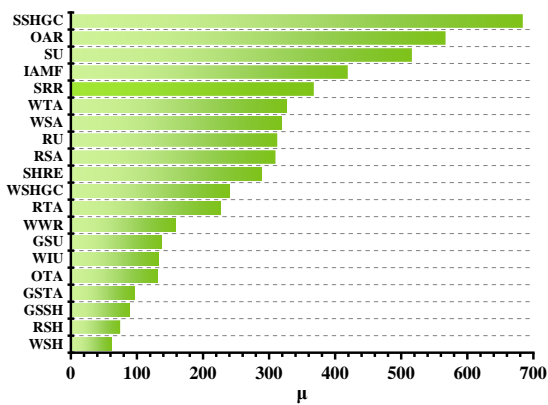
(d) Mild zone



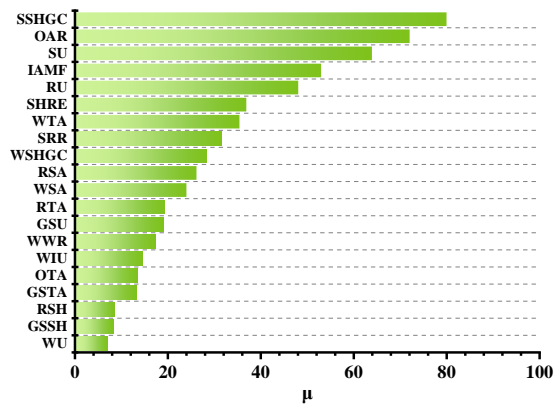
(e) Hot summer & warm winter zone

Figure 4.6 Highly sensitive (top 20) parameters of the low-rise buildings in 5 climate zones

— Building energy performance



(a) Mild zone



(b) Hot summer & warm winter zone

Figure 4.7 Highly sensitive (top 20) parameters of the low-rise buildings in climate zones

without heating provision — Winter thermal discomfort

4.4.3 Comparison of highly sensitive parameters for high-rise and low-rise buildings

In the climate zones with both heating and cooling provision, it can be seen from Figure 4.4 (a-e) and Figure 4.6 (a-e) that no matter the high-rise buildings or low-rise buildings, there are 5 top sensitive parameters not associated to the building envelope but affecting the building

energy performance. They are outdoor airflow rate, sensible heat recovery effectiveness, infiltration air mass flowrate coefficient, indoor setpoint temperature for heating and indoor setpoint temperature for cooling. However, in the climate zones without heating provision, only the indoor setpoint temperature for cooling is within the top five highly sensitive parameter not related to building envelope.

According to the rankings of the parameters, the building envelope design parameters affecting the building energy performance for the high-rise buildings and low-rise buildings are significantly different. As shown in Figure 4.4 (a-e) and Figure 4.6 (a-e), overhang parameters are the most important to the high-rise buildings in each climate zones, while skylight is the most important to the low-rise buildings. In this study, the key parameters associated to overhang including overhang tilt angle and overhang depth as fraction of height. The results show that the overhang tilt angle is always more significant than overhang depth as fraction of height in each climate zone. It can be seen from Figure 4.4 and Figure 4.6 that skylight SHGC, SRR and skylight U-value are the key design parameters associated to skylight of low-rise buildings. SRR is the highly sensitive parameters to each climate zone. Skylight U-value is more crucial to the climate zone with lower temperature, while as the air temperature increases, skylight SHGC becomes more significant.

Besides the overhang, window and wall are also the important envelope affecting building energy performance to high-rise buildings. Among the parameters associated to window, WWR is the significant one for each climate zone. Window U-value is more important to the

zones with heating in winter, while window visible light transmittance and window SHGC are more important to the areas without heating in winter. As for the parameters related to wall, wall thermal absorptance is the significant one for each climate zone, but it is ignored and rarely investigated before in previous research. Wall U-value is also significant to climate zones with heating in winter, while wall solar absorptance is important to the zones without heating in winter. Besides the skylight, roof and ground slab are also the important envelope to low-rise buildings. The ground slab U-value is important to each climate zone. The U-value of roof and window are important to the zones with heating in winter. The solar absorptance of roof and wall and overhang tilt angle are important to the regions without heating in winter.

In these areas where the thermal comfort cannot be guaranteed in winter, the consideration of both winter thermal discomfort and the building energy performance is needed. As for the parameters influencing the winter thermal discomfort of climate zones without heating provision (shown in Figure 4.5 and Figure 4.7), the top parameters are related to outdoor fresh air, including outdoor airflow rate and infiltration air mass flowrate coefficient. They are also the highly sensitive parameters affecting the building energy performance in “hot summer & warm winter zone” to both of the high-rise and the low-rise buildings. However, they are not the highly sensitive parameters affecting the building energy performance in “mild zone” where the difference of indoor and outdoor air temperature and humidity is small. Therefore, the building envelope design in such areas is actually important to the building energy performance there.

As for the building envelope of the high-rise buildings in zones without heating provision in winter, it can be seen from Figure 4.4 (d-e) and Figure 4.5 (a-b) that the wall, window, overhang and skylight are the crucial elements to both the winter thermal discomfort and the building energy performance. To compare with the high-rise buildings, the skylight becomes the most important element of the low-rise buildings affecting both winter thermal discomfort and building energy performance (as shown in Figure 4.6 (d-e) and Figure 4.7 (a-b)). Skylight SHGC, skylight U-value and SRR are the highly sensitive parameters.

4.5 Analysis on impact of thermal bridge on building energy performance

Based on the results of the sensitivity analysis in this research listed in Figure 4.4 (a-e) and Figure 4.6 (a-e), it can be seen that the 5 parameters associated to thermal bridge, including floor slab linear thermal transmittance (FTLTT), glazing transition linear thermal transmittance (GTLTT), parapet linear thermal transmittance (PLTT), corner linear thermal transmittance (CLTT) and interior wall intersection linear thermal transmittance (IWILTT), are not the crucial ones in the 5 climate zones to both the high-rise and the low-rise buildings. They are listed in the 15 (out of the 35) parameters of the least impact on building energy performance in 5 climate zones as shown in Table 8 (for the high-rise buildings) and Table 9 (for the low-rise buildings). However, in some previous research, thermal bridge has a significant impact on the building energy consumption especially in the regions where the temperature in winter is extremely low [41,66,68,143-151], while the other existing sensitivity analysis did not consider thermal bridge as a parameter of high impact [9,22,27,30,43,47,48] or considered but

concluded with its insignificance [28]. Three main reasons may lead to the different conclusions on the impact of the thermal bridge. The first reason is that, in this study, the preset ranges of the parameters associated to thermal bridge are within the normal range under the normal construction quality. In order to offer valuable references for the building envelope design for the zero/low energy buildings, the extremely poor construction quality or maintenance is not considered in this study. The second reason is that, among the large number of parameters related to the building energy performance, the rankings of the thermal bridge parameters are not the high ones. The third reason is that these 5 individual parameters related to thermal bridge are considered separately so that the impacts of individuals may not be obvious or significant.

Thermal bridges refer to the localized areas of high heat flow through walls, roofs and other insulated building envelope components. It is caused by highly conductive elements that penetrate the thermal insulation and misaligned planes of thermal insulation [66]. These paths allow heat flow to bypass the insulating layer and reduce the effectiveness of the insulation, leading to significant heat loss in localized areas.

In this section, a further assessment of the collective impact of the thermal bridge parameters is conducted in order to make a comprehensive consideration of the highly sensitive parameters affecting the building energy performance and avoid ignorance of critical ones in building optimal design. It can be seen from Table 4.7 and Table 4.8 that the 5 individual thermal bridge parameters are more influential in the “severe cold zone” compared with the other zones for

both the high-rise and the low-rise buildings. Therefore, the “severe cold zone” is selected for the further assessment of the collective impact of the thermal bridge parameters. The 5 parameters related to the linear thermal bridge are therefore assessed as a whole as a combined parameter. A combined linear thermal bridge transmittance φ_T is introduced in sensitivity analysis by replacing the 5 individual thermal bridge parameters. This combined parameter is defined as Eqs. (4.6) [66].

$$\varphi_T = \frac{\sum(\varphi \cdot L)}{\sum L} \quad (4.6)$$

The results of the sensitivity analysis using the combined linear thermal bridge transmittance are shown in Table 4.9. The 15 parameters of the least impact on building energy performance in 5 climate zones of the high-rise and low-rise buildings are listed. When comparing the sensitivity analysis results considering the impacts of thermal bridge using the 5 individual parameters, it can be seen that the ranking of the combined linear thermal bridge transmittance is close to the ranking of the 5 individual thermal bridge parameters in the “severe cold zone”. The ranking of the combined linear thermal bridge transmittance (CLTBT) for the high-rise building is 22 out of the 31 parameters and its ranking for the low-rise building is 25 out of the 31 parameters. The most sensitive individual thermal bridge parameter of the high-rise buildings is parapet linear thermal transmittance (PLTT), which is ranked 22 out of the 35 parameters. As for the low-rise buildings, the most sensitive individual parameter is the interior wall intersection linear thermal transmittance (IWILTT), which is ranked 25 out of the 35 parameters. Therefore, when the preset ranges of the parameters associated with the thermal

bridge are within the normal design range under the normal construction quality, the impacts of both the combined parameter and the individual parameters are not significant for both high-rise and low-rise buildings, though the thermal bridge parameters are more influential for high-rise buildings compared to low-rise buildings.

Table 4.7 The 15 (out of the 35 or 34) parameters of the least impact on building energy performance in 5 climate zones — High-rise buildings

Rank	Severe cold zone	Cold zone	Hot summer & cold winter zone	Mild zone	Hot summer & warm winter zone
35	CLTT	IWILTT	RSH	-	-
34	GSSH	SVLT	GSSH	CLTT	IWILTT
33	RVA	RTA	IWILTT	IWILTT	CLTT
32	RSH	FSLTT	GTLTT	GTLTT	GTLTT
31	SVLT	GSTA	RVA	RVA	PLTT
30	GSTA	RVA	SVLT	FSLTT	FSLTT
29	GTLTT	CLTT	CLTT	GSTA	RSH
28	RTA	RSA	PLTT	PLTT	SVLT
27	RSA	GSSH	RTA	GSSH	RVA
26	FSLTT	RSH	FSLTT	RSH	GSTA
25	IWILTT	GTLTT	RSA	SVLT	GSSH
24	OR	PLTT	GSTA	RTA	RU
23	WSH	WSH	WSH	WU	OR
22	PLTT	SSHGC	OR	RU	RTA
21	SSHGC	OR	GSU	WSH	WU

Table 4.8 The 15 (out of the 35 or 34) parameters of the least impact on building energy performance in 5 climate zones — Low-rise buildings

Rank	Severe cold zone	Cold zone	Hot summer & cold winter zone	Mild zone	Hot summer & warm winter zone
35	RSH	PLTT	OR	-	-
34	CLTT	GTLTT	IWILTT	PLTT	IWILTT
33	FSLTT	IWILTT	CLTT	FSLTT	PLTT
32	GTLTT	OR	RTA	IWILTT	FSLTT
31	RVA	RSH	PLTT	GTLTT	CLTT
30	PLTT	FSLTT	FSLTT	OR	GTLTT
29	SVLT	WSH	GTLTT	CLTT	OR
28	OR	CLTT	WSH	WSH	WU

27	WVA	WVA	RSH	RSH	RSH
26	WSH	RSA	RSA	WU	WSH
25	IWILTT	RTA	WSHGC	SHRE	WVA
24	LHRE	GSSH	WVA	LHRE	RVA
23	ODF	ODF	WSA	WVA	RU
22	GSSH	SVLT	ODF	RVA	RTA
21	WVLT	RVA	GSSH	RTA	ODF

Table 4.9 The 15 (out of the 35 and 31) parameters of the least impact on building energy performance in severe cold zone

High-rise buildings				Low-rise buildings			
Rank	5 individual parameters	Rank	Combined parameter	Rank	5 individual parameters	Rank	Combined parameter
35	CLTT	31	SVLT	35	RSH	31	RVA
34	GSSH	30	GSH	34	CLTT	30	WSH
33	RVA	29	RSH	33	FSLTT	29	WVA
32	RSH	28	WSH	32	GTLTT	28	RSH
31	SVLT	27	RTA	31	RVA	27	WVLT
30	GSTA	26	RVA	30	PLTT	26	SVLT
29	GTLTT	25	RSA	29	SVLT	25	CLTBT
28	RTA	24	BO	28	OR	24	BO
27	RSA	23	GTA	27	WVA	23	ODF
26	FSLTT	22	CLTBT	26	WSH	22	GSH
25	IWILTT	21	SSHGC	25	IWILTT	21	RSA
24	OR	20	WVA	24	LHRE	20	RTA
23	WSH	19	GU	23	ODF	19	LHRE
22	PLTT	18	RU	22	GSSH	18	WSHGC
21	SSHGC	17	LHRE	21	WVLT	17	GTA

4.6 Recommendations on key building design parameters to be optimized

In this study, a comprehensive analysis on the significance of the design parameters is also made by comparing the assessment results from both this study and previous studies. Among all the 35 parameters, the top 20 parameters in each climate zone listed in Fig.6-Fig.9 are identified as the highly sensitive parameters. Among them, the key design parameters, which need to be optimized at the design stage, are further discussed.

In fact, some highly sensitive parameters are not related to building envelope design. Instead, they are related to the building energy system design, such as the outdoor airflow rate, heat recovery effectiveness, and indoor setpoint temperature for heating or cooling. Therefore, they are not the parameters which need optimization in the building envelope design. In the meanwhile, the parameters related to construction quality, such as infiltration air mass flowrate coefficient, are not the parameters which need to be optimized because the construction quality is the higher the better for good building energy performance.

Therefore, the top ten highly sensitive building envelope design parameters are further discussed concerning building envelope design optimization in each climate zone, as shown in Table 4.10 (a-c). The numbers in bracket represent the ranking of each parameter among the total of 35 parameters in the sensitivity analysis. As for the climate zones with both heating and cooling provision, the building energy performance is the only objective. Therefore, among the top ten highly sensitive parameters in the list, professionals can weigh the relative importance of the parameters referring to their rankings among the 35 parameters to select the parameters for optimization. The more parameters are selected, the more comprehensive the optimal design will be, but the more demand for optimization it requires, and the more difficult it becomes for the convergence of optimization. Therefore, the professionals need to make proper compromise. For the climate zones without heating provision, both of the building energy performance and the winter thermal discomfort are the performance objectives. Therefore, the professionals can prioritize the parameters and select the optimization

parameters from both lists of the ten highly sensitive parameters affecting building energy performance and the winter thermal discomfort.

Table 4.10 (a) Parameters need to be optimization for climate zones with heating provision

Rank	Severe cold zone		Cold zone		Hot summer & cold winter zone	
	Low-rise	High-rise	Low-rise	High-rise	Low-rise	High-rise
1	Skylight U Value (4)	Window U Value (5)	SRR (5)	Overhang Tilt Angle (6)	Skylight SHGC (3)	Overhang Tilt Angle (6)
2	Roof U Value (6)	WWR (7)	Skylight U Value (7)	WWR (7)	SRR (5)	Overhang Depth as Fraction (7)
3	SRR (7)	Wall Thermal Absorptance (8)	Roof U Value (8)	Window U Value (8)	Ground Slab U Value (8)	WWR (8)
4	Ground Slab U Value (9)	Overhang Tilt Angle (9)	Ground Slab U Value (9)	Overhang Depth as Fraction (9)	Roof U Value (9)	Window Visible Light Transmittance (10)
5	Window U Value (10)	Wall U Value (10)	Skylight SHGC (10)	Wall Thermal Absorptance (10)	Skylight U Value (11)	Window U Value (11)
6	WWR (11)	Overhang Depth as Fraction (11)	Window U Value (11)	Window Visible Light Transmittance (11)	WWR (12)	Wall Thermal Absorptance (12)
7	Wall Thermal Absorptance (12)	Wall Solar Absorptance (12)	WWR (12)	Wall U Value (12)	Window U Value (13)	Wall U Value (13)
8	Wall Solar Absorptance (13)	Window SHGC (13)	Wall Thermal Absorptance (13)	Window SHGC (14)	Overhang Tilt Angle (14)	SRR (14)
9	Wall U Value (14)	Skylight U Value (14)	Overhang Tilt Angle (14)	Wall Solar Absorptance (15)	Window Visible Light Transmittance (15)	Skylight SHGC (15)
10	Overhang Tilt Angle (15)	Window Visible Light Transmittance (15)	Wall U Value (15)	SRR (16)	Skylight Visible Light Transmittance (16)	Wall Visible Absorptance (16)

Table 4.10 (b) Parameters need to be optimization for mild zone without heating provision

Rank	Low-rise		High-rise	
	Building energy consumption	Winter thermal discomfort	Building energy consumption	Winter thermal discomfort
1	Skylight SHGC (1)	Skylight SHGC (1)	Overhang Tilt Angle (2)	Wall Thermal Absorptance (3)
2	SRR (2)	Skylight U Value (3)	Overhang Depth as Fraction (3)	Wall Solar Absorptance (4)
3	Ground Slab U Value (4)	SRR (5)	Window Visible Light Transmittance (4)	Window SHGC (5)
4	Skylight U Value (5)	Wall Thermal Absorptance (6)	WWR (5)	Window U Value (7)
5	Overhang Tilt Angle (6)	Wall Solar Absorptance (7)	Window SHGC (6)	WWR (8)
6	WWR (7)	Roof U Value (8)	Wall Solar Absorptance (7)	Skylight SHGC (9)
7	Wall Solar Absorptance (8)	Roof Solar Absorptance (9)	SRR (8)	SRR (10)
8	Roof Solar Absorptance (9)	Window SHGC (11)	Skylight SHGC (9)	Overhang Tilt Angle (11)
9	Ground Slab Specific Heat (10)	Roof Thermal Absorptance (12)	Wall Thermal Absorptance (10)	Wall Specific Heat (12)
10	Window SHGC (11)	WWR (13)	Wall Visible Absorptance (13)	Skylight U Value (13)

Table 4.10 (c) Parameters need to be optimization for hot summer & warm winter zone without heating provision

Rank	Low-rise		High-rise	
	Building energy consumption	Winter thermal discomfort	Building energy consumption	Winter thermal discomfort
1	Skylight SHGC (1)	Skylight SHGC (1)	Overhang Tilt Angle (4)	Wall Thermal Absorptance (3)
2	SRR (3)	Skylight U Value (3)	Overhang Depth as Fraction (5)	Window SHGC (4)
3	Ground Slab U Value (5)	Roof U Value (5)	Window Visible Light Transmittance (6)	Window U Value (6)
4	Skylight U Value (8)	Wall Thermal Absorptance (7)	Window SHGC (8)	Wall Solar Absorptance (7)
5	Overhang Tilt Angle (9)	SRR (8)	WWR (9)	WWR (8)
6	Wall Solar Absorptance (10)	Window SHGC (9)	Wall Solar Absorptance (10)	Overhang Tilt Angle (9)
7	Roof Solar	Roof Solar	Skylight SHGC (11)	Skylight SHGC (10)

	Absorptance (11)	Absorptance (10)		
8	WWR (12)	Wall Solar Absorptance (11)	SRR (12)	Wall U Value (11)
9	Window SHGC (13)	Roof Thermal Absorptance (12)	Wall Thermal Absorptance (14)	Wall Specific Heat (12)
10	Ground Slab Thermal Absorptance (15)	Ground Slab U Value (13)	Wall Visible Absorptance (15)	SRR (13)

It can be seen that the key building envelope design parameters affecting building energy performance for high-rise buildings and low-rise buildings are significantly different, which indicates the need of different design focuses for their designs. Overhang is the most important element for high-rise buildings in all climate zones, while skylight is the most important envelope element for low-rise buildings. The key parameters related to overhang include the overhang tilt angle and overhang depth as a fraction of height, and both are seldom addressed in previous research. Overhang tilt angle is always more significant than overhang depth as fraction of height in all climate zones. Skylight SHGC, SRR and skylight U-value are the key design parameters associated with skylight of low-rise buildings.

Besides the overhang, window and wall are the most sensitive ones for high-rise buildings. As for the “severe cold zone”, window and wall are the more significant elements compared with the overhang concerning the building energy performance, while as for the “cold zone” and “hot summer & cold winter zone” with less cold weather, the overhang is the most significant element. In the “mild zone” and “hot summer & warm winter zone” without heating provision and the guarantee of the winter thermal comfort, the parameters associated to wall, window, overhang and skylight are the crucial elements to both the winter thermal discomfort and the building energy performance.

In addition to the skylight, roof and ground are also the crucial elements of low-rise buildings. The thermal characteristics of the top and the bottom surfaces are significant to the energy performance of low-rise buildings. In the climate zones with the heating provision in winter, the U-value of roof and ground slab are the highly sensitive parameters affecting the building energy performance. In the climate zones without the heating provision in winter, the ground slab U-value, the solar absorptance of roof and wall are the important parameters affecting both building energy performance and winter thermal discomfort.

When comparing the results with those of previous studies, the parameters related to thermal bridge, whether the 5 individual ones or their combination, are not crucial in all climate zones for both high-rise and low-rise buildings. These parameters do have certain impact on the building energy consumption as indicated by the sensitivity analysis results, but they are not the highly sensitive ones when their values are within the normal range (i.e., with the normal building construction quality). Wall thermal absorptance is a key parameter affecting the building energy performance in all climate zones which has been ignored before.

4.7 Summary

In this chapter, the most influential design parameters of high-rise and low-rise buildings in different climate zones are identified by sensitivity analysis. The impacts of climate and building height on the key building design focus are studied and compared. The sensitivity analysis is performed using Morris, and a total of thirty-five design parameters under five categories are considered. Five Chinese climate zones covering three typical climates in the

world are investigated. Based on results of the sensitivity analysis, the major conclusions can be briefly summarized as follows.

- The key design parameters affecting energy performance of a building are significantly different in different climate zones and for different building morphology (i.e., high-rise and low-rise in this study).
- The highly sensitive envelope design parameters of high-rise buildings are related to the envelope components, including overhang, window, and wall, in all climate zones.
- The highly sensitive envelope design parameters of low-rise buildings are related to the envelope components, including skylight, roof, and ground, in all climate zones.
- Wall thermal absorptance is a key parameter affecting the building energy performance in all climate zones which has been ignored before.

It should be noted that the key design parameters of high-rise and low-rise buildings in different climate zones are identified in this study for building optimal design concerning the common performance indicators only (i.e., energy performance and thermal comfort). However, a good building design should not only be limited to minimizing the building energy consumption while maintaining a comfortable indoor environment, but also contribute to the development of a comfortable outdoor environment by minimizing its impacts on the ambient environment. In the next chapter, we will further investigate the key building design parameters affecting the microclimate (particularly in high-density cities), and consider these parameters in building optimal design.

CHAPTER 5 INVESTIGATION ON THE MUTUAL IMPACTS OF ZERO/LOW ENERGY BUILDING DESIGN AND LOCAL MICROCLIMATE

This chapter presents a comprehensive and systematic analysis of the mutual impacts between new individual zero/low energy building design and the local microclimate considering the interaction, and the identification of the major influential parameters of zero/low energy buildings on both local microclimate and building energy performance in subtropical urban area. A large number of high-resolution microclimate and building simulations based on advanced GIS spatial analysis technique are performed under different building designs for the assessment of mutual impacts. A global sensitivity analysis is conducted to identify the major influential building parameters.

5.1 Main building parameters concerned

A total of 6 building parameters affecting building performance and local microclimate are considered in the mutual impact assessment and sensitivity analysis in this study as listed in Table 5.1. They can be classified into two main categories, i.e., building morphology and building thermal characteristics. The building morphology parameters include building height, building orientation, and building aspect ratio. The building thermal characteristics parameters include the overall heat transfer coefficient of building envelope, emissivity of wall, and heat rejection of air-conditioners. The variation ranges of the parameters are set as wide as possible

by referring to the requirements in related design codes [146,152] and the settings in previous research [13,70,89,99,152].

Building aspect ratio [15,76], building height [15,74,13,89], orientation [70,78], emissivity [14,71,72,74,84], building height [74,13,15,89] and heat transfer coefficient [71] are the key influential parameters of building design affecting local microclimate, which are widely investigated in previous studies as shown in Table 1. It is worth noticing that the heat rejection of air-conditioners, as a major source of anthropogenic heat particularly in cooling-dominated regions [73], is rarely investigated in previous studies on local microclimate but included in this study. Existing related research only focuses on the air flow and temperature near the condensing units of air-conditioners, to determine their optimum placement for enhanced system coefficient of performance [77,99]. Though the district design parameters (e.g., district density [15,71,74,76,89], district morphology [71,78,13,83,88], street height/width ratio [14,70,74,81,87] and sky view factor [81,89] are widely concerned in previous microclimate studies, they are not considered in this study because they are not the building design parameters affecting the building performance directly. In the research scenario with existing surroundings, the district design parameters which reflect the relationship of buildings can be determined by the three selected building morphology parameters.

Table 5.1 Building parameters concerned in this study

Category	Parameter	Range	Unit
Building morphology	Building height	6~200	m
	Building orientation	0~360	°
	Building aspect ratio	1:1, 1.2:1, 1.4:1, 1.5:1, 2:1, 3:1, 4:1, 5:1, 6:1, 7:1, 8:1, 9:1	-
Building thermal characteristics	Overall heat transfer coefficient of building envelope	1.1~14.0	W/(m ² ·K)
	Emissivity of wall	0~1	-
	Heat rejection of air-conditioners	75~150	W/m ²

5.2 Overall assessment procedure and methods

In this study, the mutual impacts between individual building design and local microclimate are investigated and a global sensitivity analysis is conducted by varying the building parameters simultaneously. The detailed procedure is illustrated in Figure 5.1. Firstly, 200 scenarios of building design are generated using Latin hypercube sampling method [81] according to the ranges of the main building parameters concerned. Secondly, the local microclimate under each scenario of building design is simulated using Fluent based on the district 3D geometry model generated based on GIS under the hottest hour on the summer typical design day. 3D steady Reynolds-Averaged Navier-Stokes (RANS) CFD simulations of incompressible flow are performed using RNG k- ϵ turbulent model. The typical meteorological year (TMY) weather data is used as the weather data input for the local microclimate simulation in this study. After generating the microclimate effect for each building design under the hottest hour, the microclimate effect is added to each hour of the summer typical design day (including 24 hours). Then the building energy performance for each scenario of building design is

simulated for the summer typical design day (including 24 hours) considering the microclimate effect. using EnergyPlus. The weather data generated considering the microclimate impacts is used as the weather data input. Fourthly, the values of performance indexes under different scenarios are calculated based on the simulation results of local microclimate and building energy performance. The performance indexes include: (i). the average difference between pedestrian-level (i.e., 3.0m away from the building and 1.5m height in this study) air temperatures of the district with and without the new building (local air temperature difference in short in the rest of this paper); (ii). the average difference between pedestrian-level wind velocities of the district with and without the new building (local wind velocity difference in short); (iii). the pedestrian thermal discomfort degree of the district considering local microclimate impacts (pedestrian thermal discomfort degree in short, D_{discom}); (iv). the building energy consumptions considering the interaction with local microclimate (the building energy consumption in short). Fifthly, mutual impact assessment is performed in Matlab based on the calculated performance indexes. The mutual impact assessment includes the analysis on the impacts of building design on local microclimate (e.g., air temperature, wind velocity, and pedestrian thermal discomfort), and the impacts of local microclimate on building energy performance. Based on the mutual impact assessment, the major influential building parameters on both the local microclimate and building energy performance are finally identified through a global sensitivity analysis.

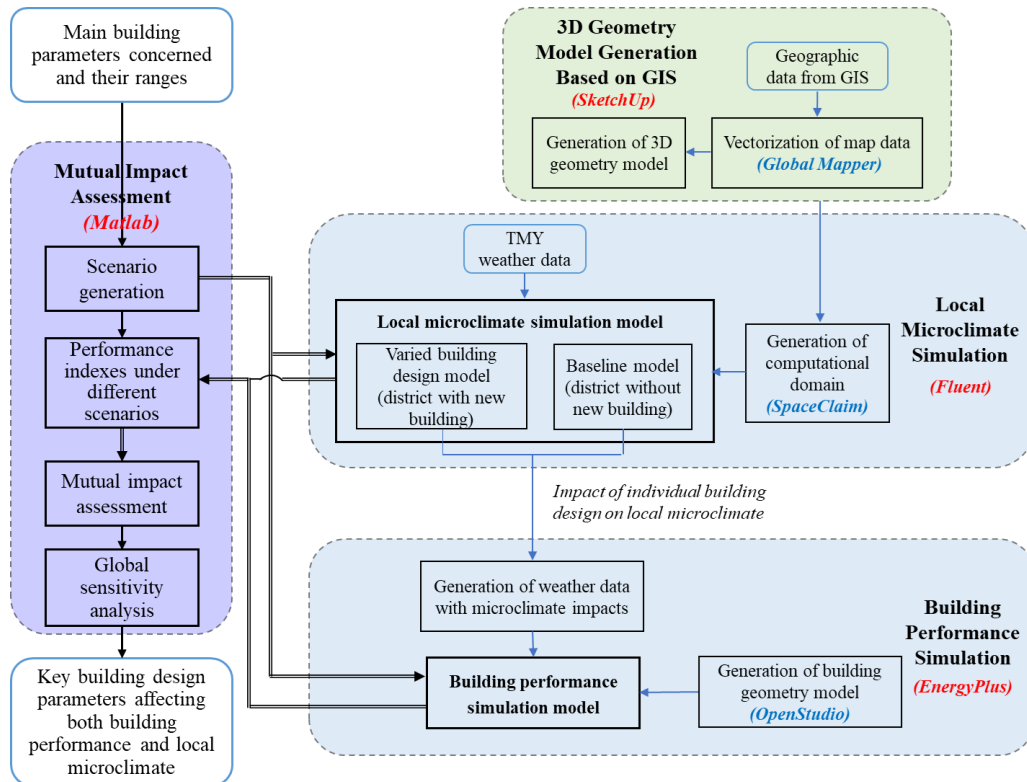


Figure 5.1 Outline of the overall research methodology and procedure

5.3 High-resolution 3D microclimate simulation and building simulation using advanced GIS-based spatial analysis techniques

5.3.1 Generation of 3D computational domain based on GIS

The investigation on the mutual impacts of individual building design and local microclimate needs very detailed and accurate geographic information. In this study, 3D structural geological model of high resolution is adopted based on advanced GIS spatial analysis technique for subsequent high-accuracy microclimate simulations. The CFD simulations of the 200 design scenarios are conducted under the most unfavorable weather condition (the hottest hour) of the summer typical design day with the prevailing wind condition in order to assist the evaluation

of the design performance and significantly reduce the computing cost. The development of high-resolution 3D microclimate simulation model involves: the generation of computational domain based on GIS, grid discretization, and the development of the microclimate simulation model, which are introduced in detail as below.

Generation of computational domain

The 3D computational domain is generated using advanced spatial analysis techniques based on GIS. GIS is a system which can store, visualize, analyze, and interpret geographic data. The geographic data includes the descriptive information of the geographic features, such as the altitude/elevation, the widths of roads, and the locations and dimensions of buildings, which are necessary for generating the computational domain for CFD (Computational Fluid Dynamics) simulation [115]. The utilization of GIS allows to account for the complexity of the urban structure and the specific surface characteristics on a fine spatial scale [153]. It can not only simplify the process of generating the computational domain while ensuring the accuracy of microclimate simulation, but also benefit the spatial analysis by reloading the simulation data back to GIS.

The generation of computational domain includes two main steps. Firstly, the geographic data of the target district is collected from Google Map. Secondly, the captured geographic data is vectorized and converted using Global Mapper to generate the 3D geometry model of the district, which contains the landforms, buildings and roads. Figure 5.2 shows the 3D geometry model of the target district in this study, which is a 1,000m×1,000m urban area in Kowloon,

Hong Kong. Based on the developed district 3D geometry model, the whole computational domain is generated using SpaceClaim. The dimension of the entire computational domain for microclimate simulation as shown in Figure 5.3 is determined to be 8,000m×4,500m×2,100m for fully developed flow according to the CFD simulation guidelines and previous research [154,155]. The maximum height of the buildings and terrain elevation is H=300m. The distance between the built area to the lateral boundaries, upper boundary and inlet boundary of the computational domain is determined as 5H. The distance between the built area to the outlet boundary of the computational domain is determined as 15H for flow re-development behind the wake region.

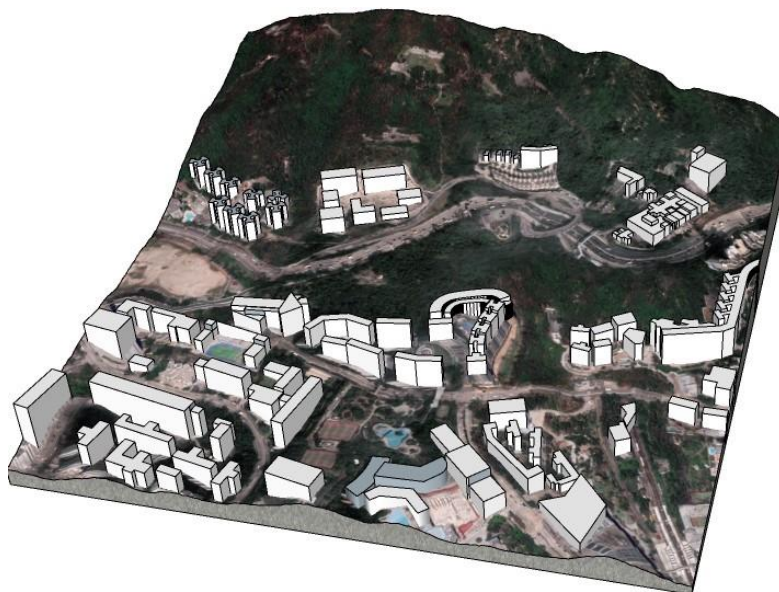


Figure 5.2 3D geometry model of the target district in SketchUp

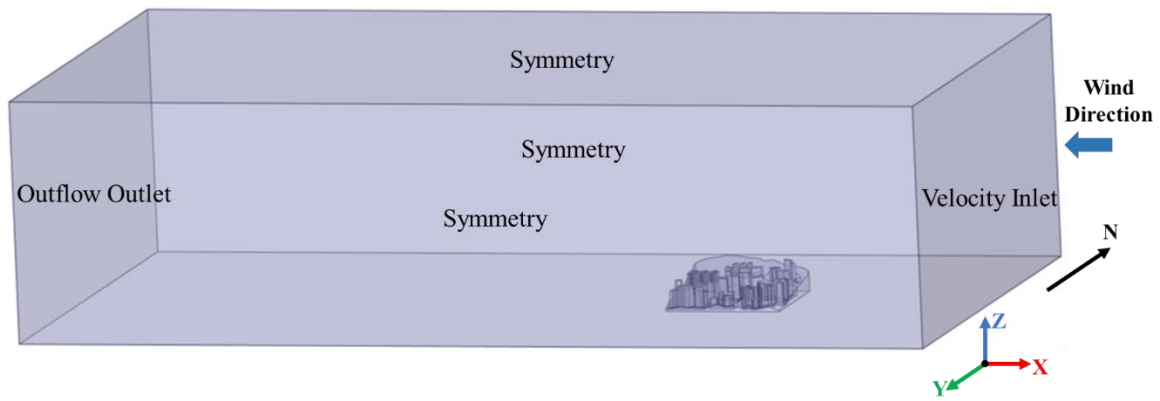


Figure 5.3 3D computational domain in SpaceClaim

Grid discretization

Grid discretization is performed using the software Meshing. The unstructured grid is used in this study in view of the complicated geometry of the target district. The grid independence verification is performed using three grid systems to find the proper grid resolution, including a coarse grid system, a basic grid system, and a fine grid system. The basic grid system is finally adopted and the grid number in the 200 cases of microclimate simulations ranges from 8.225 to 31.071 million. Local grid refinement is implemented near the wall of the buildings and the ground, while coarser mesh is for far field.

5.3.2 Development of high-resolution 3D microclimate and building simulation model

In this study, two types of 3D microclimate simulation models are developed using Fluent based on the generated computational domain and mesh in order to investigate the impacts of new building development on the local microclimate. One is the 3D simulation model of the target district without the new building, which is regarded as the baseline model for comparison. The other one is the microclimate simulation models of the target district with different designs

of individual building. The impacts of the individual building design on the local microclimate are quantified by: (i). the local air temperatures difference; (ii). the local wind velocity difference; (iii). the pedestrian thermal discomfort degree (D_{discom}). D_{discom} is defined to assess the degree of outdoor thermal discomfort at the pedestrian level. A higher absolute value means a higher degree of thermal discomfort. It is calculated based on the widely-used outdoor thermal comfort index PET [156], as shown in Eq. (5.1-5.2). Where, PET_n is the neutral physiological equivalent temperature, which is set to 28°C in this study [141]. PET_{ave} is the average PET of male (PET_{male}) and female (PET_{female}).

$$D_{discom} = PET_{ave} - PET_n \quad (5.1)$$

$$PET_{ave} = (PET_{male} + PET_{female})/2 \quad (5.2)$$

3D steady Reynolds-Averaged Navier-Stokes (RANS) CFD simulations of incompressible flow are performed using RNG k- ϵ turbulent model due to its high accuracy [154]. For the near-wall treatment, scalable wall functions with no-slip boundary condition are adopted considering the compromise between simulation accuracy and computing cost. Radiation with discrete ordinates (DO) model is adopted in the calculation. The SIMPLE scheme was used for the pressure and velocity coupling. The second-order schemes are used for discretization to improve numerical accuracy. As the prevailing wind in Hong Kong is from the east, the right surface of the computational domain is determined as the velocity inlet as shown in Figure 5.3. The vertical velocity profile U_z , the turbulent kinetic energy k_z , and the turbulence dissipation ϵ_z are calculated according to the AIJ's benchmark tests, as shown in Eqs. (5.3-5.7)

[104,142,155]. The downstream boundary is defined as outflow. The lateral and upper surfaces of the computational domain are set as the symmetry boundary conditions. The surfaces of buildings and the ground are set as the no-slip wall boundary conditions. The boundary conditions are set according to the CFD simulation guidelines and previous research [78,104,142,155,157,158]. The validation of the CFD model is conducted in order to ensure the fidelity of the CFD simulation results. The boundary conditions and parameter settings of the CFD model are validated by comparing the numerical modeling results with the wind tunnel test data of Case E wind tunnel experiment made by Architecture institute of Japan (AIJ) [159]. The wind tunnel experiment area of Case E is an actual urban area in the Niigata city of Japan, the configuration of which is similar to our study area. The CFD simulations is performed using Fluent (2019R3) in a server with an AMD EPYC 7T83 CPU at 3.40 GHz and Windows 10 Enterprise 64-bit OS. The computational time for each CFD simulation is about 1~2 hours.

$$U_z = U_s \cdot \left(\frac{z}{z_s}\right)^\alpha \quad (5.3)$$

$$k_z = 1.5 \cdot (I_z \cdot U_z)^2 \quad (5.4)$$

$$I_z = 0.39 \cdot \left(\frac{z}{10}\right)^{-\alpha} \quad (5.5)$$

$$\varepsilon_z = C_\mu^{0.75} \cdot k_z^{1.5} / l_z \quad (5.6)$$

$$l_z = 100 \cdot \left(\frac{z}{30}\right)^{0.5} \quad (5.7)$$

where, z is the vertical coordinate of the calculation point in the computational domain. U_s is the velocity at the reference height, which is set to 2.639m/s in this study. z_s is the reference height, which is set to 62m in this study. α is the power-law exponent, which is set to 0.39

according to the terrain category. I_z is the turbulent intensity. C_μ is the model constant, the value of which is 0.09. l_z is the turbulence integral length.

The internal settings and the settings of the parameters not under investigation in the simulation model are determined as shown in Table 5.2. The standard floor height is set as 3m, and the ground floor height can be 3m, 4m, or 5m. The building height is increased by increasing the floor number and varying the ground floor height. The dimension of each building design scenario is determined by Latin hypercube sampling method, which has the maximum floor area under the sampled orientation and aspect ratio in the design area available for the new building (170m×125m) and has the sampled height. The dimension can be modified by controlling the coordinate settings.

As a large number of building performance simulations are required for a comprehensive mutual impact analysis between the new building and the local microclimate, jEplus is adopted to achieve the automatic process of numerous building performance simulations. jEplus can automatically modify the parameter values (i.e., the six parameters listed in Table 3) in building simulation model according to the generated scenarios and call EnergyPlus to perform the simulation.

Table 5.2 The internal settings and the settings of the parameters not under investigation in the simulation model

Parameter	Value	Units
Window to wall ratio	0.25	-
Wall specific heat	920	J/(kg·K)
Wall thermal absorptance	0.9	-

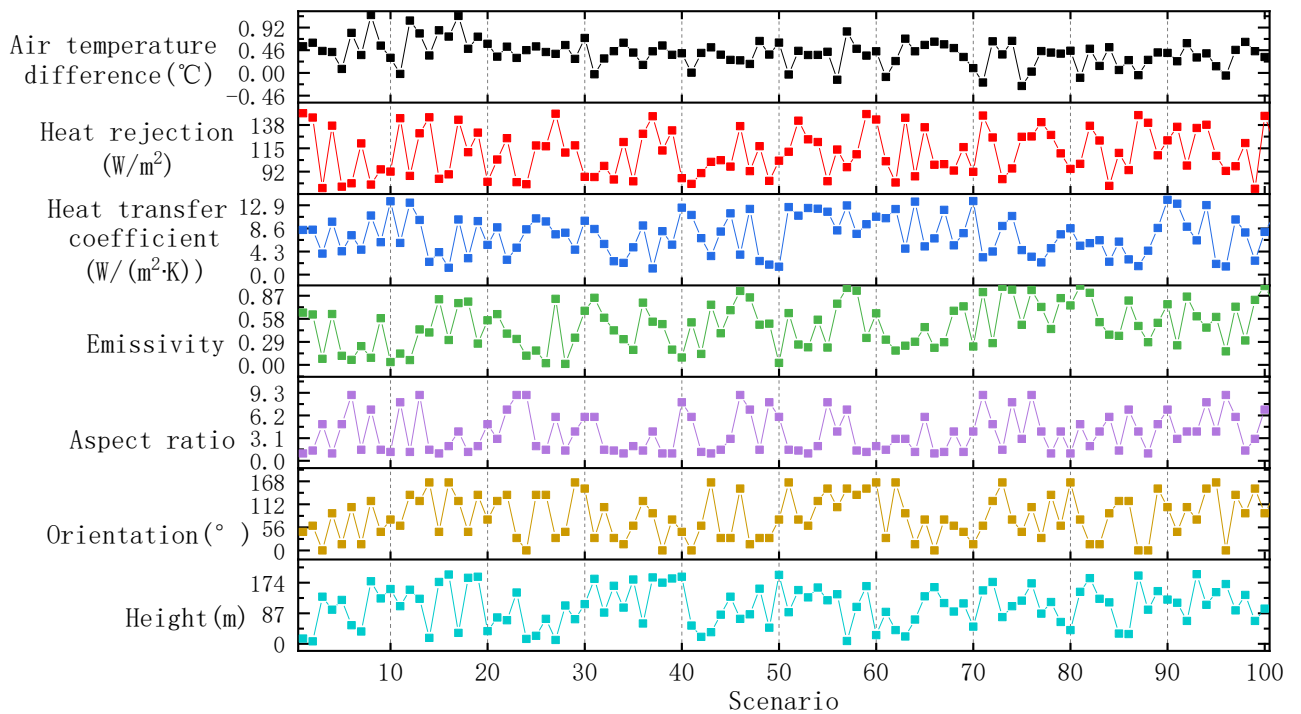
Wall solar absorptance	0.7	-
Wall visible absorptance	0.7	-
Roof specific heat	920	J/(kg·K)
Roof thermal absorptance	0.9	-
Roof solar absorptance	0.7	-
Roof visible absorptance	0.7	-
Ground slab specific heat	920	J/(kg·K)
Ground thermal absorptance	0.9	-
Window SHGC	0.15	W/(m ² ·K)
Window visible light transmittance	0.61	-
Infiltration air mass flowrate coefficient	1	1/h
Outdoor airflow rate	0.00944	m ³ / (person· s)
Indoor setpoint temperature for cooling	25.5	°C
Overhang tilt angle	90	°
Sensible heat recovery effectiveness	0.7	-
Latent heat recovery effectiveness	0.65	-
Occupancy	4	m ² /person
People load	108	W/person
Lighting load	10	W/ m ²
Electric equipment load	7.6	W/ m ²

5.4 Analysis on impacts of building design on local microclimate

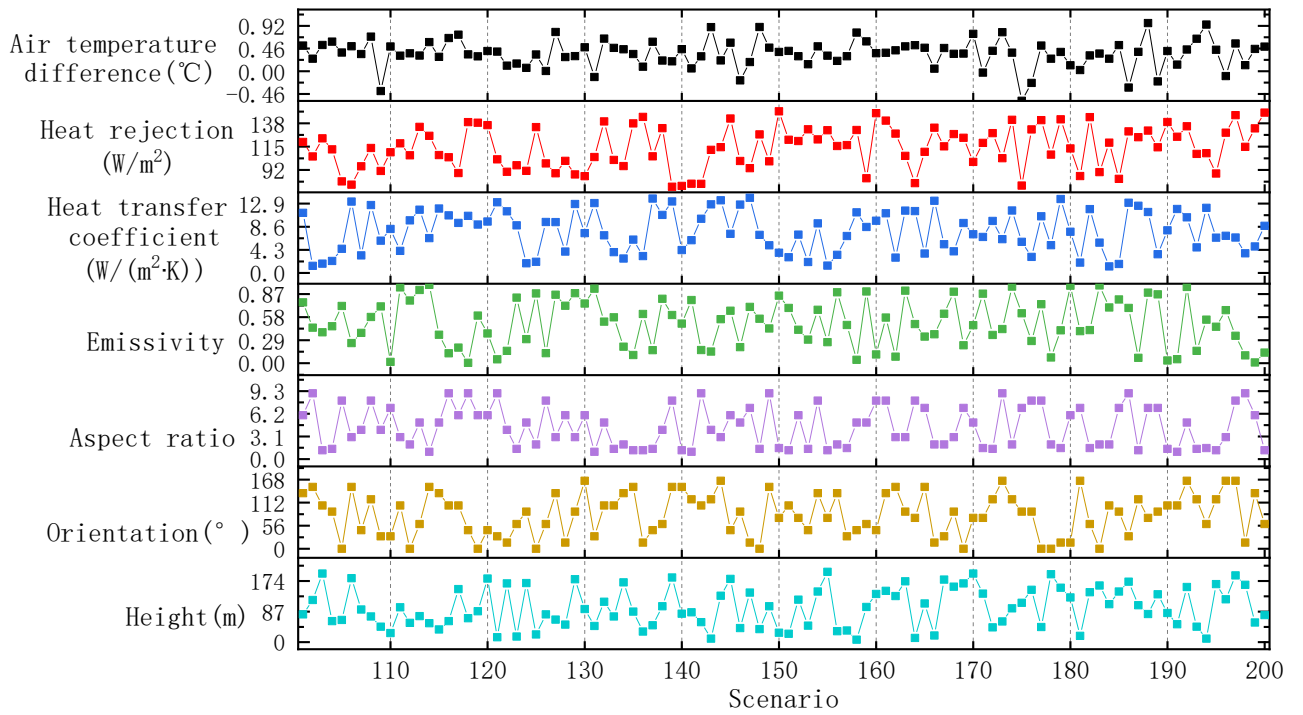
5.4.1 Impacts on local air temperature

The distributions of local air temperature differences under the 200 scenarios on the six building parameters are shown in Figure 5.4. It can be seen that the development of a new building in an existing district will not always lead to an increase in the local air temperature surrounding the building. Different building designs bring impacts of varying degrees on the local air temperature. In this research case, the local air temperature difference varies between

-0.60 K and +1.17 K under different building design scenarios. Among them, 49% of the scenarios have a decrease in the local air temperature, and 50% of the scenarios have a temperature increase higher than 0.40 K. The air temperature distributions under different target buildings in planning are significantly different. Take Scenario 87 (shown in Figure 5.5 (a)) and 37 (shown in Figure 5.5 (b)) as examples, when the building orientation increases from 0° (Scenario 87) to 90° (Scenario 37) and other 5 design variables vary by a little (0~5% of their varying ranges), the local air temperature increases by 0.48 K. This is because when the control strategy adopted in the design building maximizes the use of natural ventilation, an orientation aligning with the windward direction can promote the wind flow and thus reduce the local air temperature, otherwise, the reverse.

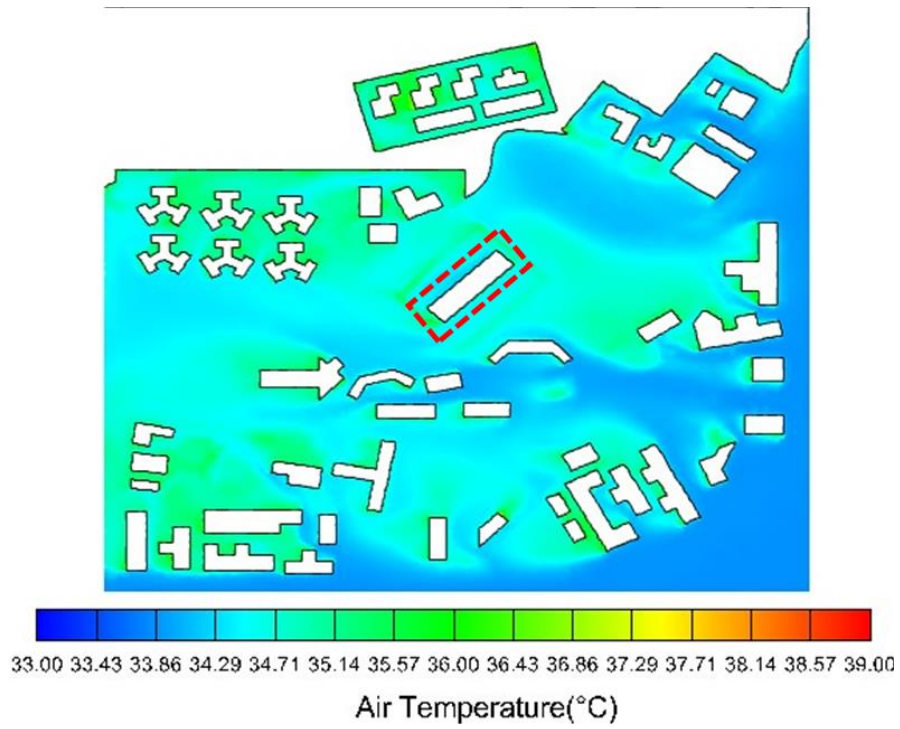


(a) Scenario 1~ Scenario 100

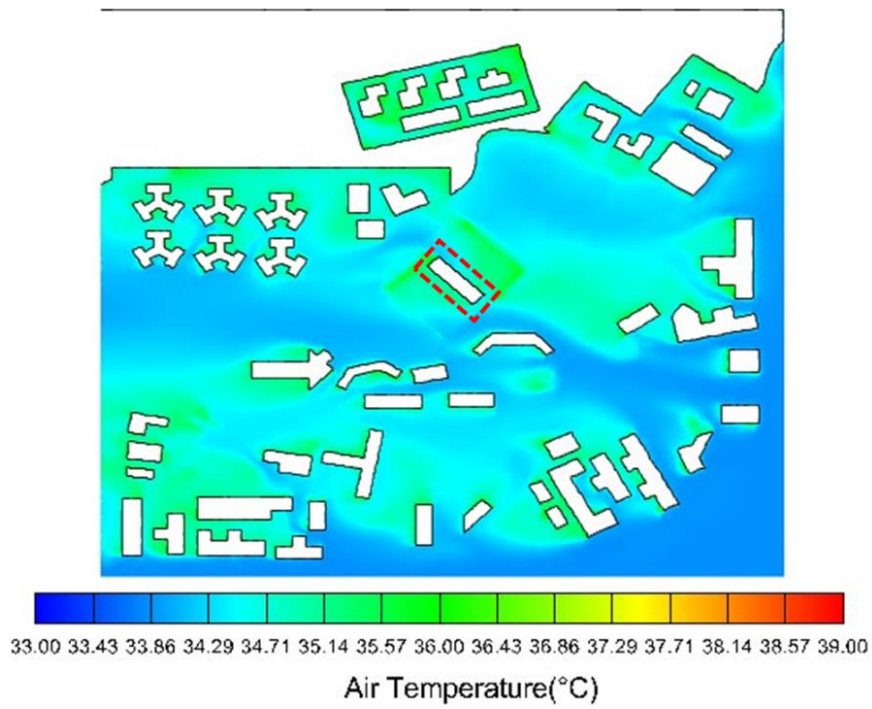


(b) Scenario 101~ Scenario 200

Figure 5.4 Local air temperature differences between with and without the new building under different scenarios



(a) Scenario 87

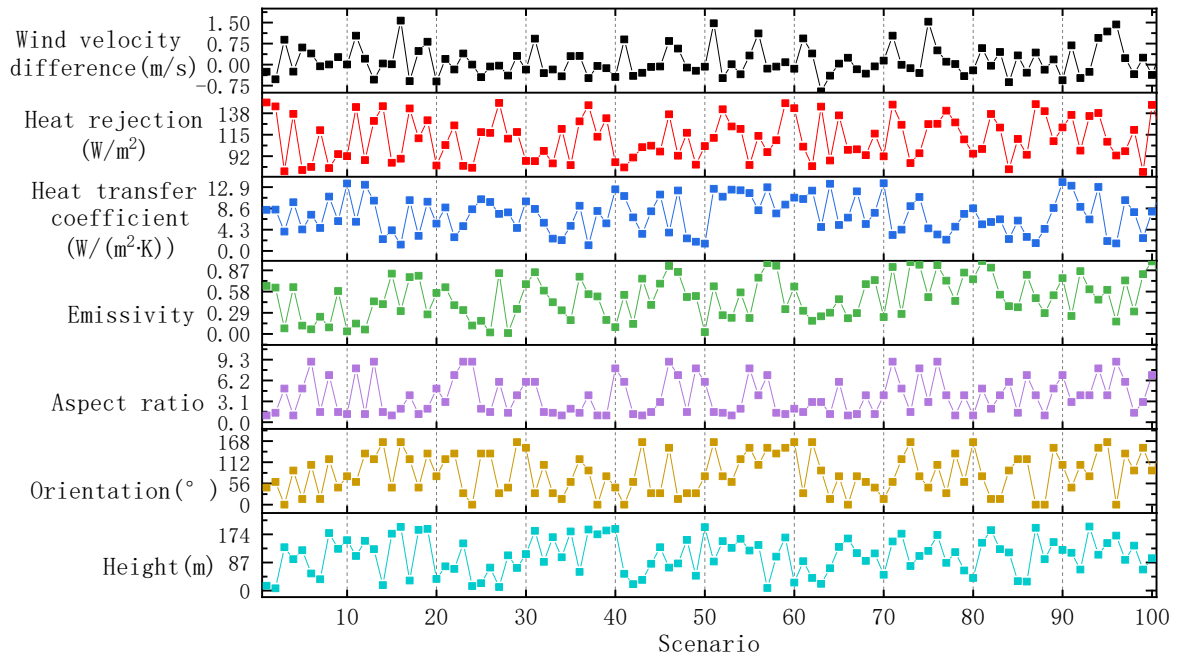


(b) Scenario 37

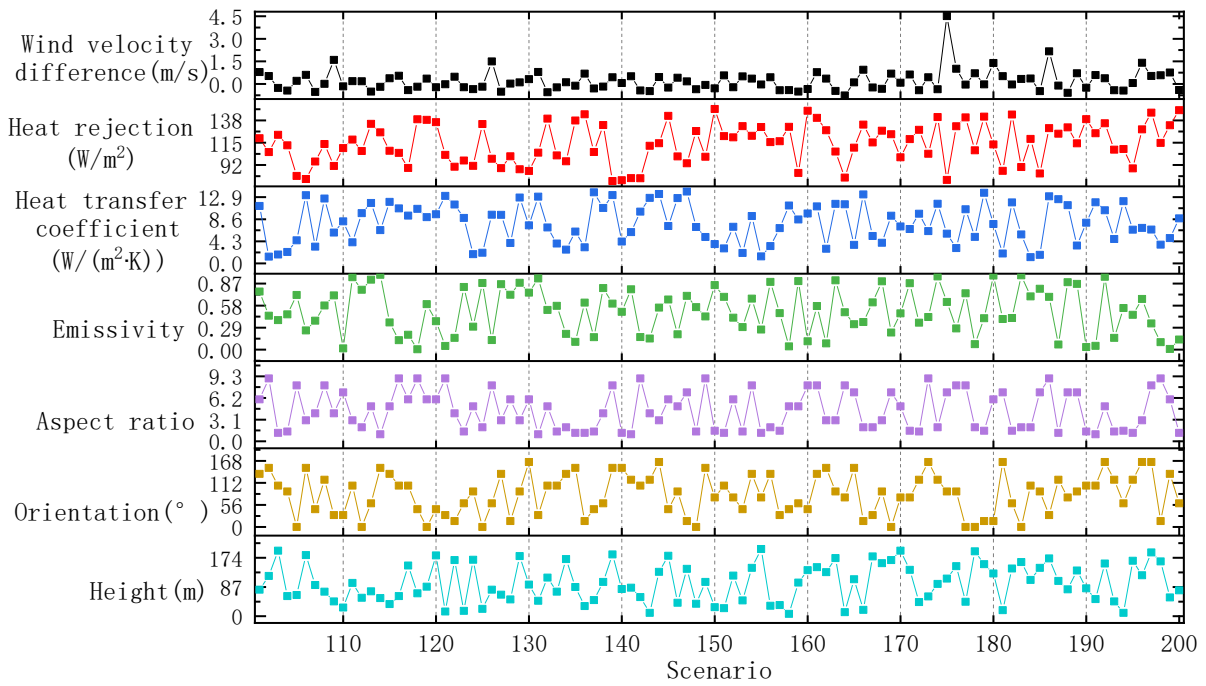
Figure 5.5 Air temperature distributions at $z=1.5\text{m}$ of magnified view of study area

5.4.2 Impacts on local wind velocity

The results of local wind velocity differences under the 200 building design scenarios are shown in Figure 5.6 (a) and Figure 5.6 (b). It can be seen that different design of a new building can lead to an increase or decrease in the local wind velocity surrounding the building. The local wind velocity difference between with and without the new building varies from -0.95m/s to +4.51m/s under the 200 design scenarios. In nearly half of the scenarios, the local wind velocity is increased and the wind velocity difference falls within a range between 0.01m/s and 0.95m/s. The average wind velocity difference under all of the scenarios is 0.15m/s. The wind velocity distributions under different building design are absolutely different. It can be observed from Figure 5.7 (a) (Scenario 33) and Figure 5.7 (b) (Scenario 23) that the building aspect ratio has considerable impacts on the local wind velocity. The increase of the aspect ratio from 1.4:1 (Scenario 33) to 9:1 (Scenario 23) can lead to 0.57m/s of velocity increase because the flow past a building which seems like a flat plate can promote the ventilation around it.

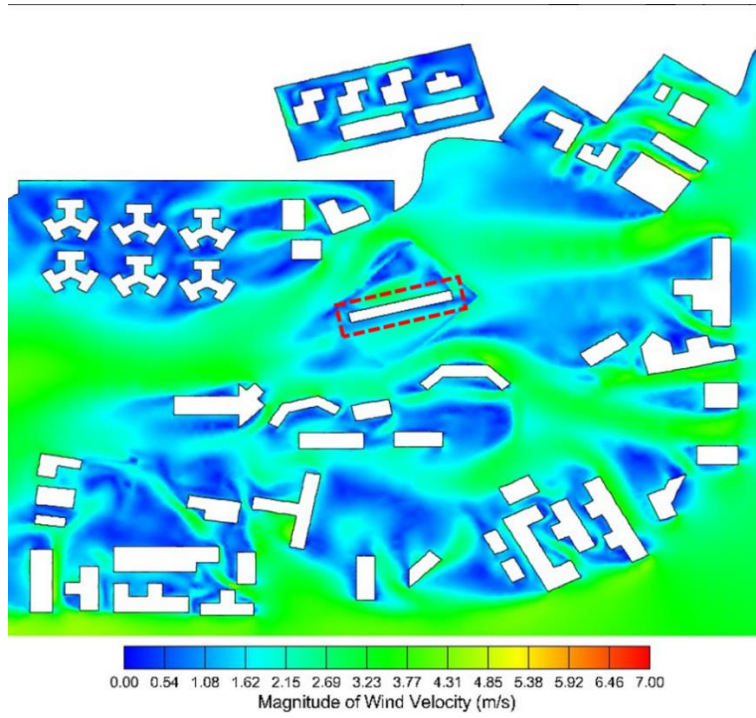


(a) Scenario 1~ Scenario 100

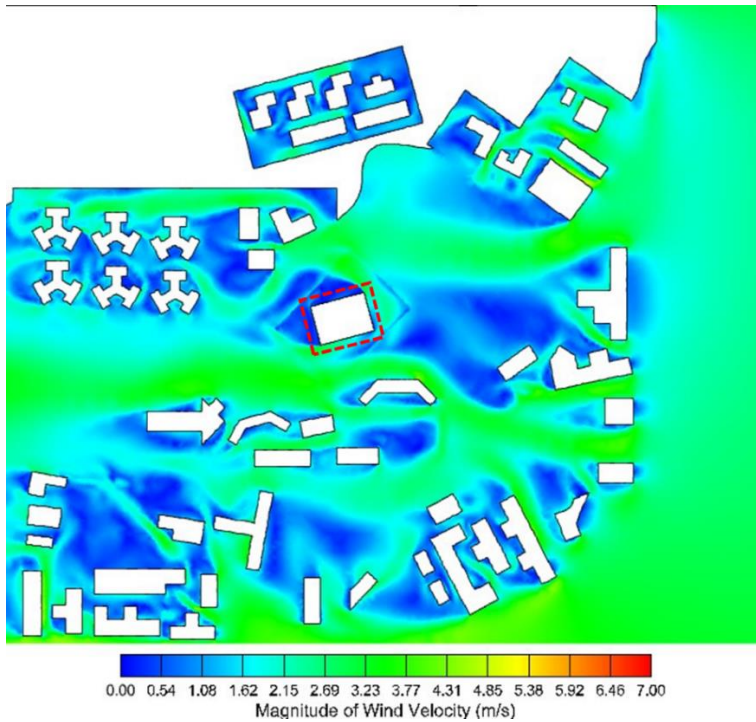


(b) Scenario 101~ Scenario 200

Figure 5.6 Local wind velocity differences between with and without the new building under different scenarios



(a) Scenario 23

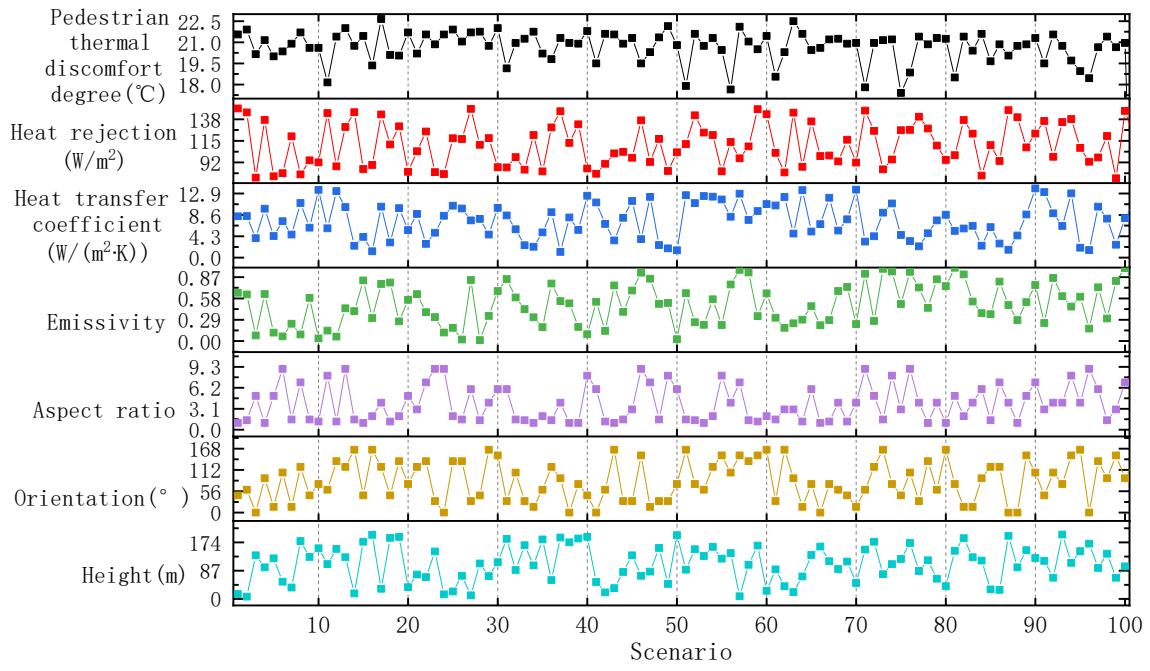


(b) Scenario 33

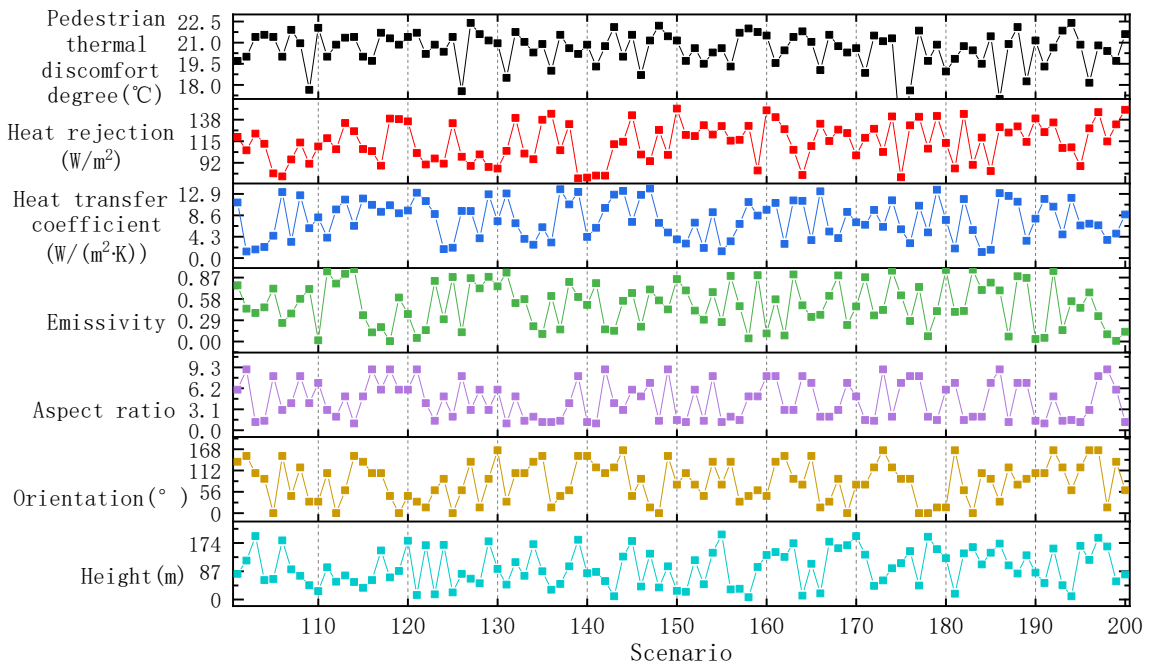
Figure 5.7 Wind velocity distributions at $z=1.5\text{m}$ of magnified view

5.4.3 Impacts on pedestrian thermal comfort

The pedestrian thermal discomfort degrees under the 200 building design scenarios are shown in Figure 5.8. It can be seen that the pedestrian thermal discomfort degree varies from 13.75°C to 22.65°C under different building design scenarios, corresponding to the thermal perception from hot to very hot. 95.5% of the scenarios have a high pedestrian thermal discomfort degree higher than 18°C. The average pedestrian thermal discomfort degree is around 20.61°C. Figure 5.9 shows the pedestrian thermal discomfort degrees of the district under the typical scenarios of building design. It can be seen that the one-variable-dominated variation (other 5 building design variables setting as the same or varying by a little) can lead to the changes of pedestrian thermal discomfort degree in the range of -1.45~3.90°C. The increase of building height from 65m (Scenario 92) to 141m (Scenario 56) can dominate the significant mitigation of pedestrian thermal discomfort (Ddiscom decrease of 3.90°C). The Ddiscom decrease of 2.10°C is dominated by the increase of building orientation from 0° (Scenario 125) to 135° (Scenario 156). The increase of the aspect ratio from 1.4:1 (Scenario 33) to 9:1 (Scenario 23) dominates the Ddiscom decrease of 0.40°C. The increase of the wall emissivity from 0.35 (Scenario 172) to 0.78 (Scenario 36) can mitigate the pedestrian thermal discomfort to 1.70°C. When the overall heat transfer coefficient increases from 1.32 W/(m²·K) (Scenario 102) to 5.13 W/(m²·K) (Scenario 149), Ddiscom increases by 1.45°C. The increase of heat rejection of air-conditioners from 96.64 W/m² (Scenario 123) to 145.23 W/m² (Scenario 2) can dominate the Ddiscom increase of 1.05°C.



(a) Scenario 1~ Scenario 100



(b) Scenario 101~ Scenario 200

Figure 5.8 Pedestrian thermal discomfort degrees under different scenarios

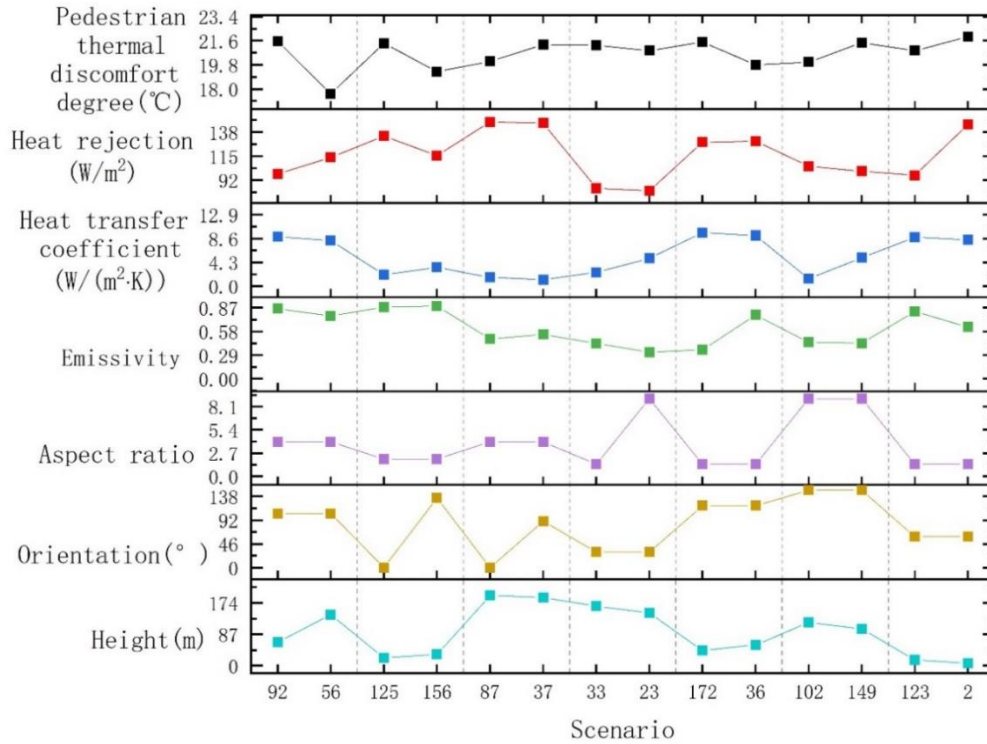


Figure 5.9 Pedestrian thermal discomfort degrees of the district with the new building under different scenarios

5.5 Analysis on impacts of local microclimate on building energy performance

The differences between building energy consumptions considering local microclimate impacts and without considering the local microclimate impacts (i.e., under TMY weather) under the 200 scenarios of building design are shown in Figure 5.10, as well as the corresponding air temperature and wind velocity differences between the local microclimate and TMY weather. It can be seen that the air temperature difference between the local microclimate and TMY weather varies from +0.18 ~ +1.96 K under different building design scenarios, while the wind velocity difference varies within a range between -3.06 m/s and +2.40 m/s. Among the 200 scenarios, all of the scenarios have a higher local air temperature than that

of TMY weather, and 99.5% of the scenarios have a lower local wind velocity than that of TMY weather. The local microclimate can lead to an increase or decrease of building energy consumption within the range between -41.75kJ/m^2 and $+291.54\text{kJ/m}^2$ compared with the TMY weather. Only 2.5% of the scenarios has a decrease in the building energy consumption due to the microclimate impact. 91% of the scenarios has an increase in the building energy consumption larger than 50kJ/m^2 . The average building energy consumption difference caused by local microclimate is 123.31kJ/m^2 . The highest building energy consumption increase happens when the air temperature difference is 1.49K and the wind velocity difference is -2.74m/s . When the air temperature difference is 1.12K and the wind velocity difference is -2.05m/s , there shows the largest decrease in the building energy consumption.

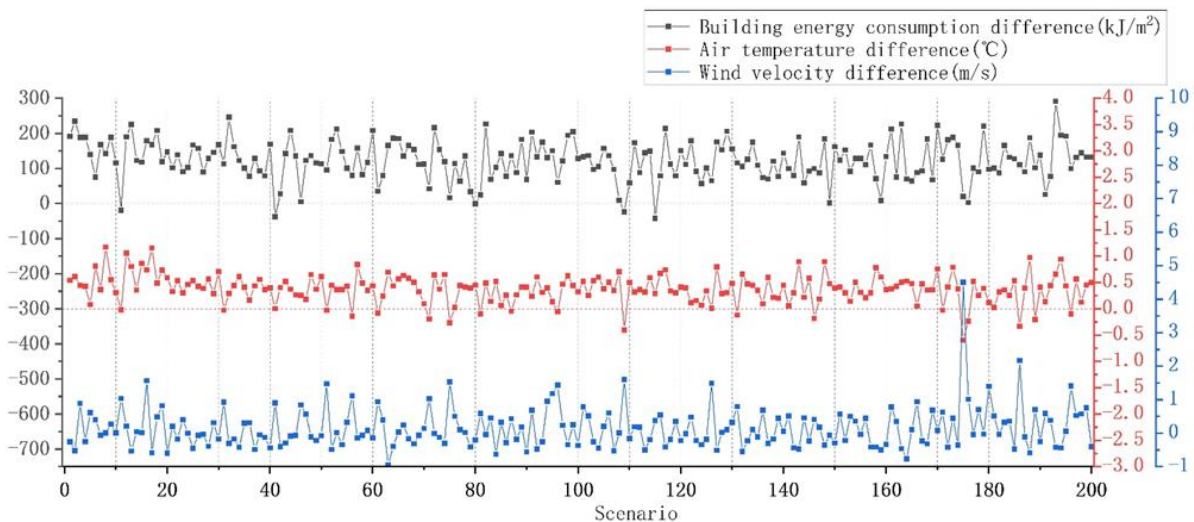


Figure 5.10 Building energy consumption, outdoor air temperature and wind velocity differences between local microclimate and TMY under different scenarios

5.6 Identification of the major influential building parameters on both local microclimate and building performance

5.6.1 Results of sensitivity analysis

In this study, regression method, as a widely-used global sensitivity analysis method, is adopted. Spearman Correlation Coefficient (SPEA) is used to measure and compare the sensitivity of each building parameter to the four performance indexes introduced in Section 5.2 to identify the major influential parameters. A positive value means a positive correlation exists between the building parameters and the performance concerned, while a negative value means negative correlation. The larger the absolute value of SPEA is, the more sensitive the building parameter is to the performance.

Figure 5.11 shows the SPEA correlation coefficient between the six building parameters and the four performance indexes concerned. It can be seen that the building orientation and wall emissivity are the highly-sensitive parameters. The building orientation and overall heat transfer coefficient are positively correlated with the local air temperature difference, while the building height, aspect ratio, wall emissivity and heat rejection of air-conditioners are negatively correlated. This means that the increase in the building height, aspect ratio and wall emissivity would increase the ambient air temperature around the target building, while the increase in the overall heat transfer coefficient would decrease the ambient air temperature. These results are similar to those in previous studies concerning the impacts of district [70,89]. The results are rational because the increase in the building height or aspect ratio would

increase the shading around the building and the ambient wind velocity around the target building, and therefore decrease the ambient air temperature. The increase in the emissivity and the decrease in the heat transfer coefficient would lead to the less heat exchange and therefore a decrease in the ambient local air temperature. The results regarding the heat rejection of air-conditioners seem inconsistent with previous studies where an increase of air temperature is observed around the condensing units of air-conditioners [77,99]. This problem will be further discussed in section 5.6.2. As for the local wind velocity difference, building height and aspect ratio are the highly-sensitive parameters. In general, the six building parameters have more significant impacts on the local wind velocity than local air temperature. The building parameters that have positive impacts are the morphology parameters (i.e., building height, orientation, and aspect ratio), and the parameters that have negative impacts are the thermal characteristic parameters (i.e., wall emissivity, overall heat transfer coefficient, and air-conditioner heat rejection). Most of these results are similar to the previous studies. However, the result related to the building height is not consistent with that in previous studies concerning the impacts of district buildings [89,104]. The results are both rational due to the difference of the research scenarios concerned. In this study, the individual building is concerned. The increase in the building height would result in the higher ambient wind velocity and accelerate the ventilation around it. For the district buildings, the increase in the average building height would block the airflow of the district and thus decrease the wind velocity.

As for the pedestrian thermal discomfort degree, the building parameters that have positive impacts are overall heat transfer coefficient, and air-conditioner heat rejection. The parameters that have negative impacts are the morphology parameters and wall emissivity. Building height and overall heat transfer coefficient are the highly-sensitive parameters. Building height is the only parameter that has negative correlation with the building energy consumption considering local microclimate impacts. Building height, aspect ratio and overall heat transfer coefficient are the highly-sensitive parameters. However, in previous studies [70] regarding the impacts of district design, emissivity is recognized as the highly sensitive parameter, while the district aspect ratio has low impact. It is worth noting that the correlations between building parameters and local microclimate are relatively low compared with those with building energy consumption. This is because the building parameters which affect both the building performance and local microclimate are only considered, and the impacts of an individual building are limited compared with a whole district. However, the impacts of the relatively sensitive parameters (e.g., building height) cannot be ignored.

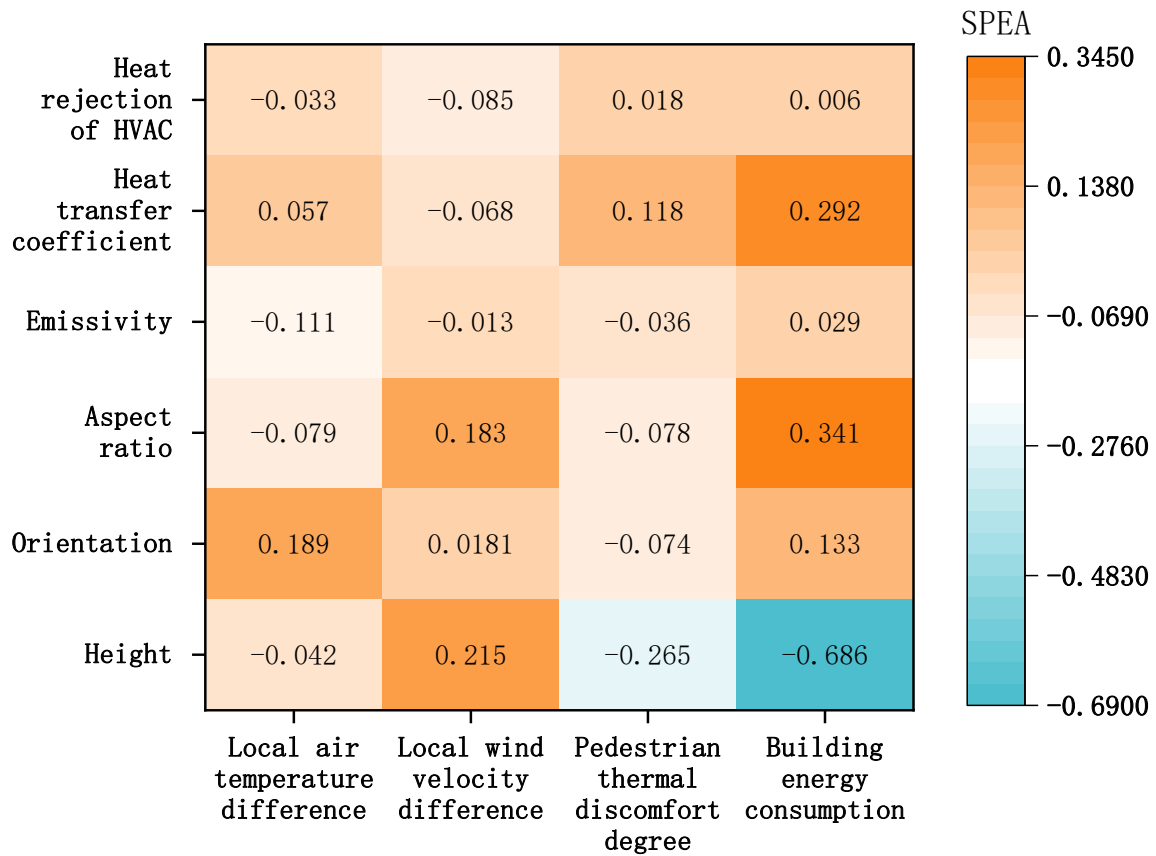


Figure 5.11 SPEA correlation coefficient between building parameters and the performance indexes concerned

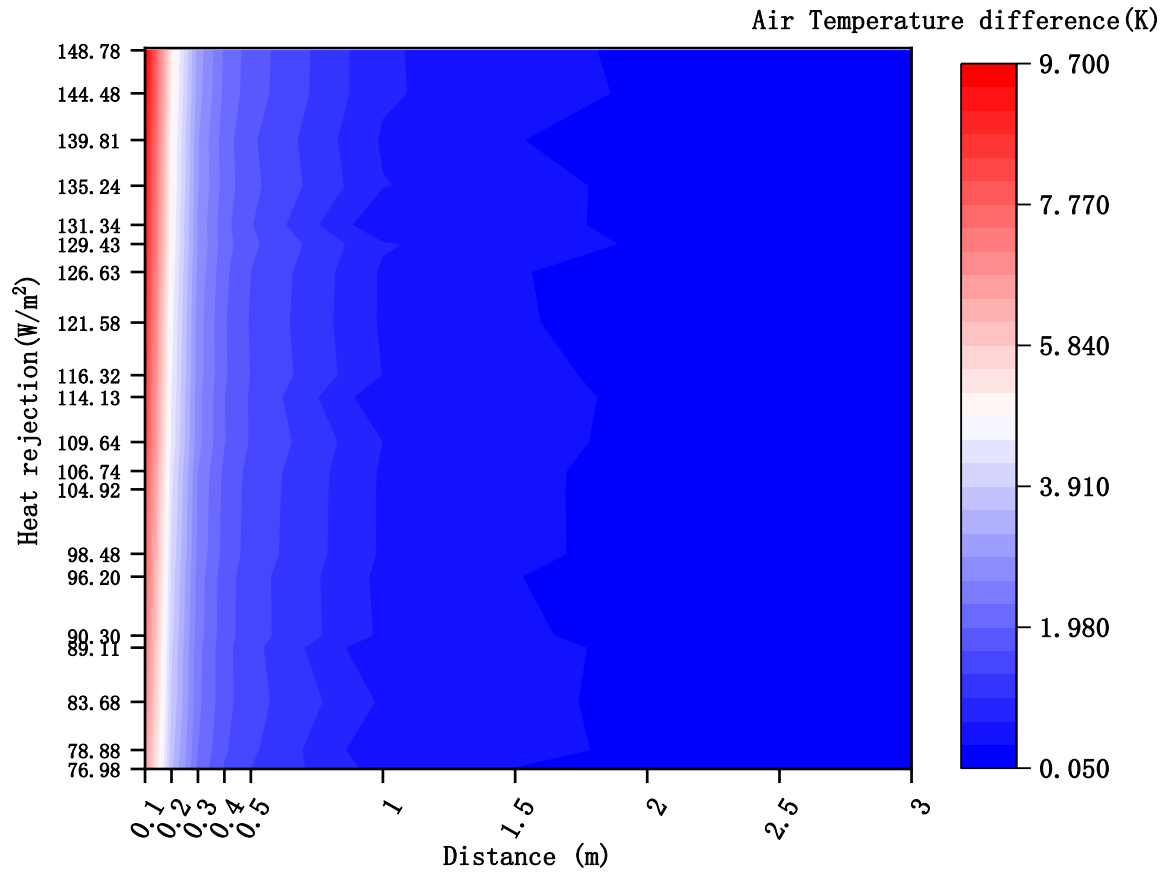
5.6.2 Discussion on the impacts of heat rejection of HVAC on local microclimate

It is worth noticing that the heat rejection of air-conditioners has negative correlations with the local air temperature and wind velocity differences, which seems inconsistent with theoretical inference. To further verify the rationality, a local sensitivity analysis of the air-conditioner heat rejection to the local microclimate is conducted by set other building parameters as fixed values. The local microclimate near the wall installed with air-conditioners, which is also the windward side, is particularly investigated, in view of stronger impacts near the air-conditioners. The windward-side local air temperature and wind velocity differences at 10

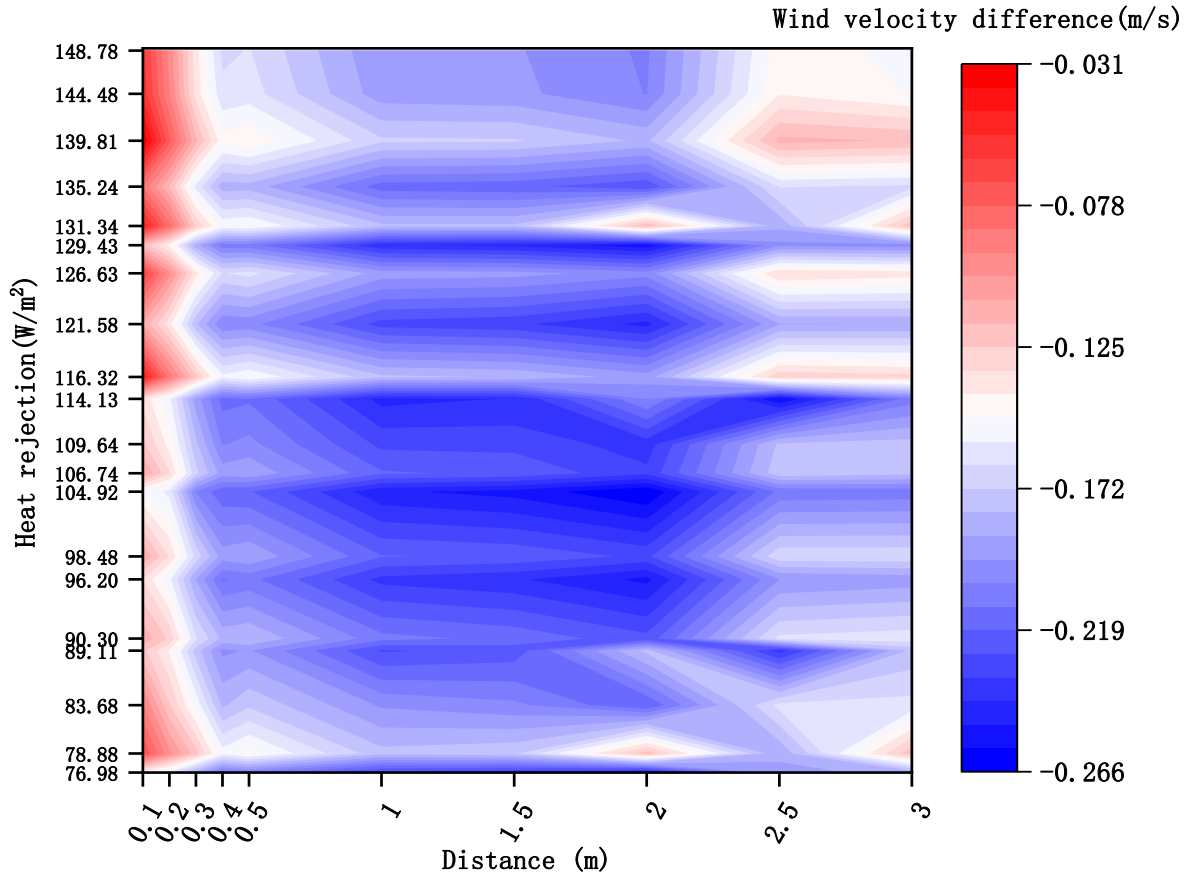
different distances (i.e., 0.1m, 0.2m, 0.3m, 0.4m, 0.5m, 1.0m, 1.5m, 2.0m, 2.5m, 3.0m) from the new building in the horizontal direction is simulated under 20 different settings of heat rejection. The settings are determined according to the random sample from the corresponding range (i.e., 75~150 W/m²). The results are shown in Figure 5.12.

It can be seen from Figure 5.12 (a) that the air conditioner heat rejection increases the windward-side local air temperature at any distance concerned. The increase of the air conditioner heat rejection also leads to the increase of ambient air temperature difference when the distance is less than 0.5m. When the microclimate at a further distance is concerned, the impacts of air-conditioner heat rejection become weak. Therefore, it is rational that the SPEA correlation coefficient between the heat rejection and local air temperature difference shown in Figure 5.15 is slightly negative, as it is calculated based on the average local air temperature differences of all sides at the distance of 3.0m where the impacts become weak at a far distance and complicated under the variation of all building parameters including building orientation. The windward-side local wind velocities at different distances are reduced due to the development of the new building as seen from Figure 5.12 (b). But the local wind velocity difference does not show an obvious increase or decrease particularly at far distances when the air-conditioner heat rejection increases, due to insignificant impact of heat buoyancy force. Therefore, the slightly negative value of the SPEA correlation coefficient between the heat rejection and local wind velocity difference (shown in Figure 5.11) does not mean an obvious

negative correlation, which is also applied for local air temperature difference. It is just the average impact under the 200 cases. Thus, the sensitivity analysis results are rational.



(a) Air temperature difference (K)



(b) Wind velocity difference (m/s)

Figure 5.12 Windward-side local microclimate differences at different distances under different settings of air-conditioner heat rejection

5.6.3 Identification of the major influential building parameters

Based on the above sensitivity analysis results, the building parameters affecting the local air temperature and wind velocity are ranked respectively, as listed in Table 5.3. It can be seen that the ranking orders of the building parameters affecting local air temperature and wind velocity are totally different. The major influential building parameters on local air temperature are building orientation and wall emissivity, while the parameter with the least impact is the heat rejection of air-conditioners. The major influential building parameters on local wind

velocity are building height and building aspect ratio, followed by the heat rejection of air-conditioners. The wall emissivity has the least impact on local wind velocity. It is worth noticing that the emissivity of wall and the heat rejection of air-conditioners, which are found to have significant impacts on local air temperature or wind velocity, are ignored in previous research.

As the pedestrian thermal comfort is widely used to evaluate the local microclimate, the building parameters affecting the pedestrian thermal discomfort degree are also ranked and compared with those affecting building energy consumption considering the microclimate impacts. The results are listed in Table 5.4. It can be seen that the major influential building parameters on pedestrian thermal discomfort degree are building height and overall heat transfer coefficient of building envelope, while the parameter with the least impact is the heat rejection of air conditioners. The ranking orders of the building parameters affecting building energy consumption are almost the same as those affecting pedestrian thermal discomfort degree, except for building orientation and overall heat transfer coefficient. The major influential parameters on building energy performance include building height, building aspect ratio, overall heat transfer coefficient of building envelope. It is recommended that the restrictions on the overall heat transfer coefficient of building envelope and building height specified in the building design guidelines or related policies should be given considering the impacts on both building energy consumption and local microclimate.

Table 5.3 Ranking of major building parameters affecting local microclimate

Performance Rank	Local air temperature	Local wind velocity
1	Building orientation	Building height
2	Emissivity of wall	Building aspect ratio
3	Building aspect ratio	Heat rejection of air-conditioners
4	Overall heat transfer coefficient of building envelope	Overall heat transfer coefficient of building envelope
5	Building height	Building orientation
6	Heat rejection of air-conditioners	Emissivity of wall

Table 5.4 Ranking of major building parameters affecting pedestrian thermal discomfort degree and building energy consumption considering microclimate impacts

Performance Rank	Pedestrian thermal discomfort (Correlation)	Building energy consumption (Correlation)
1	Building height (Negative)	Building height (Negative)
2	Overall heat transfer coefficient of building envelope (Positive)	Building aspect ratio (Positive)
3	Building aspect ratio (Negative)	Overall heat transfer coefficient of building envelope (Positive)
4	Building orientation (Negative)	Building orientation (Positive)
5	Emissivity of wall (Negative)	Emissivity of wall (Positive)
6	Heat rejection of air-conditioners (Positive)	Heat rejection of air-conditioners (Positive)

Although the ranking orders of the building parameters affecting pedestrian thermal discomfort and building energy consumption are similar, the correlations between the parameters and the performance are not the same. For instance, the building aspect ratio, building orientation and wall emissivity have negative correlations with pedestrian thermal discomfort, but positive correlations with the building energy consumption. Therefore, a building design which has the lowest building energy consumption is probably not friendly to the local microclimate. So it is necessary to consider the mutual impacts between building design and local microclimate in

the design of new buildings to improve building energy performance while minimizing the impacts on the local microclimate.

5.7 Summary

In this chapter, a comprehensive and systematic analysis is conducted to investigate the mutual impacts between new individual building design and local microclimate considering their interaction in subtropical urban area, and to identify the major influential parameters on both local microclimate and building energy performance by sensitivity analysis. The mutual impact analysis and sensitivity analysis are based on 200 sets of microclimate and building performance simulations using advanced GIS-based spatial analysis techniques. Based on the analysis results, the major conclusions can be drawn and summarized as follows.

- Strong mutual impacts exist between the new building design and urban local microclimate. In this study, different building designs lead to significant variations of local wind velocity (i.e., $-0.95\sim+4.51$ m/s), air temperature (i.e., $-0.60\sim+1.17$ K), and pedestrian thermal discomfort degree (i.e., $13.75\sim22.65^{\circ}\text{C}$). The local microclimate results in a change in the building energy consumption from -41.75kJ/m^2 to 291.54kJ/m^2 .
- The major influential parameters on local air temperature, wind velocity and pedestrian thermal discomfort are rather different. The major influential parameters on local air temperature are building orientation and wall emissivity, while the major influential parameters on local wind velocity are building height and aspect ratio. As for the

pedestrian thermal discomfort, the major influential parameters include building height and overall heat transfer coefficient of building envelope.

- The major influential parameters on both local microclimate and building energy performance are building height and overall heat transfer coefficient of building envelope. Although the ranking orders of the building parameters affecting pedestrian thermal discomfort and building energy consumption are similar, the correlations between the parameters and the performance are significantly different. Therefore, it is necessary to consider the mutual impacts between building design and local microclimate in the design of new buildings to improve building energy performance while minimizing the impacts on the local microclimate.

In this study, the thermal characteristics of the building for building performance simulation in EnergyPlus, such as the specific heat capacity, density, thickness, thermal absorptance, solar absorptance, and visible absorptance, are assumed as constant values, the impacts of which on the microclimate are ignored and could be investigated in future work. The representation of trees and roads in the study area is simplified to save computational resources.

CHAPTER 6 DEVELOPMENT OF A GENERIC DATA-DRIVEN LOCAL MICROCLIMATE MODEL CONSIDERING THE IMPACTS OF BUILDING DESIGN

This chapter presents the development of local microclimate surrogate models for efficient and accurate assessment of the impacts on the local microclimate when making optimal building design. Two complementary machine learning-based surrogate models are proposed, including an SVR-based local air temperature model and a LightGBM-based local wind velocity model. They are identified by evaluating and comparing eight alternative machine learning models. Totally four machine learning algorithms are used for each model development, including ANN, SVR, RF and LightGBM. The case study is conducted to validate the local microclimate surrogate models.

6.1 Methodology of the machine learning-based surrogate models development

This chapter presents the procedure and methods of the development of local microclimate surrogate models. The machine learning-based surrogate models are developed to predict the impacts on the local microclimate (i.e., local air temperature and wind velocity) due to the addition of new individual zero/low energy building. 200 sets of CFD simulation data corresponding to different building designs are used for the model training and validation. Four machine learning algorithms are used for each model development, including ANN, SVR, RF and light gradient boosting machine (LightGBM). A case study is conducted to validate the local microclimate surrogate models. The surrogate models that demonstrate the highest

efficiency and accuracy are recommended for predicting changes in the local microclimate during the early stages of new zero/low energy building design.

6.1.1 Outline of the surrogate models

A surrogate model refers to a simplified model for replacing the computationally expensive model, which can obtain a much faster and more efficient approximation for faster evaluations and analysis [106,108]. In this study, the machine learning-based surrogate models are developed to predict the local microclimate impacts under different designs of new individual building, replacing the computationally expensive and time-consuming microclimate simulations.

To enhance the generalizability of the surrogate model, two major works has been undertaken. One is to set the comprehensive key building parameters affecting local microclimate as the model inputs, including two major categories, i.e., building morphology and building thermal characteristics, which can provide the comprehensive and systematic prediction of the potential for individual building design's impact. The key influential building parameters are identified by a comprehensive impact analysis made previously. The variables concerning building morphology include building height, building orientation, and building aspect ratio. The parameters concerning building thermal characteristics include the overall heat transfer coefficient of building envelope, emissivity of wall, and heat rejection of air-conditioners. The other one is to set the relative changes in the local microclimate (i.e., local air temperature and wind velocity) before and after the addition of a new building as the model outputs. Compared

with existing models directly using the local microclimate parameters as the model outputs, the surrogate models developed in this study can significantly reduce the dependency on the climate conditions. The position for evaluating the relative changes refers to the four lines of 3.0m away from the building and at a height of 1.5m (described as the pedestrian-level in the rest of this thesis). The relative changes are the average changes of the four lines. The temporal condition for evaluation is under the most unfavorable weather condition (the hottest hour) of the summer typical design day in order to assist the evaluation of the design performance and significantly reduce the computing cost.

The detailed procedure of the model development is illustrated in Figure 5.1. Firstly, the dataset for model training and testing is generated via CFD simulations. Various scenarios of building design (e.g., 200 scenarios in this study) are generated using Latin hypercube sampling method according to the ranges of the identified key influential building parameters. The local microclimate (i.e., local air temperature and wind velocity) under each scenario of building design is simulated using Fluent based on the 3D district geometry model developed based on GIS. The local microclimate impacts under each scenario are calculated by comparing the simulated local microclimate with the reference scenario (i.e., before the addition of the new building). The building designs and corresponding local microclimate relative changes under all the scenarios constitute the dataset for model development. Secondly, the dataset is preprocessed by min-max normalization method to adjust the data to the range between 0 and 1, and thereby improve the stability and facilitate the convergence of the learning process while

preventing overfitting. Then the whole dataset is divided into training and testing data. Thirdly, alternative machine learning models are trained based on the training data using ANN, SVR, RF and LightGBM respectively. Fourthly, the model performances are evaluated using the testing data in terms of different performance evaluation metrics. The machine learning models with the best model performance are selected as the surrogate models for predicting the impacts on the local air temperature and wind velocity due to the variation of the new building design.

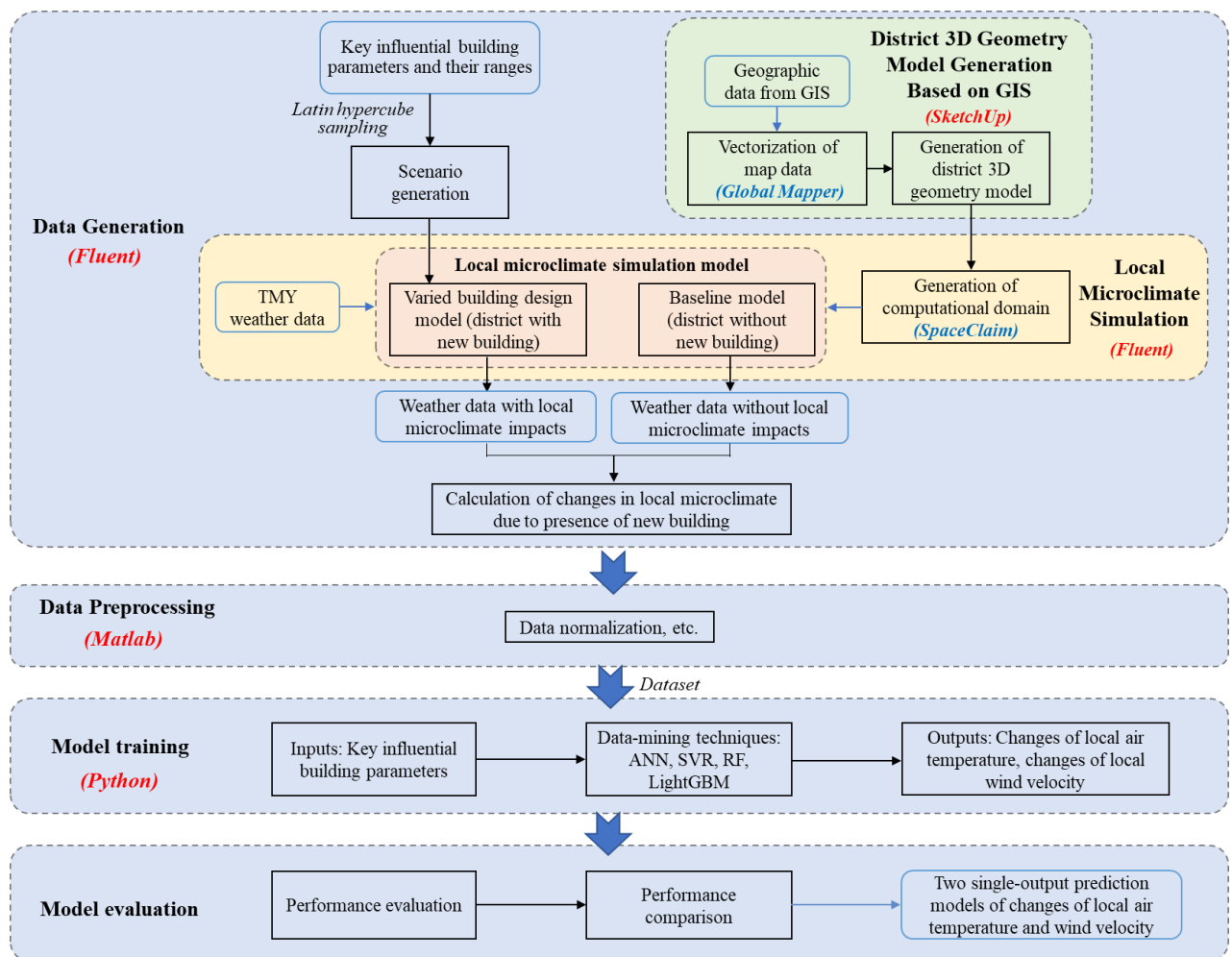


Figure 6.1 Outline of the overall research methodology and procedure

6.1.2 Machine learning techniques concerned

The four machine learning algorithms, i.e., ANN, SVR, RF and LightGBM, are selected in view of their good capability in learning and modelling the nonlinear and complex relationship. These algorithms are all used and compared for developing the surrogate models for predicting the impacts on local air temperature and wind velocity respectively, considering that different algorithms may be preferred due to their different variation characteristics.

ANN is a fundamental supervised learning algorithm in deep learning. It is highly effective in dealing with high-dimensional problems, and has been applied to numerous complex problems [105] including local microclimate prediction as summarized in Table 2.4. In this study, a feed-forward back propagation neural network is adopted. It consists of an input layer, a hidden layer, and an output layer, as shown in Figure 6.2. The input layer is composed of 6 neurons corresponding to the identified six model inputs, and the output layer involves 1 neuron corresponding to the specific model output concerned. The number of hidden neurons is to be optimized during model training.

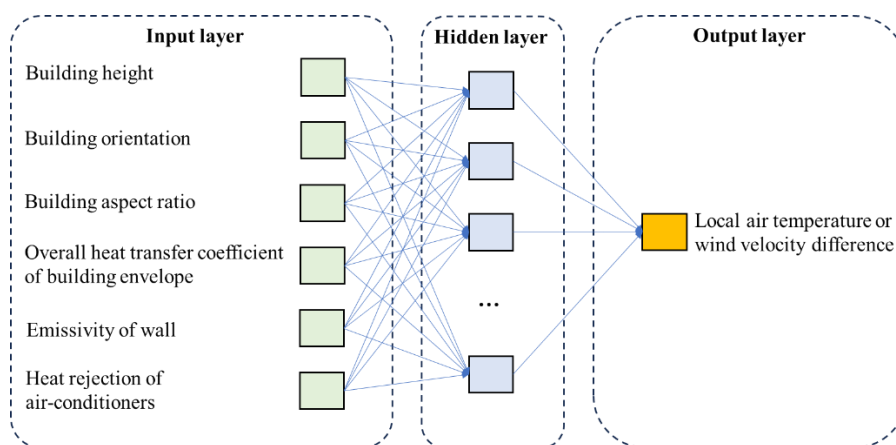


Figure 6.2 Neural network for predicting the changes of local microclimate

SVR is a widely used supervised learning algorithm in machine learning, which has distinct advantages for small datasets and can maintain a good generalization capability [160]. Given the high computational load of CFD simulations in data generation in this study, SVR could be a good option for model development with limited dataset while ensuring a high prediction accuracy. SVR is the application of the support vector machine in regression analysis, which can be utilized to solve non-linear problems, so it is selected to address the non-linear problem of local microclimate prediction in this study.

RF is an ensemble learning method consisting of a collection of decision trees. It is one of the most popular supervised learning algorithms for solving regression problems due to its simplicity, robustness and high accuracy [161]. RF is an extension of bagging method and shows the property of parallelization, in which each weak learner is trained independently. Both the random sample of data and the random feature selection add diversity and reduce the correlation among these decision trees, which maintains the generalization ability of RF. The good generalization ability can avoid the risk of overfitting and maintain the simplicity and robustness for prediction of the local microclimate relative changes. In this study, the final prediction result of this RF model is based on majority averaging of all trees in the forest to yield a more accurate and stable estimate.

LightGBM is also an ensemble learning method based on decision tree algorithms, which has been emerging in the prediction of building area and shows better prediction results [106,162,163]. Unlike RF, LightGBM is built on a gradient boosting framework, which is a

serial integration model that combines weak learners into strong learners by creating sequential models with the aim of maximizing the final model's accuracy. The highly optimized histogram-based decision tree learning algorithm is adopted to reduce the consumption of memory and calculations [162]. The prediction model of the local microclimate changes can benefit from the higher efficiency, lower memory usage and improved accuracy of LightGBM.

6.1.3 Performance evaluation metrics

Four commonly-used metrics [110-112,114] are utilized to evaluate the performance of the machine learning models, including MAE, mean squared error (MSE), normalized RMSE and median absolute deviation (MAD). They can be calculated using the Eqs. (6.1-6.4) respectively.

Where, \hat{y}_i is the predicted value. y_i is the true value. y_{max} is the maximum of the true value. y_{min} is the minimum of the true value. n is the total number of samples. MAE, MSE and MAD are scale-dependent metrics, which offer a straightforward method to quantify prediction error. They also allow a comparison between the prediction error with the measurement error of air temperature and wind velocity for practical physical interpretations. The scale-independent metric, i.e., normalized RMSE is selected to eliminate the unit difference and assess the relative performance of different models. It is within the range from 0 to 1. A lower value indicates better predictive performance of the model, while a higher value indicates poorer predictive performance. Other scale-independent metrics, such as the mean absolute percentage error (MAPE), are not considered in this study as the equation denominator (i.e., the relative changes in local wind velocity and wind velocity) may be zero [164].

Two information criteria, i.e., AIC (Akaike Information Criterion) and BIC (Bayesian Information Criterion), are utilized to evaluate the model overfitting by balancing the goodness of fit and model complexity. AIC is based on information theory, while BIC is based on Bayesian theory. Smaller values indicate better model selection. AIC and BIC can be calculated using the Eqs. (6.5-6.6) respectively. Where, $\log_{likelihood}$ is the value of the model's log-likelihood function. k is the number of parameters in the model, the value of which is 6 in this study.

$$MAE = \frac{1}{n} \sum_{i=1}^n |\hat{y}_i - y_i| \quad (6.1)$$

$$MSE = \frac{1}{n} \sum_{i=1}^n (\hat{y}_i - y_i)^2 \quad (6.2)$$

$$\text{normalized } RMSE = \sqrt{\frac{\sum_{i=1}^n (\hat{y}_i - y_i)^2}{n}} / (y_{max} - y_{min}) \quad (6.3)$$

$$MAD = \text{median}(|\hat{y}_1 - y_1|, \dots, |\hat{y}_n - y_n|) \quad (6.4)$$

$$AIC = -2\log_{likelihood} + 2k \quad (6.5)$$

$$BIC = -2\log_{likelihood} + k \cdot \log(n) \quad (6.6)$$

6.2 Development of alternative data-driven models

6.2.1 Data generation and preprocessing

The local microclimate surrounding the building is simulated using Fluent under different building designs obtained by varying the six influential building parameters concerned as shown in Table 6.1. 200 scenarios are generated using Latin hypercube sampling method

according to the ranges of the parameters for microclimate simulations as shown in Section 5.1 [166].

Based on the simulation results, the changes in the local microclimate due to the addition of the new building are calculated under the 200 scenarios, including: (i). the average relative change at the pedestrian-level (i.e., 3.0m away from the building and 1.5m height in this study) air temperatures in the district before and after the addition of the new building (local air temperature change for short in the rest of this paper); (ii). the average relative change on pedestrian-level wind velocity in the district before and after the addition of the new building (local wind velocity change for short). Then the dataset of local air temperature impacts and local wind velocity impacts, together with corresponding building parameters, are normalized for model training and testing.

6.2.2 Training of the machine learning models

Single-output machine learning models are developed to predict the local air temperature difference and local wind velocity difference respectively, using the four selected machine learning algorithms. The single-output prediction models can realize more accurate prediction results than one multiple-output prediction model [104,105]. 90% of the 200 dataset is used for the model training, while the rest (i.e., 10%) is used for testing. The 10-fold cross validation and parameter grid search are utilized for hyperparameter optimization during the model training. The optimization range and optimization results of hyperparameter in grid search are listed in Table 6.1.

For the ANN model, the number of hidden neurons is optimized within a range between 10 and 1000. The learning rate is optimized within a range from 0.00001 to 1. Different activation functions (i.e., 'identity', 'logistic', 'tanh' and 'relu') and solvers (i.e., 'lbfgs', 'sgd', and 'adam') are compared respectively to select the proper ones. For the SVR model, the kernel function of Gaussian radial basis is utilized in this study. The regularization parameter C is optimized within a range between 0.0001 and 100000. A larger C tends to make the model more prone to overfitting, while a smaller C is more likely to cause underfitting. The kernel coefficient gamma is optimized within a range from 0.0001 to 12.8. For the RF model, the bootstrap samples method is adopted to reduce the variance of the predictions and improve the predictive performance. The number of trees in the forest is optimized within a range between 10 and 1000. The maximum depth of the tree is optimized within a range from 2 to 15. For the LightGBM model, the gradient boosting decision tree is adopted. The number of boosted trees is optimized within a range from 10 to 1000. The maximum tree depth and leaves for the base learners are optimized within the ranges of 2-15 and 3-39 respectively. The learning rate is optimized within a range between 0.00001 and 1. The subsample ratio of the training instance and the columns when constructing each tree are optimized within a range from 0.8 to 1. The hyperparameter optimization results for the prediction model of local air temperature difference and local wind velocity difference are listed in Table 6.1.

Table 6.1 Hyperparameter optimization for the prediction model of local microclimate impacts

Machine learning model	Hyperparameter	Optimization range	Optimization value	
			Local air temperature model	Local wind velocity model
ANN	Numbers of hidden layers	1, 2, 4, 5, 10	1	1
	Hidden layer size	10, 50, 100, 200, 300, 400, 500, 800, 1000	10	1000
	Learning rate	1e-5, 1e-4, 0.001, 0.005, 0.01, 0.05, 0.1, 0.5, 1	0.1	1e-5
	Activation functions	'identity', 'logistic', 'tanh', 'relu'	tanh	tanh
	Solver	'lbfgs', 'sgd', 'adam'	stochastic gradient descent	stochastic gradient descent
SVR	Regularization parameter	1e-4, 0.001, 0.01, 0.1, 1, 10, 100, 1000, 10000, 100000	1	10
	Kernel coefficient gamma	1e-4, 0.001, 0.005, 0.01, 0.05, 0.1, 0.2, 0.4, 0.6, 0.8, 1.6, 3.2, 6.4, 12.8	0.001	1e-5
RF	Number of trees	10, 100, 200, 500, 1000	10	10
	Maximum depth of tree	2, 3, 4, 5, 10, 15	5	5
LightGBM	Number of trees	10, 100, 200, 500, 1000	1000	1000
	Maximum depth of tree	2, 3, 4, 5, 10, 15	2	2
	Maximum tree leaves	3, 7, 15, 31, 1023, 32767	3	3
	Learning rate	1e-5, 1e-4, 0.001, 0.005, 0.01, 0.05, 0.1, 0.5, 1	1e-5	0.05
	subsample ratio	0.8, 0.9, 1	1	1

6.3 Results of local microclimate prediction

6.3.1 Local air temperature impact prediction

The predicted local air temperature change given by different machine learning models is shown in Figure 6.3. A positive value means the pedestrian-level local air temperature is increased due to the addition of the new building. Where, a negative value indicates the pedestrian-level local air temperature is decreased. The comparison of the pedestrian-level local air temperature distributions (calculated by CFD simulations) before and after the addition of the new building, taking Case 8 as an example, are shown in Figure 6.4 and Figure 6.5. The area concerned is marked in Figure 6.5. As shown in Figure 6.3, the actual local air temperature change (i.e., that given by CFD simulations) is predominantly positive with minimal variation, ranging from -0.21 to 1.15 °C. The predicted local air temperature impacts given by the four machine learning models show the similar pattern. Although significant increases or decreases of the actual local air temperature profiles can be observed occasionally, the SVR model can effectively capture these variations. The RF model can also reflect the variations, but the trends are not always correct. In contrast, the ANN and LightGBM models lack the sensitivity to predict the variations of the impact due to different new building designs on the local air temperature, although the discrepancies between their predictions and the predictions of other two models are not substantial.

The local air temperatures are predicted by adding the predicted local air temperature changes to the corresponding simulated local air temperature in the reference case (i.e., before the

addition of the new building). The results are presented in Figure 6.6, together with the “actual” local air temperature (i.e., given by CFD simulation). According to the lines representing the error of +0.5 °C and -0.5 °C, the majority of the predicted local air temperature based on the four machine learning models fall within this range. The prediction performance of the four machine learning models appears to be good, with insignificant differences between them.

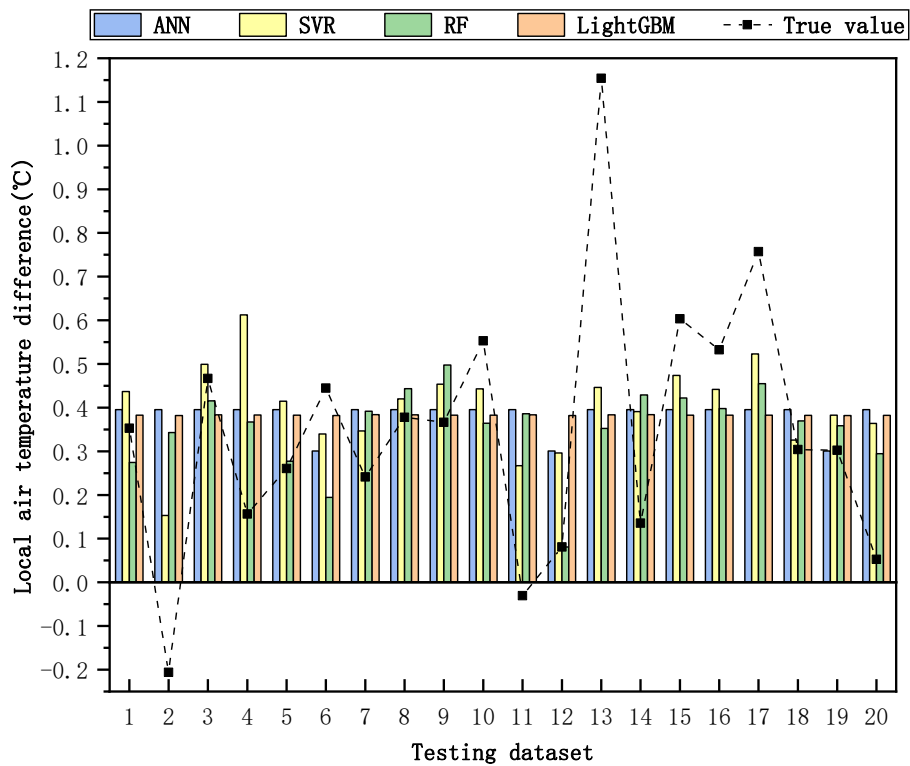


Figure 6.3 Predicted local air temperature difference given by different machine learning models

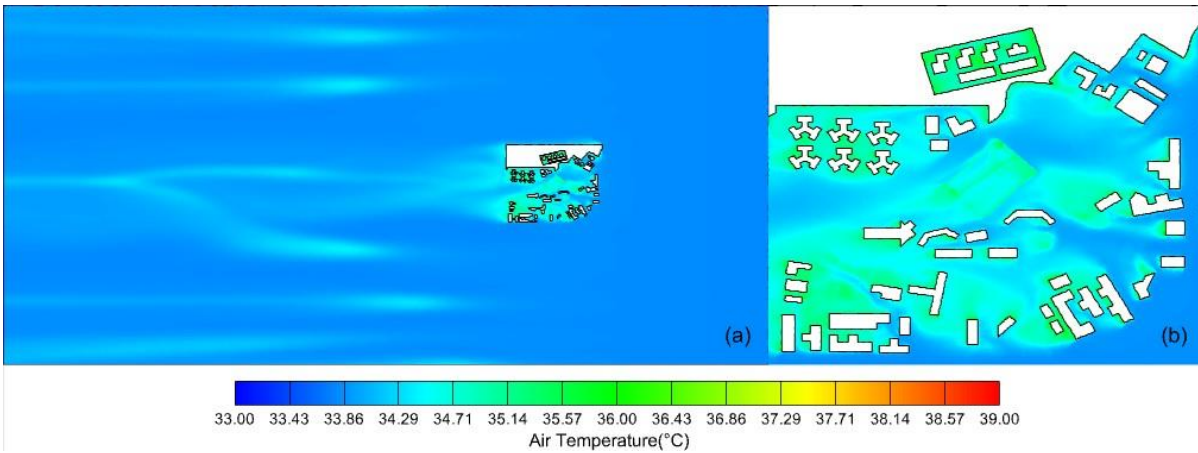


Figure 6.4 Pedestrian-level local air temperature distribution of the reference case calculated by CFD simulations (a). entire computational domain; (b). magnified view of the district without new building in development

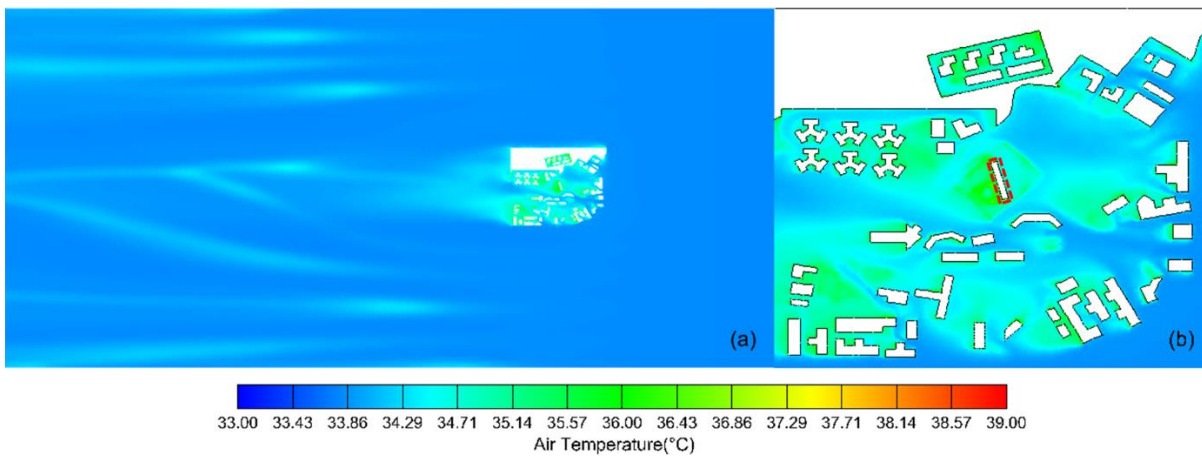


Figure 6.5 Pedestrian-level local air temperature distribution of the Case 8 calculated by CFD simulations (a). entire computational domain; (b). magnified view of the district with new building in development

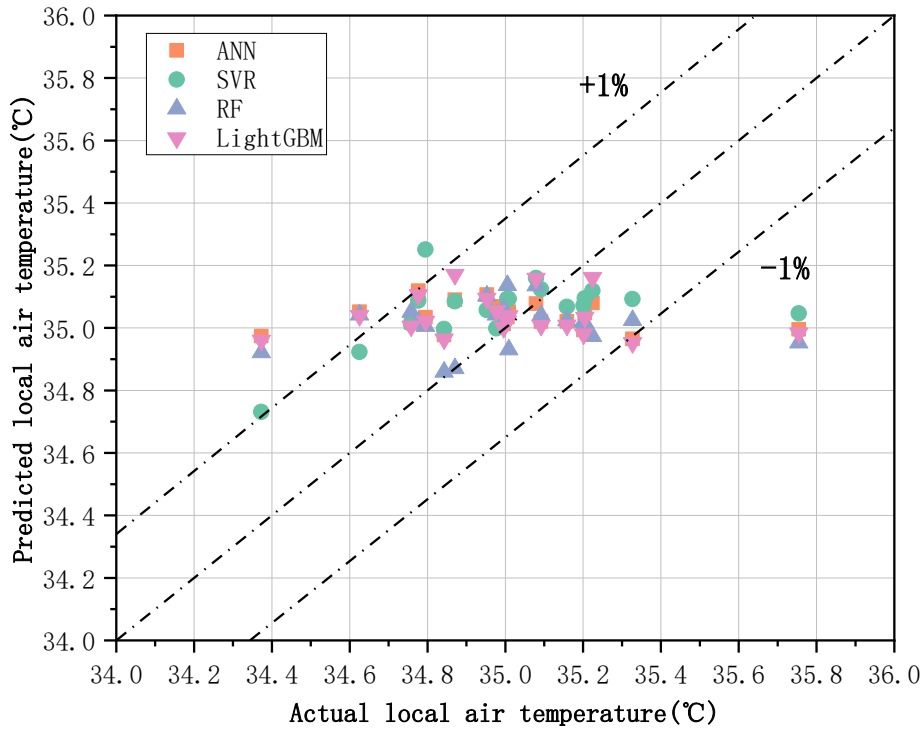


Figure 6.6 Predicted local air temperature vs actual local air temperature

6.3.2 Local wind velocity impact prediction

The predicted local wind velocity change given by different machine learning models is shown in Figure 6.7. A positive value indicates that the addition of the new building enhances the pedestrian-level local wind velocity, while a negative value means the addition of the new building reduces the pedestrian-level local wind velocity. The comparison of the pedestrian-level local wind velocity distributions (calculated by CFD simulations) before and after the addition of the new building, take Case 33 as an example, are shown in Figure 6.8 and Figure 6.9. The area concerned is marked in Figure 6.9. As shown in Figure 6.10, the actual local wind velocity change (i.e., that given by CFD simulations) fluctuates significantly between positive and negative under different test cases. The variations of the actual local wind velocity

change between each case are noticeable, ranging from -0.63 to 1.47 °C. Most of the prediction results given by the four machine learning models exhibit similar patterns. Although there are occasional significant increases or decreases in the actual local wind velocity change, the four machine learning models can mostly track the variation trends. However, the prediction results given by different models exhibit distinct characteristics. The ANN and LightGBM models are more sensitive in predicting the variation trends of the local wind velocity change, compared with the RF and SVR models. The ANN model can mostly predict the correct direction of variation, while the LightGBM model is sensitive enough to predict the peak values. Although the RF and SVR models are more sensitive in predicting the variations of local air temperature change, they lack sensitivity in predicting the impact on the local wind velocity. It can be observed that the predicted local wind velocity change given by the RF and SVR models are negative while the actual value is positive in a few cases. The discrepancies between the predicted values given by the four machine learning algorithms and the true values do not appear to be significant.

The predicted local wind velocities are calculated for the relative error analysis, by adding the predicted local wind velocity changes to the corresponding simulated local wind velocity of the reference case (i.e., before the addition of the new building). The results are presented in Figure 6.10. The dashed lines in the figure represent the relative error of +20% and -20%. It can be seen that the majority of the predicted local wind velocities based on the four machine learning models under the test cases predicted fall within this range. Though these models can

hardly provide accurate prediction results when the actual local wind velocity (i.e., given by CFD simulation) is extremely large or small, the prediction performances of the four machine learning models appear to be good, with insignificant differences between them.

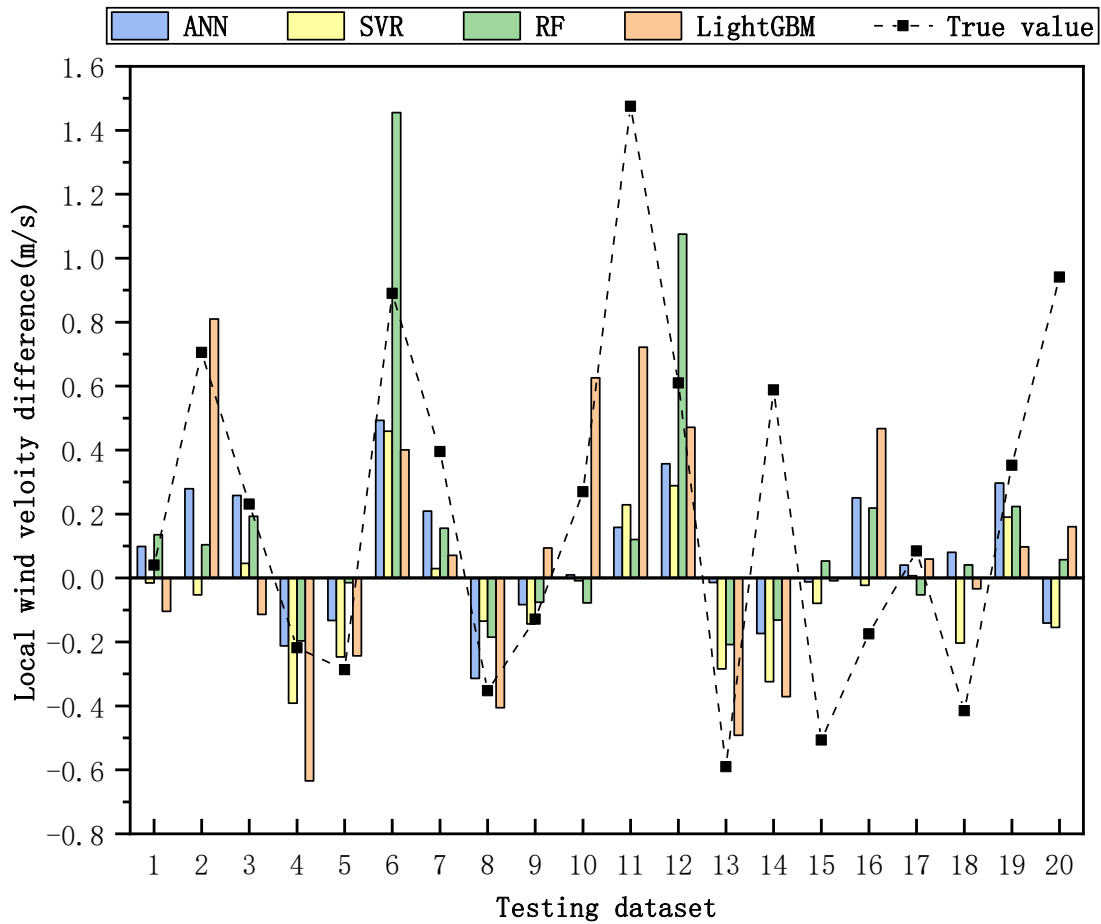


Figure 6.7 Predicted local wind velocity difference given by different machine learning models

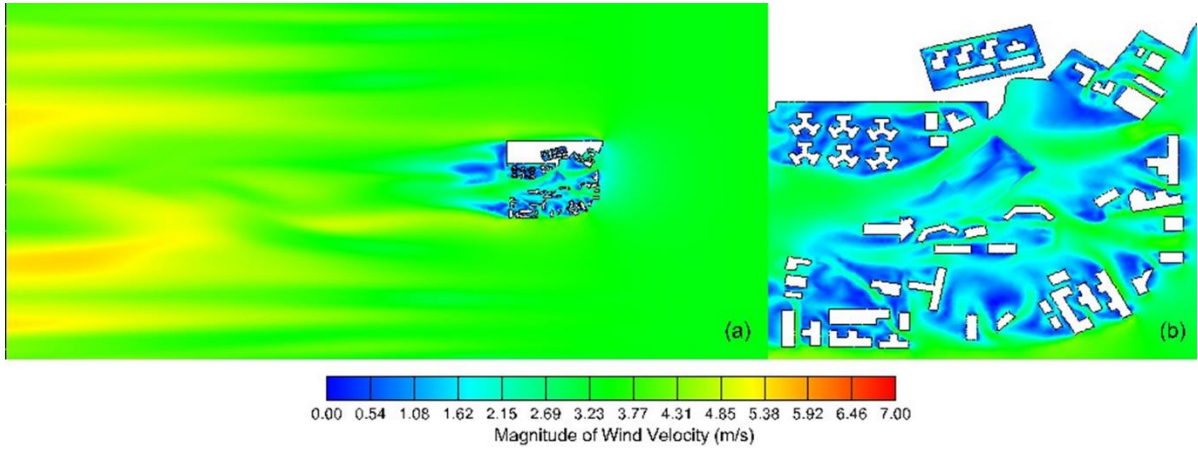


Figure 6.8 Pedestrian-level local wind velocity distribution of the reference case calculated by CFD simulations (a). entire computational domain; (b). magnified view of the district without new building in development

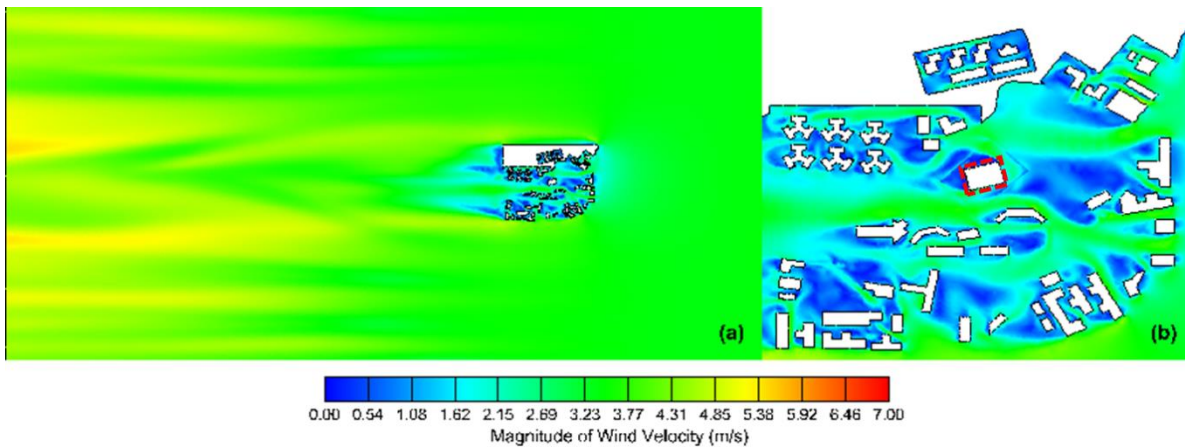


Figure 6.9 Pedestrian-level local air temperature distribution of the Case 33 calculated by CFD simulations (a). entire computational domain; (b). magnified view of the district with new building in development

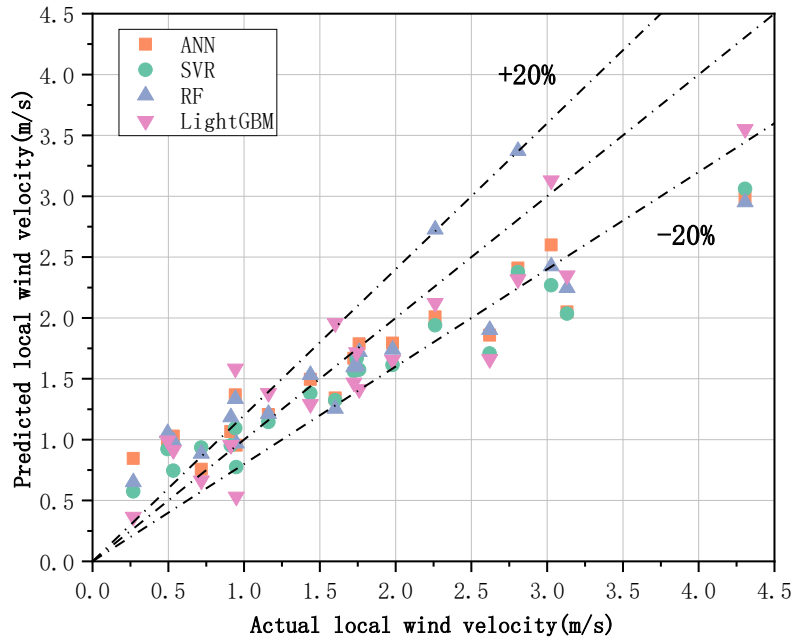


Figure 6.10 Predicted local wind velocity vs actual wind velocity

6.4 Performance validation of alternative data-driven models

6.4.1 Model performance for local air temperature impact prediction

The four machine learning models for local air temperature impact prediction are evaluated and compared in terms of the computational load and prediction accuracy. The computational load concerns two aspects, i.e., the time required for model development, and the time needed for local microclimate prediction. In this study, the computations are performed using the Scikit-learn machine learning library in Python (64 3.2.2) in a PC with an i7-3770 CPU at 3.40 GHz and Windows 7 Enterprise 64-bit OS. The total computing time required for model development using the training dataset and local air temperature impact prediction using the testing dataset is 1.72s, 0.58s, 3.83s and 0.07s respectively for the ANN, SVR, RF and LightGBM models per prediction. LightGBM proved to be the most efficient method, with its

computing time being nearly one-eighth of SVR's and one-twenty-fifth of ANN's. RF appears to be the most computationally demanding method for local air temperature impact prediction.

The predictions errors of the four machine learning models under the test cases are presented in Fig.6.11. It can be seen that the range of the prediction error for the SVR model is the smallest. But the error distributions of the four models are similar. The median values of the prediction errors of the ANN, SVR, RF and LightGBM models are 0.036°C, 0.082°C, 0.037°C, 0.054°C, respectively. The majority (25%~75%) of the prediction errors for the ANN, SVR, RF and LightGBM models fall within the ranges of -0.140~0.230°C, -0.098~0.235°C, -0.158~0.181°C, -0.117~0.238°C. This indicates that the prediction performances of the four machine learning models are commendable, with errors less than the error range of an air thermometer (i.e., $\pm 0.5^\circ\text{C}$). The MAE, MSE, RMSE and MAD of the four machine learning models in predicting local air temperature are also calculated and compared, as presented in Table 6.2. It can be seen that the SVR model exhibits the best performance. Its MAE (i.e., 0.194°C), MSE (i.e., 0.065°C), normalized RMSE (i.e., 0.187) and MAD (i.e., 0.120°C) is the smallest among the four models. The differences in MAE, MSE, normalized RMSE and MAD between the ANN, RF and LightGBM models are minimal, which are around 0.023°C, 0.019°C, 0.026, and 0.041°C higher than those of the SVR model.

The information criteria of the four machine learning models in predicting local air temperature are also calculated and presented in Table 4. It can be seen that both AIC (i.e., 50.055) and BIC

(i.e., 56.029) of the SVR model are the smallest among the four machine learning models, which indicates the best performance of balancing the model fit and complexity.

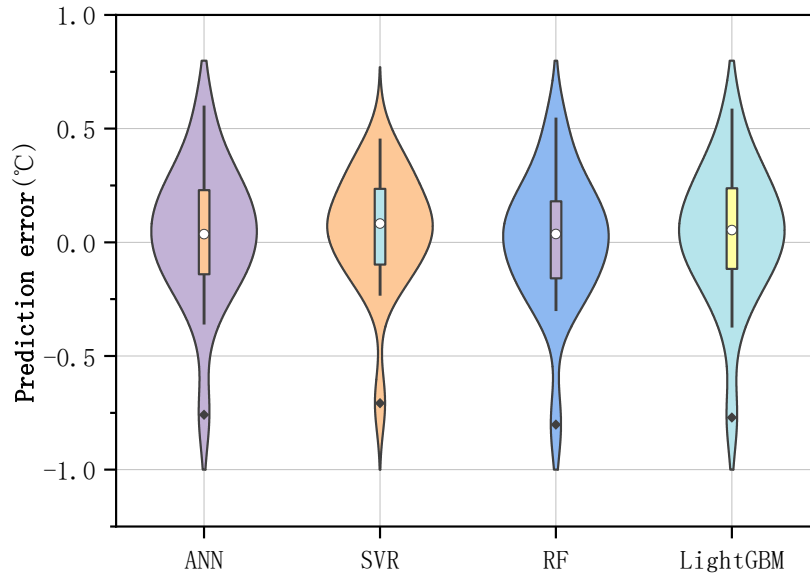


Figure 6.11 Prediction errors of different machine learning models in predicting local air temperature difference

Table 6.2 Performance of different machine learning models for local air temperature difference prediction

Metrics \ Models	MAE	MSE	normalized RMSE	MAD	AIC	BIC
ANN	0.220	0.085	0.215	0.156	50.464	56.438
SVR	0.194	0.065	0.187	0.120	50.055	56.029
RF	0.209	0.080	0.208	0.166	50.366	56.340
LightGBM	0.221	0.086	0.216	0.160	50.481	56.456

6.4.2 Model performance for local wind velocity impact prediction

The four machine learning models for local wind velocity impact prediction are also evaluated and compared in terms of the computational load and prediction accuracy. The total computing time required for model development and local wind velocity difference prediction is 2.41s,

0.55s, 3.83s and 0.07s respectively for the ANN, SVR, RF and LightGBM models per prediction. Similar to the local air temperature impact prediction model, LightGBM proved to be the most efficient method for local wind velocity impact prediction, with its computing time being less than half of SVR's and one-tenth of ANN's. RF is also the most computationally demanding method for local wind velocity impact prediction, with its computing time being fifty times higher than LightGBM's.

The prediction errors of the four machine learning models under the test cases are summarized in Figure 6.12. It can be seen that the ANN model has the smallest error range, while the LightGBM model has no obvious outlier. The error distributions of the four models are obviously different. The median values of the prediction errors of the ANN, SVR, RF and LightGBM models are -0.019m/s, -0.168m/s, 0.037m/s, 0.096m/s, respectively. The majority of the prediction errors for the ANN, SVR, RF and LightGBM models fall within the ranges of -0.328~-0.106m/s, -0.398~-0.096m/s, -0.294~-0.388m/s, 0.380~-0.163m/s, respectively. This indicates that the prediction performances of the four models are good, with the errors less than the error range of a thermoelectric anemometer for outdoor meteorological parameter detection (i.e., 0~1m/s). The MAE, MSE, normalized RMSE and MAD of the four machine learning models in predicting the local wind velocity impact are also calculated and presented in Table 5. It can be seen that LightGBM exhibits the best performance. It has the smallest MAE, MSE and normalized RMSE (0.352m/s, 0.192m/s and 0.212) among the four models, even though

the differences of MAE, MSE, normalized RMSE and MAD between the four models are minimal.

The information criteria of the four machine learning models in predicting local wind velocity are also calculated and presented in Table 6.3. It can be seen that both AIC (i.e., 52.604) and BIC (i.e., 58.578) of the LightGBM model are significant smaller than them of the other three machine learning models, which indicates the best performance of balancing the model fit and complexity.

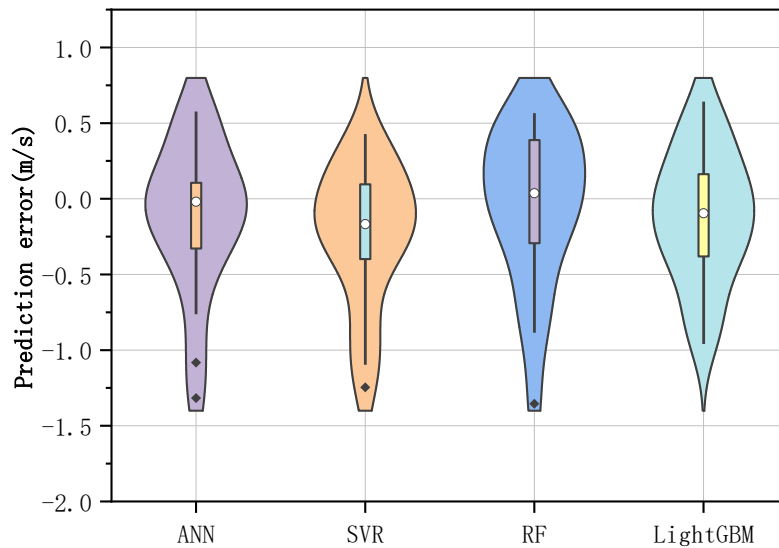


Figure 6.12 Prediction errors of different machine learning models in predicting local wind velocity difference

Table 6.3 Performance of different machine learning models for local wind velocity difference prediction

Metrics \ Models	MAE	MSE	normalized RMSE	MAD	AIC	BIC
ANN	0.355	0.252	0.243	0.256	53.788	59.762
SVR	0.372	0.258	0.246	0.248	53.911	59.885
RF	0.394	0.259	0.247	0.248	53.943	59.917
LightGBM	0.352	0.192	0.212	0.335	52.604	58.578

6.5 Discussion on the model efficiency and accuracy

In this study, the device used for computation of the machine learning models is the PC with an i7-3770 CPU running at 3.40 GHz and running Windows 7 Enterprise 64-bit OS. The instantaneous machine learning model of local microclimate prediction can allow the designer to make a local climate assessment in seconds at the early stage of building design compared with the need of over 5 hours when using CFD simulation. The total time consumption required for model development and local microclimate prediction for a single prediction is around 0.14s~7.66s. Once the development of the machine learning model completes, the prediction results can be obtained instantaneously, the time consumption of which is less than 1s. The total time consumption required for model development and local air temperature impact prediction for a single prediction is 1.72s, 0.58s, 3.83s and 0.07s respectively for the ANN, SVR, RF and LightGBM models, while the single prediction of local wind velocity impact costs 2.41s, 0.55s, 3.83s and 0.07s respectively for the ANN, SVR, RF and LightGBM models. As for the CFD simulation, the total time consumption for a single CFD simulation of the local microclimate is around 5.38 h or 320 min. The time consumption mainly includes the time for grid discretization and the time for CFD simulation. On the same device, the average time consumption for grid discretization of the 200 cases is around 20 mins. Each CFD simulation costs around five hours on the same device, which includes the automatic process of the mesh improvement, parameter setting, model simulation and results processing.

Comparing with the current deep learning models in local microclimate prediction under varied district or building designs, this study demonstrates a significant reduction in time consumption. When compared to existing GAN models, this study achieves a time reduction for model training from about 20 hours to about 2 minutes. Similarly, when compared to current CNN models, this study achieves a time reduction for model training from about 16 hours to about 2 minutes. In this study, the time consumption for the model training of local wind velocity impact is around 1.55min, 6min, 2.23min and 1.65min respectively for the ANN, SVR, RF and LightGBM models, while the time consumption for the model training of local air temperature impact is around 2.17min, 5.93min, 2.23min and 1.55min respectively. However, the development of GAN models and CNN models relies on large dataset. The number of samples based on CFD simulations used in studies with GAN models is around 500~3000 [108-110], which is 2.5~15 times consumption for data preparation of it in this study. The time consumption for existing GAN model training (including hyperparameter tuning and data processing) is around 20h using 2665 samples [109], and the prediction time is around 4~10s for a single prediction [108,109]. As for CNN models, the samples based on CFD simulations are around 3400~3500 [113,116], which is 17~18 times consumption for data preparation of it in this study. The time consumption for model training is around 16h using 3400 samples, and the prediction time is around 0.005s for a single prediction.

As for the model accuracy, the local microclimate prediction for pedestrian level in this study can keep the same order of accuracy as the GAN models and the CNN models, while greatly

reduce the time needed for data preparation, model training and prediction. The LightGBM-based local wind velocity prediction model in this study can achieve an MAE of 0.35m/s, an MSE of 0.26m/s and an RMSE of 0.44m/s at pedestrian level using the dataset of 200 CFD simulation results. The LightGBM model shows the better accuracy in the prediction of local wind velocity than SVR and RF, which is consistent with the results in previous research [18]. It was concluded that the gradient boosting regression predicted the wind velocity parameters with the higher accuracy than SVR and RF. The SVR model for local air temperature prediction proposed by this study can achieve an MAE of 0.19°C, an MSE of 0.07°C and an RMSE of 0.26°C at pedestrian level. Comparing with GAN-based local wind velocity prediction model, the MAE at the pedestrian level is 0.5m/s using the dataset of 1025 CFD simulation results [110]. In some local areas around the buildings, the MAE is more than 3.75m/s when using the dataset of 564 CFD simulation results with a prediction time of 4s [108]. The RMSE of local wind velocity prediction is around 0.16~0.63m/s using the dataset of 1025 CFD simulation results with the prediction time of 5~10s and the model training time of 20h [109]. Most of the errors in the computational domain are within the error range of a thermoelectric anemometer for outdoor meteorological parameter detection (i.e., 0~1m/s), indicating a high-accuracy prediction of local wind velocity. As for the near-instantaneous CNN prediction model of local wind velocity (the prediction time is around 0.005s) using the dataset of 3400 CFD simulation results with the model training time of 16h, though the MSE is less than 0.5m/s in the most of the computational domain, it is more than 0.5 surrounding the buildings [109].

6.6 Recommendation on the data-driven model for microclimate simulation

Based on the performance evaluation, the SVR-based local air temperature prediction model and LightGBM-based local wind velocity prediction model offer the best overall performance and are, therefore, recommended as the surrogate models for fast local microclimate impact predictions in new individual building design in Hong Kong.

As for the local air temperature impact prediction, SVR exhibits the best prediction performance in terms of prediction accuracy, whose MAE, MSE, normalized RMSE and MAD is 0.194°C, 0.065°C, 0.187 and 0.120°C respectively. SVR also exhibits the best performance of balancing the model fit and complexity to mitigate the risk of overfitting, whose AIC and BIC is 50.055 and 56.029 respectively. LightGBM and SVR are proven to be the more efficient methods among the four algorithms, whose computing time is 0.07s and 0.58s respectively. Given that the computing time for each CFD simulation is over five hours, the difference between the computing time of the LightGBM and SVR models is minimal. As for the local wind velocity impact prediction, the LightGBM model exhibits the best performance in terms of prediction accuracy, as it has the smallest MAE, MSE and normalized RMSE (0.352m/s, 0.192m/s and 0.212) among the four models. LightGBM also exhibits the best performance of balancing the model fit and complexity, whose AIC and BIC are 52.604 and 58.578 respectively. LightGBM is proven to be the most efficient method among the four algorithms in terms of the computing time. The computing time of the LightGBM model is 0.07s. Comparing with the conventional CFD simulation which requires over five hours for each

simulation, the use of the LightGBM model can significantly reduce the computing time, making the consideration of microclimate impact in building design optimization feasible.

6.7 Summary

In this chapter, machine learning-based surrogate models are developed to predict the impacts of local microclimate (i.e., local air temperature and wind velocity) due to the addition of a new individual building in high-density urban area. Two complementary machine learning-based surrogate models are identified and recommended for their high accuracy and high efficiency, including an SVR-based local air temperature model and a LightGBM-based local wind velocity model. Totally four machine learning algorithms are evaluated and compared for each model development, including ANN, SVR, RF and LightGBM. Six key influential building parameters are selected as the model inputs based on a comprehensive impact analysis made previously. 200 sets of CFD simulation data corresponding to different building designs are used for the model training and testing. The developed surrogate models can assist designers for fast and accurate prediction of the impacts on the local microclimate at the early design stage of new construction and renovation of buildings for preferred local microclimate and/or avoiding negative impacts on local microclimate. Based on the results, the major conclusions can be briefly summarized as follows.

- The machine learning models dramatically reduce computation time (from over 5 hours to less than a second) for local microclimate prediction, compared with using CFD

simulations. LightGBM and SVR are the efficient methods for both local air temperature and wind velocity prediction, while RF is the most computational expensive method.

- ANN, SVR, RF and LightGBM show good performance of local microclimate prediction, providing the same order of accuracy of CFD simulations. The prediction errors of local air temperature based on these four algorithms are below the error range of an air thermometer ($\pm 0.5^{\circ}\text{C}$), and SVR shows the best performance. The prediction errors of local wind velocity based on the four algorithms are below the error range of thermoelectric anemometer (0~1m/s), and LightGBM shows the best performance.
- The single-output prediction model of local air temperature based on SVR is recommended due to their high efficiency, high accuracy and low risk of over-fitting, The computation time is 0.58s, and its MAE and normalized RMSE (0.194 $^{\circ}\text{C}$ and 0.187) are the smallest among the four methods.
- The single-output prediction model of local wind velocity based on LightGBM is recommended due to their high efficiency, high accuracy and low risk of over-fitting. The computation time is 0.07s, and its MAE and normalized RMSE (0.352m/s and 0.212) are the smallest among the four methods.

CHAPTER 7 DEVELOPMENT OF A COORDINATED DESIGN OPTIMIZATION METHOD OF ZERO/LOW ENERGY BUILDINGS CONSIDERING THEIR INTERACTION WITH LOCAL MICROCLIMATE

This chapter presents the procedure and methods of the proposed coordinated design optimization method for improving building energy performance while mitigating the unacceptable negative impacts of local microclimate, considering the interactions between them. The local microclimate surrogate models and automated building simulation are combined with the optimizer to enhance the efficiency and generalizability. The multi-objective optimization for extensive design variables is therefore facilitated. The global optimal solutions identified are evaluated by the entropy-TOPSIS method, and the best solution is finally recommended. A case study in Hong Kong is utilized to test and validate the proposed method.

7.1 Procedure of coordinated design optimization and optimization problem formulation

The building design variables (i.e. building aspect ratio and building orientation) have opposite effects on the two objectives of energy performance-driven design and local microclimate-driven design, which will be further elaborated in Section 7.3.1. Therefore, proposed coordinated design optimization considering the mutual impacts of a building and its microclimate is essential.

7.1.1 Overall procedure and major steps

The multi-objective optimization is adopted for the coordinated optimal design of a building and its local microclimate to effectively identify the global optimal design solutions considering their mutual impacts. The detailed procedure of the coordinated design optimization is illustrated in Figure 7.1.

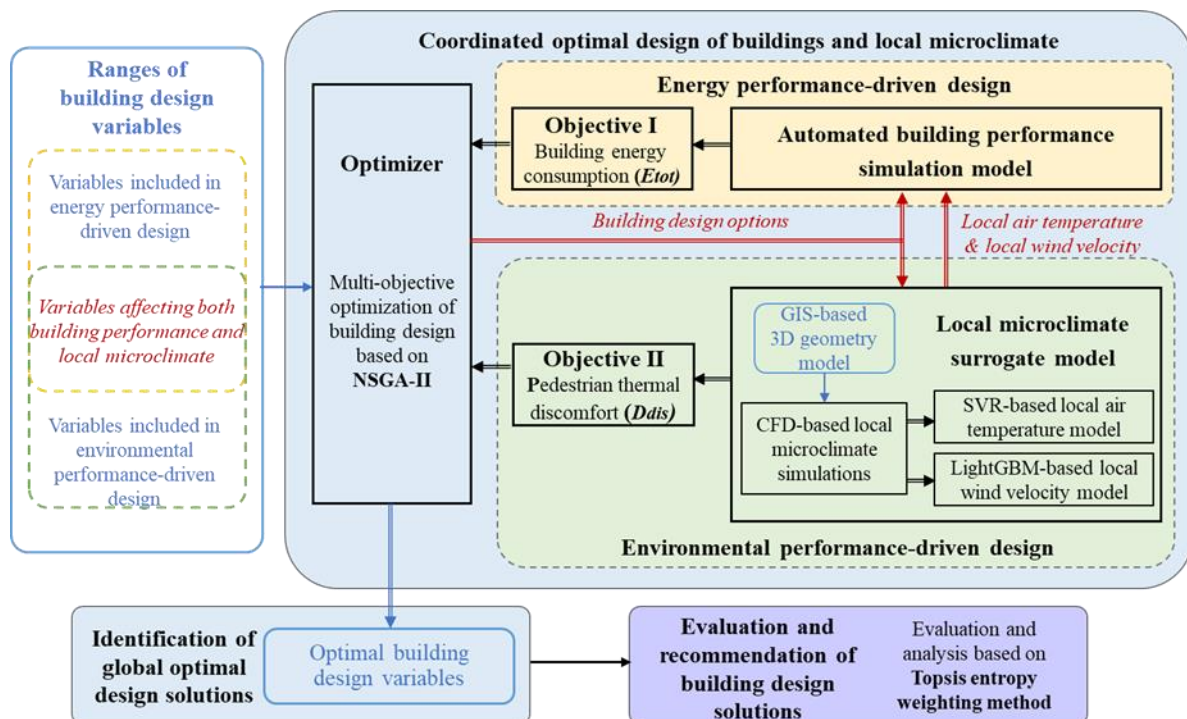


Figure 7.1 Outline of the overall research methodology and procedure

The coordinated design optimization involves the energy performance-driven design and the environmental performance-driven design. The building design variables affecting building energy performance and local microclimate are optimized. The ranges of the variables are preset for the optimizer to generate building design options. The multi-objective optimization is conducted to identify the optimal building design solutions using non-dominated

evolutionary algorithm NSGA-II [139], which minimizes the optimization objectives of both energy performance-driven design and environmental performance-driven design, subject to the satisfaction of the design constraints.

The optimization objective of energy performance-driven design is calculated using the automated building performance simulation in the software Energyplus, which is integrated with the optimizer based on the optimization technique through Eppy toolkit in Python in order to ensure the generalizability, fidelity and automation. The optimization objective of environmental performance-driven design is calculated using the local microclimate surrogate models with high accuracy and high efficiency, including an SVR-based surrogate model of local air temperature and a LightGBM-based surrogate model of local wind velocity. These surrogate models are developed based on the typical scenario of high-density urban district which can ensure the model generalizability. The results of a large number of 3D high-resolution microclimate simulations based on CFD simulation and advanced GIS spatial analysis technique are used for the surrogate model development. The prediction results of local microclimate under different building design options are provided not only for the calculation of environmental performance-driven design objective concerning the pedestrian thermal comfort, but also for the automated building energy performance simulation, in order to consider the mutual impacts between building design and local microclimate.

Based on the energy and environmental performance evaluation of the building design options, the optimizer identifies the Pareto front including a few global optimal solutions of

simultaneous building and local microclimate optimization. Finally, the Pareto optimal solutions are evaluated and the best design solution is recommended using the entropy-TOPSIS method.

In this study, two major efforts have been made to enhance the efficiency, generalizability and automation of the optimization model. Firstly, the automated building performance simulation, using the software EnergyPlus, is integrated with the optimization technique through Eppy toolkit in Python. Once design optimization is needed in a new design scenario, the building performance simulation will proceed automatically with need to modify the ranges of building design variables and settings of parameters in Python only. Secondly, the surrogate models of local microclimate are also integrated with the optimization solver, which predict the local microclimate instantaneously given the ranges of design variables for a new design scenario.

7.1.2 Formulation of the optimization problems

The coordinated design optimization problem of a building and its local microclimate is formulated as Eq. (7.1). Where, F is the design optimization objective. X is the building design variables. The subscript “*ene*” refers to the energy performance, and the subscript “*env*” refers to the environmental performance. The building design variables are optimized within their searching ranges, subject to the design constraint C as shown in Eq. (7.2).

$$\text{Minimize: } F = (F_{ene}, F_{env}) \quad (7.1)$$

$$\text{Subject to: } X_{min} \leq X \leq X_{max}$$

$$C(X) \leq 0 \quad (7.2)$$

7.2 Building design variables and optimization objectives

7.2.1 Building design variables concerned

Totally eleven building design variables affecting building energy performance and local microclimate are considered in the coordinated design optimization. They are overhang tilt angle, window SHGC, window to wall ratio, wall solar absorptance, skylight SHGC, skylight to roof ratio, building height, building aspect ratio, overall heat transfer coefficient of building envelope, building orientation and emissivity of wall. These design variables are selected based on the results of a systematic and comprehensive sensitivity analysis on the key building design parameters affecting building energy performance and local microclimate in subtropical regions in Chapter 4 and Chapter 5. They are optimized in their searching ranges as listed in Table 7.1. The ranges are determined according to the requirements of building energy efficiency [144,146,165] and the settings in previous studies [83,88,152].

Table 7.1 Design variables of coordinated optimal design of building and local microclimate

Category	Design variables	Abbreviation	Value Range	Units
Building design	Overhang tilt angle	OTA	0~180	°
	Window SHGC	WSHGC	0~0.48	W/(m ² ·K)
	Window to wall ratio	WWR	0.1~0.4	-
	Wall solar absorptance	WSA	0.1~0.9	-
	Skylight SHGC	SSHGC	0.1~0.3	W/(m ² ·K)
	Skylight to roof ratio	SRR	0~0.9	-
Building design and local microclimate design	Building height	BH	6~200	m
	Building aspect ratio	BAR	1~9	-
	Overall heat transfer	OHTC	1.1~14.0	W/(m ² ·K)

	coefficient of building envelope			
	Building orientation	BO	0~360	°
Local microclimate design	Emissivity of wall	EW	0~1	-

7.2.2 Optimization objectives

In this study, two design objectives are adopted in the coordinated design optimization. One evaluates the energy performance of the building, and the other evaluates the local environmental performance surrounding the building.

Optimization objective evaluating energy performance

The energy performance objective (F_{ene}) is formulated as shown in Eqs. (7.3), which is adopted to evaluate the building energy consumption affected by the local microclimate. The total building energy consumption includes the total electricity consumption for cooling, lighting and other equipment on a typical design day. The building design variables are optimized to minimize this objective to achieve a higher energy efficiency of the building designed. This objective is quantified by the automated building energy performance simulation under the most unfavorable weather condition, i.e., the typical summer design day under clear sky conditions, which accounts for the local microclimate effect. The typical summer design day under clear sky conditions is utilized to assess the building energy consumption under extreme climate conditions. Thus, the representative daily building energy consumption can be analyzed [88,99].

$$\begin{aligned}
F_{ene} = E_{tot} &= E_{CE} + E_{LE} + E_{EE} & (7.3) \\
&= Q_{CL}/SCOP_s + E_{LE} + E_{EE}
\end{aligned}$$

where, E_{tot} is total building energy consumption (kWh/m²). E_{CE} is the electricity consumption for cooling (kWh/m²), calculated based on the cooling demand (Q_{CL}) of the building (kWh/m²) and the overall coefficient of performance of the air-conditioning system ($SCOP_s$). In this study, $SCOP_s$ is set to 4. E_{LE} is the lighting electricity consumption (kWh/m²). E_{EE} is the electricity consumption (kWh/m²) of other electric equipment.

Optimization objective evaluating environmental performance

The environmental performance objective (F_{env}) is adopted to evaluate the pedestrian thermal discomfort under the local microclimate, which is affected by the building design. It is formulated as shown in Eqs. (7.4-7.5). The building design variables are optimized to minimize this objective to improve the outdoor thermal comfort surrounding the building. In this study, pedestrian-level refers to the position of 3.0m away from the building and at a height of 1.5m. This objective is quantified under the most unfavorable weather condition, i.e., the hottest hour in the typical summer design day under clear sky conditions with the prevailing wind condition. The hottest hour is utilized to assess the pedestrian thermal discomfort under extreme climate conditions and significantly reduce the computing cost [13,14,79,80,82]..

$$F_{env} = D_{discom} = PET_{ave} - PET_n \quad (7.4)$$

$$PET_{ave} = (PET_{male} + PET_{female})/2 \quad (7.5)$$

where, D_{dis} is the pedestrian thermal discomfort degree ($^{\circ}\text{C}$). A higher absolute value indicates a higher degree of thermal discomfort. PET_n is the neutral physiological equivalent temperature, which is set to 28°C in Hong Kong [141]. PET_{ave} is the average PET of male (PET_{male}) and female (PET_{female}). The PET_{male} and PET_{female} are calculated by `pythermalcomfort.models` toolkit in Python utilizing the developed local microclimate surrogate models..

7.3 Preprocessing of design optimization

7.3.1 The needs of coordinated design

In this section, the need of coordinated design optimization of a building and its local microclimate is elaborated. Figure 7.2 shows the relationship between the design variables and objectives of the energy performance-driven design and the environmental performance-driven design. The positive sign refers to the positive relationship between the design variable on the optimization objective, while the negative sign refers to the negative relationship. The impacts are investigated in Chapter 4 and Chapter 5. It can be seen that there are four building variables affecting both building energy performance and local microclimate. They are the building height, building aspect ratio, overall heat transfer coefficient of building envelope and building orientation. However, some of these design variables (i.e. building aspect ratio and building orientation) have opposite effects on the two optimization objectives (i.e. total building energy consumption and pedestrian thermal discomfort degree). The increase of building aspect ratio leads to higher building energy consumption but lower pedestrian thermal discomfort. Similarly, when the building orientation increases, the pedestrian thermal discomfort decreases

but the building energy consumption increases. That means a building design which has the lowest building energy consumption is probably not friendly to the local microclimate. Therefore, it is necessary to coordinate the building and local microclimate design to make a balance between the improvements of building energy performance and local microclimate.

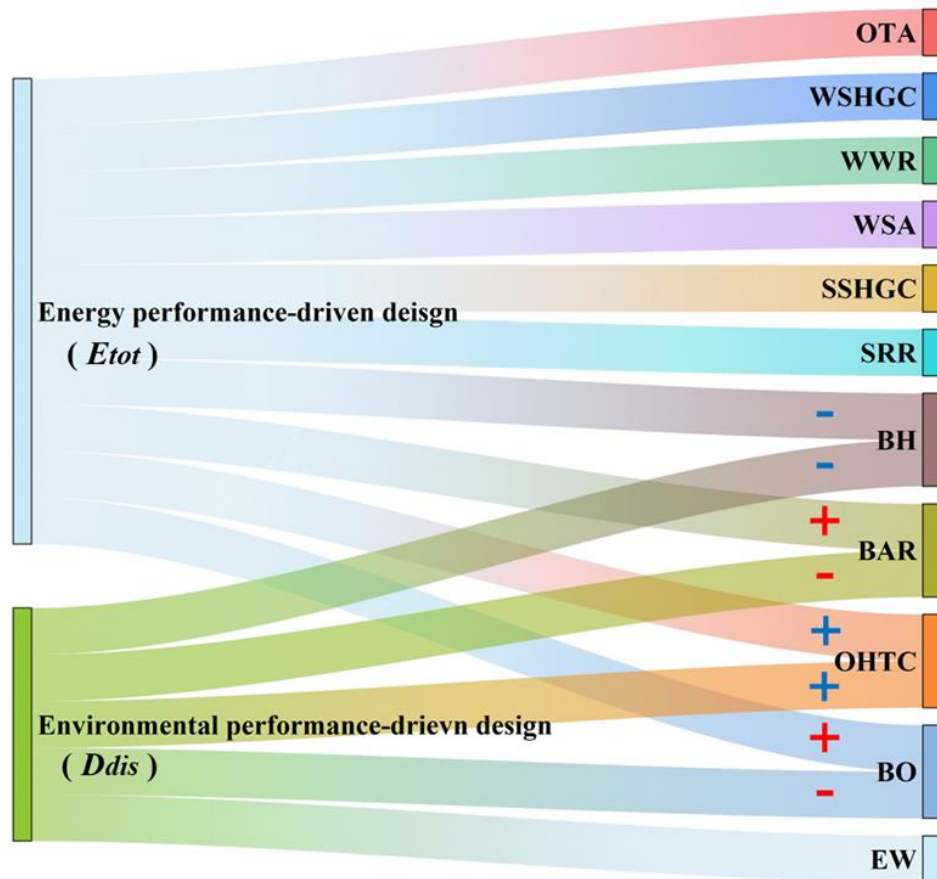


Figure 7.2 The relationship between design variables and objectives of the energy performance-driven design and the environmental performance-driven design

7.3.2 Automated building performance simulation model

The automated building performance simulation model is utilized to calculate the building energy consumption, considering the interaction with the local microclimate on a typical

summer design day. The building performance model is developed using the software EnergyPlus, which is combined with optimization techniques using the Eppy toolkit in Python. The detailed settings of the control logic and schedules for the air-conditioning and lighting systems in the EnergyPlus model are detailed in Chapter 3.

7.3.3 Local microclimate surrogate model

The fast and efficient surrogate models of local microclimate are adopted in order to significantly reduce the computing time while keeping the same order of accuracy with CFD simulations. Two single-output surrogate models are developed for the prediction of the local air temperature and wind velocity respectively, which are the major microclimate parameters affecting thermal comfort. Single-output surrogate models are adopted as different machine learning methods are appropriate for different prediction purposes and they demonstrate higher accuracy than the multi-output surrogate model in the test and validation. The inputs of the surrogate models are five key building design variables affecting local microclimate, as shown in Figure 7.2. The output of the local air temperature surrogate model is the change of the local air temperature affected by the building design. The output of the local wind velocity surrogate model is the change of the local wind velocity affected by the building design.

The surrogate models of high computing efficiency and prediction accuracy have been developed in a Chapter 6. The developed SVR-based local air temperature surrogate model has a high prediction accuracy (i.e., MAE of 0.194), and the prediction time is at the millisecond level for a single prediction. The LightGBM-based local wind velocity surrogate model has a

MAE of 0.352 and the prediction time is at the millisecond level for each prediction. The computations are performed on a PC with an i7-3770 CPU at 3.40 GHz and Windows 7 Enterprise 64-bit OS using the Scikit-learn machine learning library in Python 3.2.2 (64-bit). The generalizability and automation of the models are enhanced by incorporating various design scenarios in model training and integrating the model with the optimization technique in Python.

7.4 Design constraints of the validation case

Some constraints on the building geometry are considered in the coordinated design optimization, which are shown in Eqs. (7.6-7.7). The building volume for each building design option is fixed to provide the expected floor area for accommodating occupants, which is determined as 127,500 m³ in this study. The width of the new building (d) is constrained within a range from 15m to 125m, considering the minimum width requirements and the maximum available site area. Where, BH is the building height (m). BAR is the building aspect ratio..

$$BH \cdot BAR \cdot d^2 = 127500 \quad (7.6)$$

$$15 \ll d \ll 125 \quad (7.7)$$

7.5 Results and analysis of optimization case study

7.5.1 Optimal design results of building and its local microclimate

The purpose of the coordinated design optimization is to identify the global optimal building design solutions which minimizes both total building energy consumption (E_{tot}) and the

pedestrian thermal discomfort (D_{dis}), by considering the interactions between the building and its local microclimate. NSGA-II algorithm is adopted in this study for the multi-objective optimization due to its good performance and fast convergence speed. It has the structure of evolutionary algorithm, in which the non-dominated sorting approach and crowded comparison operator are utilized to rank and preserve the elitism solutions [107]. The initial population was set as 100 designs and 80 iterations were conducted for the evolutionary search process to converge and obtain the final Pareto solutions. .

The historical samples of building design and the identified Pareto optimal set in the coordinated design optimization are shown in Figure 7.3. A total ten global optimal solutions are identified as the Pareto front, each of which is not dominated by other solutions. The detailed optimization results are listed in Table 7.2. If the priority of the building design is to improve building energy performance, the total building energy consumption on typical summer design day can be as low as 0.060 kWh/m² and the pedestrian thermal discomfort degree would be 8.580°C. The building energy consumption under this scenario is reduced by up to 63.34% (0.104 kWh/m²) compared with historical samples. As the pedestrian thermal comfort improves, the building energy consumption increases. When the priority is to improve pedestrian thermal comfort, the pedestrian thermal discomfort degree can be as low as 7.785°C, which is reduced by 9.3% (i.e., 0.795 K) compared to the scenario where the priority is given to building energy performance, and is reduced by 19.41% (i.e., 1.875 K) compared with historical samples. The building energy consumption on typical summer design day under this

scenario is 0.066 kWh/m², which is increased by 0.007 kWh/m² compared to the scenario where the priority is given to building energy performance.

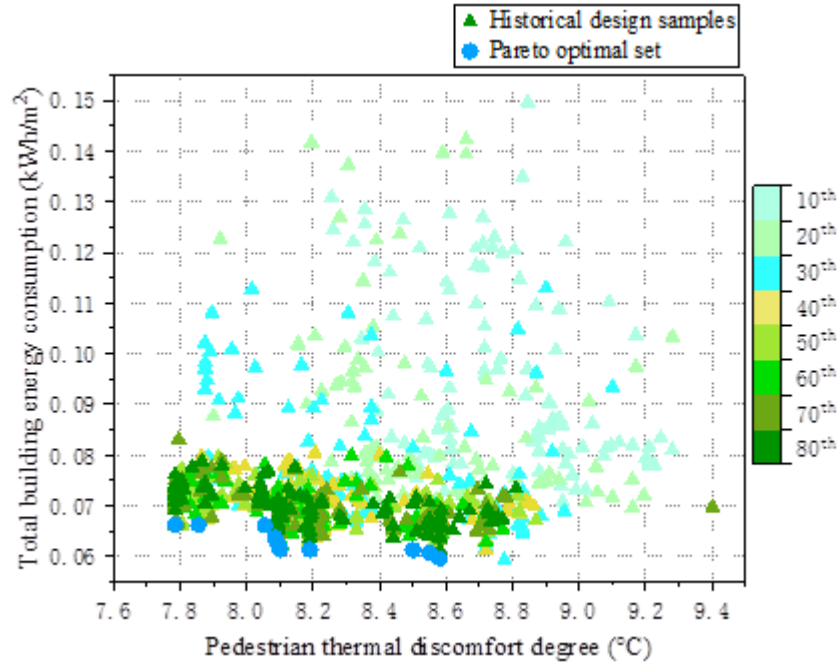


Figure 7.3 Historical design samples (1st to 80th generation) and Pareto optimal set in the coordinated optimal design

The searching range, mean value, median value and distribution of the Pareto front of the building design variables are shown in Figure 7.4. It can be observed that within a wide range of the variables to be optimized, the impact of variables on energy consumption and thermal discomfort is not monotonic. The Pareto front suggests that the optimal range for overhang tilt angle of 125~170°, window SHGC of 0.01~0.06 W/(m²·K), window to wall ratio of 0.2~0.3, wall solar absorptance around 0.1, skylight SHGC of around 0.3W/(m²·K), skylight to roof ratio of 0.01~0.05, building height of 180~191m, building aspect ratio of 1.3~1.8, overall heat transfer coefficient of building envelope of 1.5~5.7 W/(m²·K), building orientation of 8~18°,

and emissivity of wall of 0.6~0.7 can minimize the building energy consumption while mitigating the pedestrian thermal discomfort in the test case. The optimization results of window SHGC, window to wall ratio, skylight SHGC and skylight to roof ratio can effectively meet the Chinese standards for near zero energy buildings and energy efficiency of buildings in subtropical regions [144,146,165]. Within the permissible range, a larger overhang angle can more effectively block sunlight and reduce solar heat gain, thus reducing the energy consumption for cooling. A smaller wall solar absorptance can reduce the solar heat gain of the wall, consequently increasing the cooling load of the building. As for the four design variables involved in both energy performance-driven design and environmental driven-design, a larger building height and more compact building geometry (i.e., BAR of 1.3~1.8) is suggested in this optimization case, however, an optimal range of height (i.e., 180 to 191m) is proposed rather than pursuing sheer magnitude. A high-rise building with a low aspect ratio has relatively few interface areas for conducting heat exchange with the outdoors, thus reducing the building energy demands [167,168]. Meanwhile, the effects of the vertical meteorological pattern can lead to a lower air temperature and a higher wind speed in the vertical direction as height increases [169,170], thereby decreasing the cooling loads per unit area [171-174]. It is recommended to consider a lower overall heat transfer coefficient of the building envelope to alleviate both building energy consumption and pedestrian thermal discomfort, which is consistent with the result in Chapter 5. However, an optimal range (i.e., 1.5 to 5.7 W/(m²·K)) is proposed, and smaller values are not always optimal (i.e., less than 1.5 W/(m²·K)). In the test case, a windward orientation (i.e., 8~18°) helps direct wind flow along the sides of the building,

thereby reducing the surrounding air temperature and enhancing both the building energy performance and pedestrian thermal comfort.

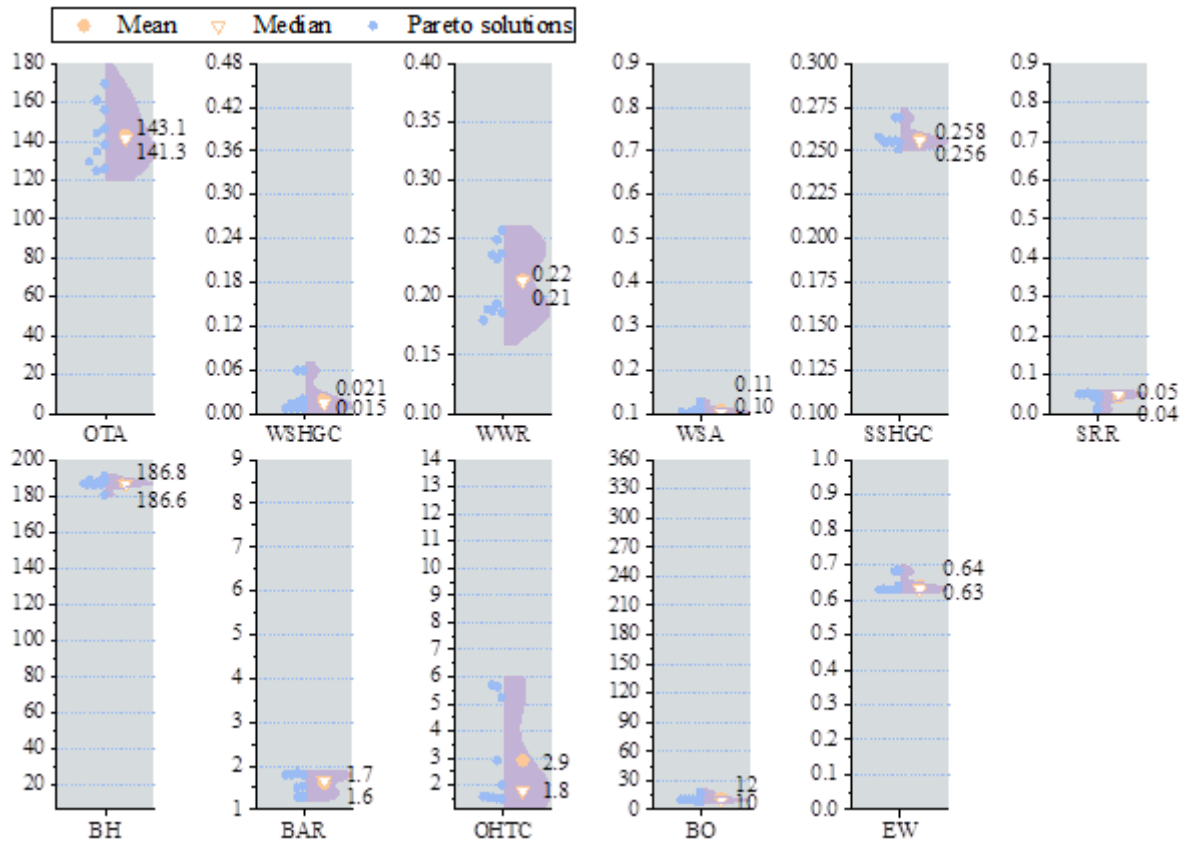


Figure 7.4 Searching range, and mean value, median value and distribution of the Pareto front of the building design variables

Table 7.2 Pareto optimal solutions of the coordinated optimal design of building and local microclimate

Scheme number	Building design variables											Optimization	
	OTA	WSHGC	WWR	WSA	SSHGC	SRR	BH	BAR	OHTC	BO	EW	E _{tot}	D _{dis}
1	169.607	0.015	0.237	0.104	0.255	0.051	188.260	1.288	1.508	18.021	0.683	0.060	8.580
2	125.856	0.015	0.257	0.107	0.256	0.052	186.339	1.298	1.510	11.664	0.682	0.061	8.550
3	161.050	0.020	0.187	0.104	0.269	0.049	180.446	1.530	1.555	8.356	0.641	0.061	8.500
4	146.566	0.007	0.233	0.108	0.251	0.007	187.638	1.328	1.578	10.028	0.629	0.061	8.190
5	156.230	0.059	0.194	0.102	0.255	0.044	186.344	1.827	2.021	8.220	0.629	0.061	8.100
6	144.303	0.014	0.188	0.127	0.256	0.053	186.343	1.848	1.597	10.466	0.629	0.062	8.095
7	124.921	0.007	0.236	0.101	0.255	0.051	188.451	1.803	2.911	10.476	0.629	0.064	8.085
8	129.530	0.007	0.189	0.104	0.256	0.036	186.343	1.803	5.242	10.459	0.630	0.066	8.055
9	138.218	0.059	0.180	0.105	0.258	0.050	190.995	1.511	5.635	17.064	0.629	0.066	7.855
10	134.863	0.007	0.249	0.115	0.269	0.014	186.842	1.794	5.704	10.341	0.629	0.066	7.785

7.5.2 Solution evaluation and recommendation based on entropy-TOPSIS method

In this study, the entropy-TOPSIS method is utilized for the evaluation of the Pareto optimal solutions obtained by the coordinated design optimization to select the best solution maximizing the overall benefits concerning building energy performance and pedestrian thermal comfort. The entropy-TOPSIS method mainly includes two stages. In the first stage, the Shannon's entropy weight method is utilized to give weight to each design variable which is determined as the evaluation criteria in this study. In the second stage, the TOPSIS technique is applied to ranking the Pareto optimal solutions.

Shannon's entropy is a measure of the uncertainty in information representing the average intrinsic information transmitted for decision-making [175]. The smaller the information entropy is, the greater the weight is. The Shannon's entropy weight method includes the process of normalization of the decision matrix, calculation of information entropy and calculation of weight for evaluation criteria. In order to make comparison across the evaluation criteria, the data in decision matrix with various criterion dimensions is normalized to the non-dimensional criterion. The decision matrix is normalized as $P=[p_{i,j}]m \times n$, $i=1,2,\dots,m$; $j=1,2,\dots,n$. In this study, $p_{i,j}$ is the value of the building design variable in a design scheme after normalization. m is determined as 14 which is the number of Pareto optimal solutions to be evaluated, n is determined as 11 which is the number of evaluation criteria. The information entropy for each evaluation criteria is formulated as Eq. (7.8). The weight given to each evaluation criteria is formulated as Eq. (7.9). The weighted matrix is formulated as Eq. (7.10).

$$E_j = -(\ln m)^{-1} \sum_{i=1}^m p_{i,j} \ln p_{i,j} \quad (7.8)$$

$$w_j = (1 - E_j) / (n - \sum_{j=1}^n E_j) \quad (7.9)$$

$$p_{i,j}^w = w_j \cdot p_{i,j} \quad (7.10)$$

The technique for order preference by similarity to ideal solution (TOPSIS) used for ranking is one of the well-known methods in multi-criteria decision making. The best solution determined by TOPSIS has the shortest distance to the positive ideal solution while having the farthest distance to the negative ideal solution. The positive ideal solution can maximize the benefit criteria and minimize the cost criteria. On the contrary, the negative ideal solution can maximize the cost criteria and minimize the benefit criteria [176]. The positive ideal solution and negative ideal solution of each evaluation criterion can be determined as Eq. (7.11-7.12), respectively. The Euclidean Distance of each Pareto optimal solution to the positive ideal solution and the negative ideal solution is formulated as Eq. (7.13-7.14). The relative closeness of each Pareto optimal solution to the ideal solution, which is used as the score of comprehensive evaluation, is formulated as Eq. (7.15). The larger the value is, the closer the solution to the positive idea solution is, and the better the design performance of the solution will be.

$$p_j^+ = \max(p_{i,j}^w), i \in [1, m] \quad (7.11)$$

$$p_j^- = \min(p_{i,j}^w), i \in [1, m] \quad (7.12)$$

$$d_i^+ = \sqrt{\sum_{j=1}^n (p_{i,j}^w - p_j^+)^2}, i \in [1, m] \quad (7.13)$$

$$d_i^- = \sqrt{\sum_{j=1}^n (p_{i,j}^w - p_j^-)^2}, i \in [1, m] \quad (7.14)$$

$$C_i = d_i^- / (d_i^+ + d_i^-), i \in [1, m] \quad (7.15)$$

In this study, minimizing the total building energy consumption and mitigating the pedestrian thermal discomfort are of equal importance. The scores of the solutions are normalized to the range of 0~1 for ranking. The larger the score obtained by the solution, the better the performance of energy and local microclimate of the building design, which will result in a

higher ranking for the solution. The rankings and scores of the ten Pareto optimal solutions evaluated by the entropy-TOPSIS method are shown in Figure 7.5. The best solution (Scheme 2) with the highest score (i.e., 0.826) is marked on the Pareto front in Figure 7.6. It can be observed that it is the building design scheme that has the total building energy consumption of 0.061kWh/m^2 (the second lowest total building energy consumption), 1835.1 kWh for the entire building on a typical summer design day, and the pedestrian thermal discomfort degree of 8.55°C (the second highest pedestrian thermal discomfort degree) on a typical summer design day. Scheme 2 has a building height of 186m, building orientation of 12° , building aspect ratio of 1.3, emissivity of wall of 0.7, heat transfer coefficient of building envelope of $1.5\text{ W}/(\text{m}^2\cdot\text{K})$, overhang tilt angle of 126° , window SHGC of $0.015\text{ W}/(\text{m}^2\cdot\text{K})$, window to wall ratio of 0.26, wall solar absorptance of 0.1, skylight SHGC of $0.256\text{ W}/(\text{m}^2\cdot\text{K})$, skylight to roof ratio of 0.05. The solution (Scheme 10) with the lowest score (i.e., 0.009) is also marked on the Pareto front in Fig. 9. It can be observed that it has the largest total building energy consumption of 0.066kWh/m^2 , 1835.1 kWh for the entire building on a typical summer design day, and the lowest pedestrian thermal discomfort degree of 7.785°C on a typical summer design day. Scheme 10 has a building height of 135m, building orientation of 10° , building aspect ratio of 1.8, emissivity of wall of 0.629, heat transfer coefficient of building envelope of $5.7\text{ W}/(\text{m}^2\cdot\text{K})$, overhang tilt angle of 135° , window SHGC of $0.007\text{ W}/(\text{m}^2\cdot\text{K})$, window to wall ratio of 0.25, wall solar absorptance of 0.1, skylight SHGC of $0.269\text{ W}/(\text{m}^2\cdot\text{K})$, skylight to roof ratio of 0.01.

As the building height is identified as the variable negative impacts on both total building energy consumption and pedestrian thermal discomfort in previous research, it is considered as a beneficial criterion in this study. That means a larger value of it can benefit both of the building energy performance and local microclimate, as proposed in Scheme 2. Meanwhile, as the overall heat transfer coefficient has positive impacts on both total building energy

consumption and pedestrian thermal discomfort, it is therefore determined as the cost criteria to be minimized in this study, as proposed in Scheme 2. When compared to historical building design solutions, the recommended best solution (Scheme 2) can save up to 62.9% (0.103 kWh/m² of total building energy consumption and 3109.4 kWh for the entire building on a typical summer design day, while mitigating pedestrian thermal discomfort by up to 11.5% (1.11K) to prevent unacceptable extreme weather.

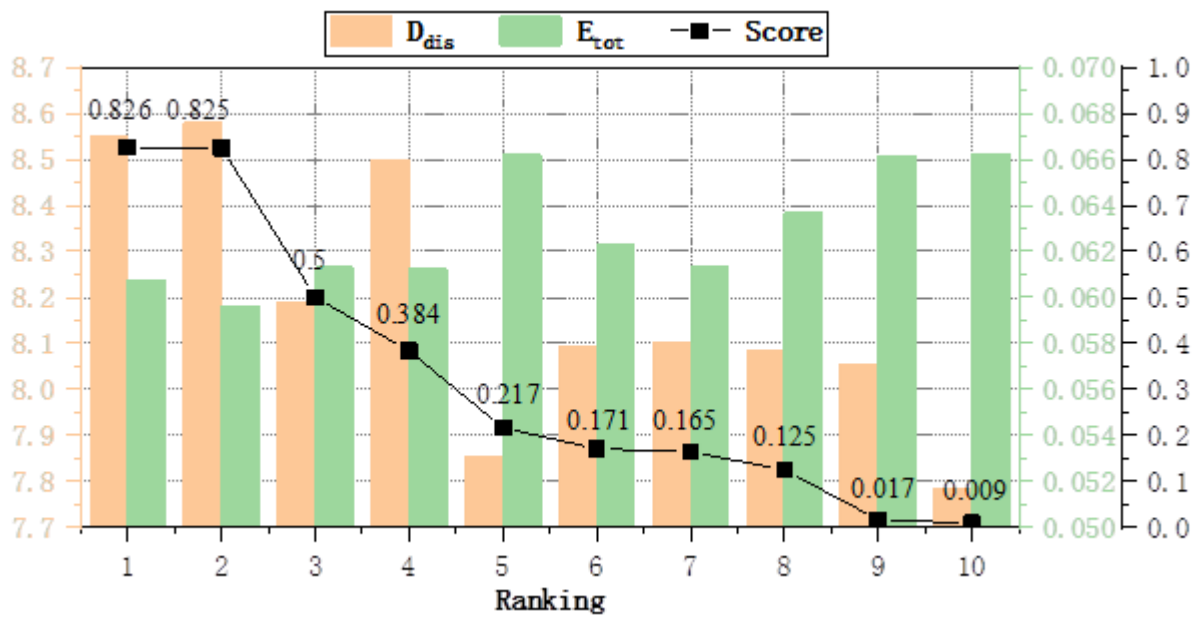


Figure 7.5 Rankings and scores of the Pareto optimal solutions evaluated by entropy-TOPSIS method

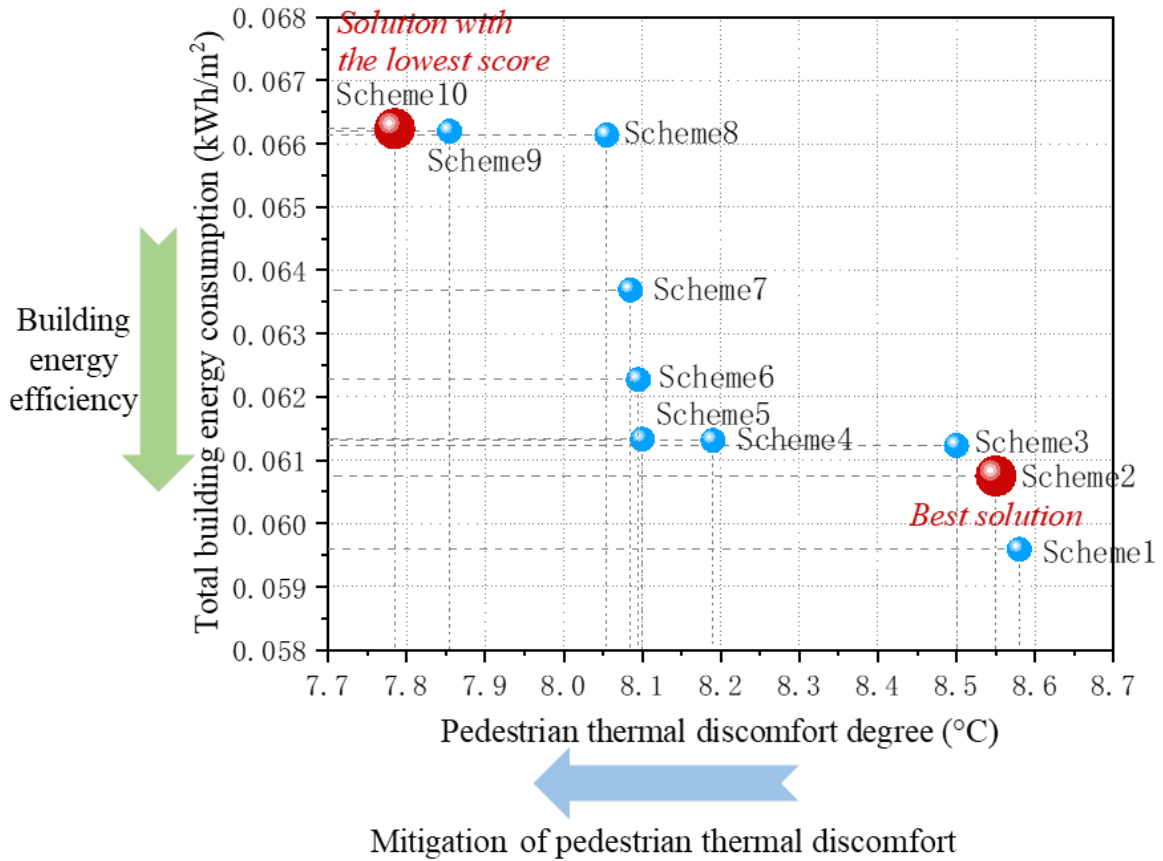


Figure 7.6 The best solution on the Pareto front

7.5.3 Discussion on optimization complexity and computation cost

In this study, the computing time of the design optimization can be reduced by 99.98% (i.e., from 42684.44 to 8.89 hours) compared with that using conventional simulation methods. The performance evaluation of each building design option, including the automated building performance simulation and the surrogate model-based local microclimate simulation, totally costs about 4 seconds. In this coordinated optimal design, a total of 8000 evaluations including 100 populations for 80 generations are conducted to converge, which takes about 8.89 hours. As for the conventional performance evaluation utilizing EnergyPlus and CFD simulations, the total computing time consumption is estimated to be around 42684.44 hours, given that each EnergyPlus and CFD simulation take about 4s and 5.33 hours (19204 seconds) respectively. The device used for computation is a PC with an i7-3770 CPU at 3.40 GHz and Windows 7

Enterprise 64-bit OS. The coordinated design optimization, automated building performance simulation model and local microclimate surrogate model development are conducted in Python 3.2.2 (64-bit).

Even taking into account the computing time for surrogate model development, the proposed method can still save 41608.75 hours and 97.48% of the total computing time for the coordinated design optimization compared with the conventional simulation methods (i.e., from 42684.44 to 1075.69 hours). The utilization of the surrogate models for local microclimate prediction saves a large amount of time compared with the time-consuming CFD simulation. Once the model development completes, the prediction time is at millisecond level. To develop the surrogate models, totally 200 high-resolution CFD simulations are proceeded for obtaining the training dataset. Each CFD simulation, including the automatic process of mesh improvement, parameter setting, model simulation and result processing, takes about 5.33 hours using Fluent 2019 (R3). The total time for developing the SVR-based local air temperature surrogate model (including the time for hyperparameter tuning and data processing) is around 1.65min, while the time for developing the LightGBM-based local wind velocity surrogate model is around 5.93 minutes. Thus, the development of the local microclimate surrogate models totally costs 64,008 minutes (i.e., 3,840,455 seconds).

In order to weigh up the computational cost in the design optimization, a linear model (as shown in Figure 7.7) is developed to make a comparison of the proposed method in this study and the traditional method. Where, x is the sampling design solutions (i.e., generations*populations) included in the design optimization. $C1$ is the computing time for the traditional method. $C2$ is the computing time including that for surrogate model development. It can be observed in Fig. 10 that when the number of samples exceeds 200, the proposed method in this study has a significant advantage over the traditional method in terms of computational efficiency. For the design optimization involving numerous design variables

(i.e., 11 in this study), adequate iterations and samplings are necessary to converge and identify the global optimum solution, and to avoid local optimum. The proposed method in this study can provide the designers with a comprehensive and efficient analysis of building design and local microclimate considering the interaction between them.

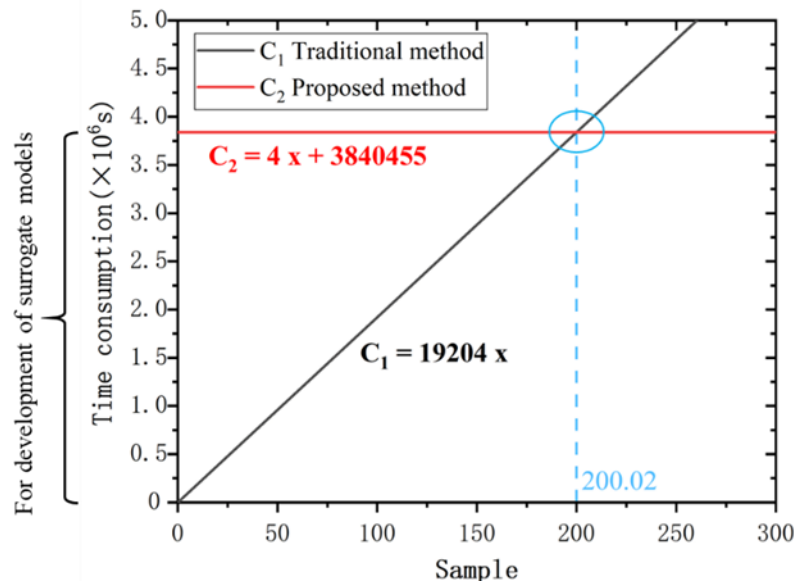


Figure 7.7 Comparison of time consumption for traditional method and proposed method

7.6 Summary

In this chapter, a coordinated design optimization method is proposed for improving building energy performance while mitigating the unacceptable negative impacts of local microclimate, considering their mutual impacts. The automated optimization solver combines the surrogate models of local microclimate and the building performance simulation software EnergyPlus with the optimization technique through Eppy toolkit in Python, which enhances the efficiency, generalizability and automation of the optimization model. The multi-objective optimization using NSGA-II for extensive design variables is therefore facilitated. The Pareto optimal solution set is identified by NSGA-II, reaching the compromise design solutions of building energy performance and pedestrian thermal comfort. The solutions are evaluated by the entropy-TOPSIS method, and the best solution is finally recommended. The case study in Hong

Kong is utilized to test and validate the proposed method. The coordinated optimal design proposed in this study can fill the gap of the simultaneous design optimization of building and local microclimate and provide global optimal design solutions to improve building energy performance while improving the local microclimate and/or avoiding unacceptable negative impacts in an efficient, generic and automatic way. Based on results of the optimization case study, the major conclusions can be briefly summarized as follows.

- The coordinated design optimization building and its local microclimate is necessary when some building design variables lead to conflicting impacts. The Pareto optimal solutions identified by the proposed method can reach compromise building design solutions of energy efficiency and pedestrian thermal comfort, which and help to save total building energy consumption about 59.5~63.6% ($0.097\sim 0.104\text{kWh/m}^2$) while mitigating the pedestrian thermal discomfort about 11.2~19.4% ($1.08\sim 1.88\text{K}$) on typical summer design day.
- The Pareto front suggests the optimal ranges of building design variables that can minimize the building energy consumption while mitigating the pedestrian thermal discomfort in the test case in subtropical areas (i.e., window to wall ratio of 0.2~0.3, wall solar absorptance around of 0.1, skylight to roof ratio of 0.01~0.05, building height of 180~191m, building aspect ratio of 1.3~1.8, overall heat transfer coefficient of building envelope of 1.5~5.7 $\text{W}/(\text{m}^2\cdot\text{K})$, and building orientation of 8~18°).
- The best design solution recommended by the entropy-TOPSIS method, with a larger building height and a smaller overall heat transfer coefficient within the optimal range, can save up to 62.9% (0.103 kWh/m^2) of total building energy consumption and 3109.4 kWh for the entire building on a typical summer design day, while mitigating pedestrian thermal discomfort by up to 11.5% (1.11K) to prevent unacceptable extreme weather.

- The coordinated design optimization method proposed in this study can reduce the computation time by 99.98% (i.e., from 42684.44 to 8.89 hours), and reduce the total computational cost by 97.48% (i.e., from 42684.44 to 1075.69 hours) compared with that using conventional simulation methods. When the samples exceed 200, the proposed method has a great advantage over the traditional method in time saving.

In this study, only the most unfavorable weather condition is used to evaluate the coordinated optimal design performance. This approach assesses representative pedestrian thermal discomfort and total building energy consumption under extreme climate conditions while significantly reducing computing costs. Performances under other conditions are not considered, and annual total building energy consumption is not addressed. The optimization results are validated with a test case in subtropical regions, and recommendations are provided for these areas.

CHAPTER 8 CONCLUSION AND FUTURE WORK

This chapter presents the main contributions of this PhD project, and the conclusions of the work conducted in this PhD project are summarized. The recommendations for future research on the research subjects are concerned in the end.

8.1 Main contribution of this study

This PhD study proposed the identification of the most influential design parameters of zero/low energy buildings considering the impacts of climate and building height, the mutual impacts between zero/low energy building design and the local microclimate, the local microclimate surrogate models and coordinated design optimization method for the zero/low energy building and local microclimate considering the mutual impacts. The main contributions are summarized as follows:

1. A systematic and comparative study on the key design parameters of zero/low energy building envelopes is conducted. The most influential design parameters of high-rise and low-rise buildings in different climate zones are identified by sensitivity analysis and the impacts of climate and building height are studied and compared. The key design parameters affecting winter thermal discomfort in the climate zones typically without heating provision are also identified. The impact of thermal bridge on building energy performance is further investigated.
2. The mutual impacts between zero/low energy building design and the local microclimate considering the interactions are investigated, and the major influential building parameters on both local microclimate and building energy performance in subtropical urban area are identified. A large number of high-resolution microclimate and building simulations based on advanced GIS spatial analysis technique are performed under different building designs

for the mutual impact assessment. A global sensitivity analysis is conducted to identify the major influential building parameters.

3. Machine learning-based surrogate models with high efficiency and high accuracy are developed to predict the impacts on local microclimate (i.e., local air temperature and wind velocity) due to the addition of a new individual building. Four machine learning algorithms are evaluated and compared for the model development, including ANN, SVR, RF, and LightGBM.
4. A coordinated design optimization method is proposed for zero/low energy building and local microclimate to effectively identify the global optimal design solutions considering the interactions between them. The automated building simulation and local microclimate surrogate models are combined with the optimizer to enhance the efficiency and generalizability. The multi-objective optimization for extensive design variables is therefore facilitated. The Pareto optimal solutions obtained are evaluated by the entropy-TOPSIS method, and the best solution is finally recommended.

8.2 Conclusions

Conclusions on identification of key design parameters of zero/low energy buildings

1. The key design parameters affecting energy performance of a building are significantly different in different climate zones and for different building morphology (i.e., high-rise and low-rise in this study).
2. The highly sensitive envelope design parameters of high-rise buildings are related to the envelope components including overhang, window and wall in all climate zones.
3. The highly sensitive envelope design parameters of low-rise buildings are related to the envelope components including skylight, roof and ground in all climate zones.

4. Wall thermal absorptance is a key parameter affecting building energy performance in all climate zones, which has been ignored before.

Conclusions on mutual impacts of zero/low energy building design and local microclimate

1. Strong mutual impacts exist between the new building design and urban local microclimate. In this study, different building designs lead to significant variations of local wind velocity (i.e., -0.95~+4.51 m/s), air temperature (i.e., -0.60~+1.17 K), and pedestrian thermal discomfort degree (i.e., 13.75~22.65 °C). The local microclimate results in a change in the building energy consumption from -41.75kJ/m² to 291.54kJ/m².
2. The major influential parameters on local air temperature, wind velocity and pedestrian thermal discomfort are rather different. The major influential parameters on local air temperature are building orientation and wall emissivity, while the major influential parameters on local wind velocity are building height and aspect ratio. As for the pedestrian thermal discomfort, the major influential parameters include building height and overall heat transfer coefficient of building envelope.
3. The major influential parameters on both local microclimate and building energy performance are building height and overall heat transfer coefficient of building envelope. Although the ranking orders of the building parameters affecting pedestrian thermal discomfort and building energy consumption are similar, the correlations between the parameters and the performance are significantly different. Therefore, it is necessary to consider the mutual impacts between building design and local microclimate in the design of new buildings to improve building energy performance while minimizing the impacts on the local microclimate.

In this study, the thermal characteristics of the building for building performance simulation in EnergyPlus, such as the specific heat capacity, density, thickness, thermal absorptance, solar

absorptance, and visible absorptance, are assumed as constant values, the impacts of which on the microclimate are ignored and could be investigated in future work. The representation of trees and roads in the study area is simplified to save computational resources.

Conclusions on generic data-driven model of local microclimate

1. The machine learning models dramatically reduce computation time (from over 5 hours to less than a second) for local microclimate prediction, compared with using CFD simulations. LightGBM and SVR are the efficient methods for both local air temperature and wind velocity prediction, while RF is the most computational expensive method.
2. ANN, SVR, RF and LightGBM show good performance of local microclimate prediction, providing the same order of accuracy of CFD simulations. The prediction errors of local air temperature based on these four algorithms are below the error range of an air thermometer ($\pm 0.5^{\circ}\text{C}$), and SVR shows the best performance. The prediction errors of local wind velocity based on the four algorithms are below the error range of thermoelectric anemometer (0~1m/s), and LightGBM shows the best performance.
3. The single-output prediction model of local air temperature based on SVR is recommended due to their high efficiency and high accuracy, The computation time is 0.58s, and its MAE and RMSE (0.194 and 0.255) are the smallest among the four methods.
4. The single-output prediction model of local wind velocity based on LightGBM is recommended due to their high efficiency and high accuracy. The computation time is 0.07s, and its MAE and RMSE (0.352 and 0.439) are the smallest among the four methods.

Conclusions on coordinated design optimization

1. The coordinated design optimization building and its local microclimate is necessary when some building design variables lead to conflicting impacts. The Pareto optimal solutions identified by the proposed method can reach compromise building design solutions of

energy efficiency and pedestrian thermal comfort, which and help to save total building energy consumption about 59.5~63.6% (0.097~0.104kWh/m²) while mitigating the pedestrian thermal discomfort about 11.2~19.4% (1.08~1.88K) on typical summer design day.

2. The Pareto front suggests the optimal ranges of building design variables that can minimize the building energy consumption while mitigating the pedestrian thermal discomfort in the test case in subtropical areas (i.e., window to wall ratio of 0.2~0.3, wall solar absorptance around of 0.1, skylight to roof ratio of 0.01~0.05, building height of 180~191m, building aspect ratio of 1.3~1.8, overall heat transfer coefficient of building envelope of 1.5~5.7 W/(m²·K), and building orientation of 8~18°).
3. The best design solution recommended by the entropy-TOPSIS method, with a larger building height and a smaller overall heat transfer coefficient within the optimal range, can save up to 62.9% (0.103 kWh/m²) of total building energy consumption and 3109.4 kWh for the entire building on a typical summer design day, while mitigating pedestrian thermal discomfort by up to 11.5% (1.11K) to prevent unacceptable extreme weather.
4. The coordinated design optimization method proposed in this study can reduce the computation time by 99.98% (i.e., from 42684.44 to 8.89 hours), and reduce the total computational cost by 97.48% (i.e., from 42684.44 to 1075.69 hours) compared with that using conventional simulation methods. When the samples exceed 200, the proposed method has a great advantage over the traditional method in time saving.

In this study, only the most unfavorable weather condition is used to evaluate the coordinated optimal design performance. This approach assesses representative pedestrian thermal discomfort and total building energy consumption under extreme climate conditions while significantly reducing computing costs. Performances under other conditions are not considered, and annual total building energy consumption is not addressed. The optimization

results are validated with a test case in subtropical regions, and recommendations are provided for these areas.

8.3 Recommendations for future work

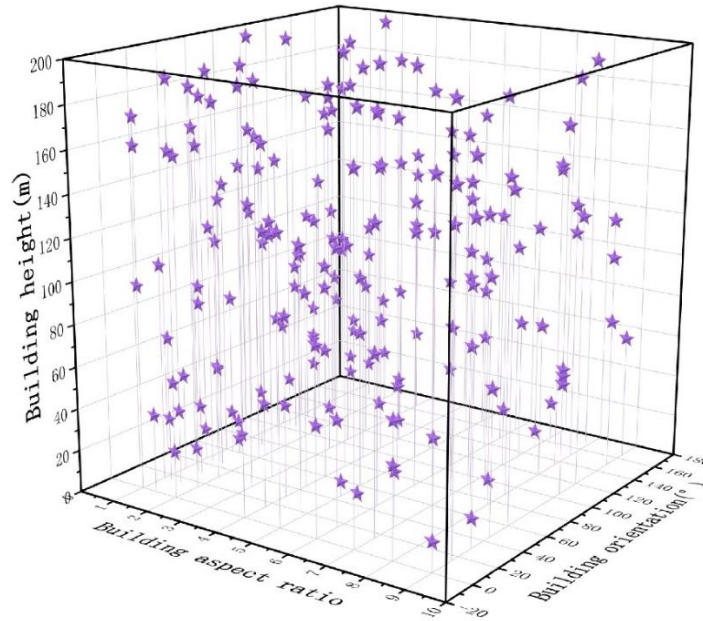
This PhD study has made significant efforts to address the mutual impacts between zero/low energy buildings and the local microclimate in the coordinated design optimization of them. In future studies, more efforts can be made on the following aspects to further enhance the methods and the convenience for practical applications.

1. The coordinated design optimization in this study mainly concerned about building energy efficiency and pedestrian thermal comfort, while the indoor thermal comfort and life cycle cost of zero/low energy buildings, which are also significant in design practices, are not addressed in this study. Therefore, the indoor thermal comfort and the life cycle cost of the zero/low energy building can be taken into consideration in coordinated design optimization of building and its local microclimate
2. In this study, the variations of local air temperature affecting the indoor air temperature play a role in the coordinated natural ventilation and air-conditioning controls in building simulation. However, the local wind velocity which can affect the natural ventilation is not concerned in natural ventilation control. Therefore, the natural ventilation control strategies considering the impact of local wind velocity can be proposed to enhance the natural ventilation and energy efficiency of zero/low energy building
3. The zero/low energy building adopts the cooling system using water-cooled electric chillers in this study. Renewable energy systems, such as photovoltaic power generation, are commonly utilized in the design of zero/low energy buildings. Therefore, the coordinated design optimization is needed to make trade-offs between the power generation, the energy consumption, and the impacts on the local microclimate in future

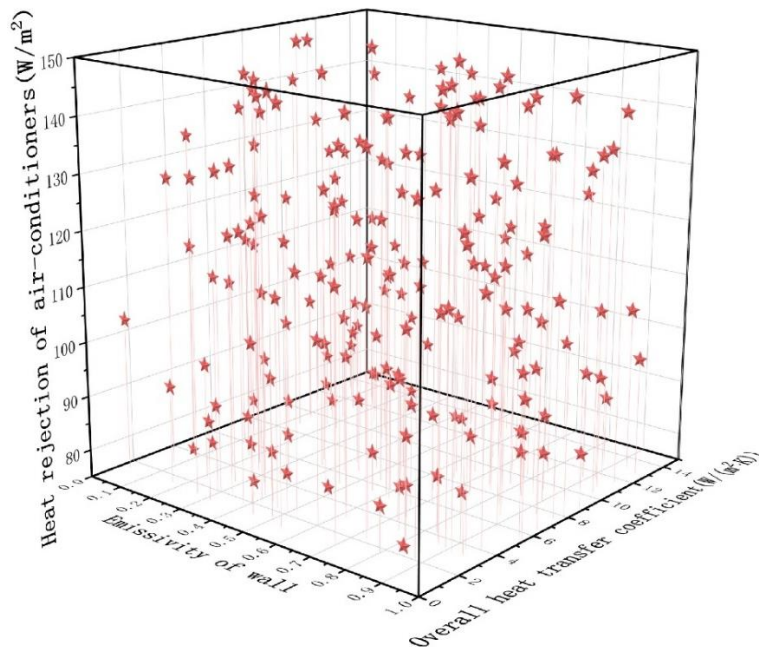
zero/low energy building design in high-density cities to facilitate the achievement of carbon neutrality.

4. The impacts of local microclimate on building energy performance are significant. Therefore, the impacts of local microclimate variations should not be ignored in energy-saving strategies. In the future studies, optimal energy management strategies considering the impacts of local microclimate variations will be proposed.

APPENDIX



(a)



(b)

Figure A1 Distribution of the 200 scenarios generated by Latin hypercube sampling method

(a). building morphology; (b). building thermal characteristics.

Table A1 200 scenarios generated by Latin hypercube sampling method

Scenario	Building height	Building orientation	Building aspect ratio	Overall heat transfer coefficient of building envelope	Emissivity of wall	Heat rejection of air-conditioners
1	15	45	1	0.657	8.305	149.548
2	7	60	1.4	0.633	8.348	145.232
3	134	0	5	0.076	3.917	75.847
4	97	90	1	0.640	9.843	137.288
5	125	15	5	0.114	4.351	77.165
6	53	105	9	0.063	7.311	80.455
7	35	15	1.5	0.236	4.640	119.782
8	178	120	7	0.089	10.980	79.247
9	129	45	1.5	0.586	6.026	94.245
10	156	75	1.2	0.036	13.647	91.987
11	107	60	8	0.141	5.888	144.532
12	154	135	1.2	0.060	13.392	87.873
13	128	120	9	0.445	10.169	129.703
14	17	165	1.5	0.407	2.373	145.503
15	176	45	1	0.825	4.170	84.923
16	197	165	2	0.313	1.269	89.259
17	31	120	4	0.777	10.261	143.123
18	188	45	1.2	0.796	3.042	111.163
19	191	135	2	0.267	9.944	130.444
20	36	75	5	0.561	5.522	82.044
21	75	120	3	0.638	8.788	103.946
22	67	135	7	0.392	2.758	124.880
23	146	30	9	0.326	5.002	81.630
24	14	0	9	0.115	8.413	79.609
25	23	135	2	0.179	10.448	117.717
26	71	135	1.5	0.021	9.898	116.974
27	11	30	6	0.831	7.501	149.040
28	109	45	1.4	0.012	7.805	110.737
29	70	165	4	0.342	4.651	117.877
30	113	150	6	0.680	10.019	86.931
31	185	30	6	0.844	8.493	86.619
32	89	105	1.5	0.593	5.702	97.682
33	165	30	1.4	0.433	2.488	84.265
34	103	15	1	0.323	2.186	121.119

35	183	60	2	0.188	5.083	82.495
36	58	120	1.4	0.782	9.126	129.247
37	189	90	4	0.544	1.156	146.579
38	174	0	1	0.513	8.067	112.822
39	186	75	1	0.192	5.572	132.556
40	191	45	8	0.092	12.445	85.477
41	52	0	6	0.534	11.105	79.896
42	20	60	1.2	0.138	6.777	90.588
43	33	165	1	0.756	3.455	101.580
44	83	30	1.5	0.398	8.003	103.210
45	134	30	3	0.688	11.405	96.947
46	71	150	9	0.929	3.717	136.826
47	84	15	7	0.848	12.223	92.534
48	157	30	1.5	0.506	2.532	117.085
49	46	30	8	0.518	1.863	82.915
50	196	75	6	0.025	1.479	102.773
51	90	165	1.5	0.651	12.565	111.566
52	153	75	1.4	0.256	10.959	142.172
53	132	60	1	0.221	12.387	123.790
54	160	120	2	0.568	12.259	121.205
55	124	150	8	0.218	11.700	82.554
56	141	105	4	0.770	8.223	113.689
57	8	150	7	0.968	12.875	96.339
58	105	135	1.4	0.933	7.570	109.068
59	164	150	1.2	0.339	9.369	148.674
60	25	165	2	0.648	10.763	143.353
61	91	30	1.5	0.317	10.500	102.236
62	39	165	3	0.181	12.194	81.334
63	21	90	3	0.241	4.837	145.051
64	69	15	1.2	0.291	13.582	87.369
65	135	75	6	0.475	5.257	135.708
66	161	0	1	0.215	6.733	98.769
67	116	75	1.2	0.285	12.047	99.337
68	92	60	4	0.681	5.444	93.045
69	115	45	1.2	0.736	7.717	116.101
70	49	15	4	0.230	13.686	91.786
71	152	60	9	0.916	3.227	147.171
72	176	120	5	0.273	4.291	125.635
73	76	165	1.5	0.983	9.035	84.609
74	107	75	8	0.947	10.893	95.166
75	123	45	3	0.503	4.567	126.288
76	172	105	9	0.942	3.324	126.668

77	86	30	4	0.728	2.282	140.647
78	119	135	1	0.451	4.895	128.147
79	62	60	4	0.840	7.484	109.940
80	39	165	1	0.747	8.621	94.676
81	148	75	5	0.998	5.385	99.650
82	187	15	2	0.907	5.850	137.143
83	128	15	4	0.537	6.395	122.603
84	118	90	6	0.380	2.406	77.946
85	29	120	1.4	0.365	6.142	110.393
86	28	120	7	0.809	2.840	93.562
87	194	0	4	0.489	1.588	147.630
88	97	0	1	0.285	4.445	140.142
89	150	150	5	0.528	8.677	108.070
90	126	105	7	0.763	13.930	122.801
91	117	45	3	0.246	13.190	136.176
92	65	105	4	0.858	8.916	97.926
93	198	75	4	0.610	6.366	135.035
94	111	150	8	0.469	12.921	138.140
95	147	165	4	0.603	2.001	107.484
96	170	0	9	0.170	1.524	92.686
97	95	135	6	0.731	10.248	97.335
98	139	90	1.4	0.307	7.836	120.089
99	65	150	3	0.817	2.587	75.087
100	100	90	7	0.991	7.941	146.900
101	79	135	6	0.765	11.183	119.573
102	120	150	9	0.446	1.318	105.329
103	195	105	1.2	0.389	1.734	123.142
104	60	90	1.4	0.464	2.234	112.303
105	63	0	8	0.720	4.498	80.751
106	182	150	3	0.253	13.284	77.542
107	93	45	4	0.382	3.255	95.584
108	73	120	8	0.581	12.621	113.592
109	44	30	4	0.713	5.999	91.001
110	26	30	7	0.017	8.174	109.403
111	99	105	3	0.953	4.107	118.161
112	55	0	2	0.788	9.786	106.445
113	74	60	5	0.921	11.772	134.465
114	54	150	1	0.986	6.484	125.568
115	36	135	5	0.358	11.982	106.713
116	60	105	9	0.124	10.700	104.549
117	151	105	6	0.195	9.295	88.922
118	68	45	9	0.005	10.614	139.076

119	88	0	6	0.598	9.001	138.495
120	181	45	6	0.374	9.556	136.091
121	14	30	9	0.048	13.136	102.455
122	167	15	4	0.155	11.457	90.161
123	16	60	1.4	0.825	8.852	96.641
124	168	90	5	0.302	1.791	91.140
125	22	0	2	0.877	2.077	134.238
126	79	60	8	0.126	9.485	98.407
127	64	135	3	0.861	9.452	88.683
128	50	15	6	0.723	3.978	100.949
129	179	90	3	0.880	12.826	87.613
130	94	165	6	0.750	7.399	85.856
131	46	30	1	0.938	12.995	104.776
132	115	105	5	0.523	6.991	139.747
133	73	105	1.4	0.577	3.862	101.900
134	170	135	2	0.207	2.685	95.818
135	87	150	1.2	0.102	6.196	137.862
136	30	15	1.2	0.619	3.129	144.257
137	48	45	1.4	0.164	13.837	105.437
138	102	60	4	0.810	10.789	133.160
139	184	150	8	0.605	13.302	75.484
140	81	150	1.2	0.498	4.250	76.326
141	85	120	1	0.795	6.090	78.456
142	57	105	9	0.165	10.075	78.365
143	10	120	4	0.146	12.760	111.782
144	132	165	3	0.554	13.517	114.472
145	180	45	6	0.660	7.269	142.597
146	40	90	5	0.202	12.708	100.863
147	141	15	7	0.709	13.994	93.767
148	37	0	1.4	0.559	7.093	126.989
149	102	150	9	0.437	5.133	100.453
150	27	75	1.5	0.850	3.760	149.725
151	24	105	1.2	0.695	2.921	121.711
152	121	75	6	0.421	7.123	120.462
153	47	45	1.4	0.296	2.036	132.044
154	144	135	8	0.672	9.221	122.115
155	200	75	1.2	0.264	1.370	131.148
156	31	135	2	0.892	3.376	115.552
157	33	30	1.5	0.481	6.868	116.516
158	7	45	5	0.043	11.273	131.326
159	100	60	5	0.902	8.545	83.876
160	137	45	8	0.109	9.723	147.930

161	146	135	8	0.575	11.096	140.532
162	131	150	3	0.082	2.853	127.753
163	173	90	3	0.912	11.594	105.877
164	12	75	8	0.493	11.502	79.019
165	110	150	7	0.334	3.614	109.808
166	19	15	2	0.364	13.431	133.649
167	178	30	2	0.622	5.335	115.249
168	158	90	3	0.899	4.010	127.342
169	167	0	7	0.225	9.277	123.655
170	195	75	5	0.478	7.199	99.897
171	138	75	1.5	0.874	6.693	118.700
172	42	120	1.4	0.355	9.662	128.251
173	59	165	9	0.429	6.287	103.522
174	96	120	2	0.963	11.622	141.439
175	112	90	7	0.629	5.781	76.573
176	149	90	8	0.280	2.990	131.909
177	43	0	8	0.741	10.541	141.052
178	193	0	2	0.072	5.166	107.174
179	155	15	1.5	0.413	13.746	141.789
180	127	15	6	0.975	7.659	113.145
181	18	165	7	0.404	1.927	85.941
182	142	60	1.5	0.417	11.862	143.957
183	161	0	2	0.978	5.647	89.893
184	108	105	2	0.700	1.220	118.892
185	144	90	7	0.802	1.658	83.294
186	172	30	9	0.695	13.051	129.972
187	105	120	1.2	0.068	12.507	124.242
188	80	75	7	0.887	11.332	130.781
189	136	90	7	0.866	3.489	114.360
190	83	105	1.4	0.034	7.929	139.216
191	51	105	1	0.050	11.902	124.667
192	157	165	5	0.959	10.350	134.996
193	44	120	1.4	0.155	4.757	107.756
194	10	60	1.5	0.547	12.104	108.457
195	165	120	1.2	0.458	6.574	88.459
196	122	165	3	0.667	6.920	128.745
197	190	165	8	0.345	6.594	145.989
198	163	15	9	0.098	3.660	114.820
199	56	135	6	0.009	4.915	132.953
200	77	60	1.2	0.133	8.755	148.467

REFERENCE

- [1] Dai H, Su Y, Kuang L, et al. Contemplation on China's Energy-Development Strategies and Initiatives in the Context of its Carbon Neutrality Goal[J]. Engineering, 2021.
- [2] Pan W, Pan M. Policy Scenarios of Zero Carbon Building for Hong Kong: To Survive or To Lead?[C]//World Sustainable Built Environment (WSBE) Conference 2017. The Construction Industry Council (CIC) and the Hong Kong Green Building Council (HKGBC)., 2017.
- [3] Torcellini P, Pless S, Deru M, et al. Zero energy buildings: a critical look at the definition[R]. National Renewable Energy Lab.(NREL), Golden, CO (United States), 2006.
- [4] Sartori I, Napolitano A, Voss K. Net zero energy buildings: A consistent definition framework[J]. Energy and buildings, 2012, 48: 220-232.
- [5] Hernandez P, Kenny P. From net energy to zero energy buildings: Defining life cycle zero energy buildings (LC-ZEB)[J]. Energy and Buildings, 2010, 42(6): 815-821.
- [6] Belussi L, Barozzi B, Bellazzi A, et al. A review of performance of zero energy buildings and energy efficiency solutions[J]. Journal of Building Engineering, 2019, 25: 100772.
- [7] Li D H W, Yang L, Lam J C. Zero energy buildings and sustainable development implications—A review[J]. Energy, 2013, 54: 1-10.
- [8] Marszal A J, Heiselberg P, Bourrelle J S, et al. Zero Energy Building—A review of definitions and calculation methodologies[J]. Energy and buildings, 2011, 43(4): 971-979.
- [9] Chen X, Yang H. Integrated energy performance optimization of a passively designed high-rise residential building in different climatic zones of China[J]. Applied energy, 2018, 215: 145-158.

- [10] Chen M, Gong Y, Lu D, et al. Build a people-oriented urbanization: China's new-type urbanization dream and Anhui model[J]. *Land use policy*, 2019, 80: 1-9.
- [11] Sun, L., Chen, J., Li, Q., & Huang, D. (2020). Dramatic uneven urbanization of large cities throughout the world in recent decades. *Nature communications*, 11(1), 5366.
- [12] Xie X, Sahin O, Luo Z, et al. Impact of neighbourhood-scale climate characteristics on building heating demand and night ventilation cooling potential[J]. *Renewable Energy*, 2020, 150: 943-956.
- [13] Allegrini J, Carmeliet J. Coupled CFD and building energy simulations for studying the impacts of building height topology and buoyancy on local urban microclimates[J]. *Urban Climate*, 2017, 21: 278-305.
- [14] Tsoka S. Investigating the relationship between urban spaces morphology and local microclimate: A study for Thessaloniki[J]. *Procedia Environmental Sciences*, 2017, 38: 674-681.
- [15] Shen P, Liu J, Wang M. Fast generation of microclimate weather data for building simulation under heat island using map capturing and clustering technique[J]. *Sustainable Cities and Society*, 2021, 71: 102954.
- [16] Zinzi M, Carnielo E, Mattoni B. On the relation between urban climate and energy performance of buildings. A three-years experience in Rome, Italy[J]. *Applied Energy*, 2018, 221: 148-160.
- [17] Akbari, H., Konopacki, S., & Pomerantz, M. (1999). Cooling energy savings potential of reflective roofs for residential and commercial buildings in the United States. *Energy*, 24(5), 391-407.

- [18] Zhu, Y., Zhang, Q., Zeng, L., Wang, J., Zou, S., & Zheng, H. (2023). An advanced control strategy for optimizing the operation state of chillers with cold storage technology in data center. *Energy and Buildings*, 301, 113684.
- [19] Sadineni, S. B., & Boehm, R. F. (2012). Measurements and simulations for peak electrical load reduction in cooling dominated climate. *Energy*, 37(1), 689-697.
- [20] Li, D. H., Lam, T. N., Chan, W. W., & Mak, A. H. (2009). Energy and cost analysis of semi-transparent photovoltaic in office buildings. *Applied Energy*, 86(5), 722-729.
- [21] Tazay, A. F., Ibrahim, A. M. A., Noureldeen, O., & Hamdan, I. (2020). Modeling, control, and performance evaluation of grid-tied hybrid PV/wind power generation system: Case study of Gabel El-Zeit region, Egypt. *IEEE Access*, 8, 96528-96542.
- [22] Mosha Zhao, Hartwig M. Künzel, Florian Antretter. Parameters influencing the energy performance of residential buildings in different Chinese climate zones. *Energy and Buildings* 2015; 96:64-75.
- [23] Yu J, Tian L, Yang C, et al. Sensitivity analysis of energy performance for high-rise residential envelope in hot summer and cold winter zone of China[J]. *Energy and Buildings*, 2013, 64: 264-274.
- [24] Yuehong Lu, Shengwei Wang, Chengchu Yan, Kui Shan. Impacts of renewable energy system design inputs on the performance robustness of net zero energy buildings. *Energy* 2015, 93:1595-1606.
- [25] Viorel Badescu, Nadine Laaser, Ruxandra Crutescu. Warm season cooling requirements for passive buildings in Southeastern Europe (Romania). *Energy* 2010, 35:3284-3300.

- [26] Paulo Filipe de Almeida Ferreira Tavaresa, António Manuel de Oliveira Gomes Martinsb. Energy efficient building design using sensitivity analysis—A case study. *Energy and Buildings* 2007.
- [27] Yuang Guo, Dewancker Bart. Optimization of design parameters for office buildings with climatic adaptability based on energy demand and thermal comfort. *Sustainability* 2020; 12:3540.
- [28] Per Heiselberg, Henrik Brohus, Allan Hesselholt, Henrik Rasmussen, Erkki Seinre, Sara Thomas. Application of sensitivity analysis in design of sustainable buildings. *Renewable Energy* 2009; 34:2030–2036.
- [29] Rahmi Andarini, Hermann Schranzhofer, Wolfgang Streicher. Energy Simulation for a Typical Small Office Building in Indonesia. *Proceedings: The First International Conference on Building Energy and Environment 2008*, 255-261.
- [30] Guohui Feng, Xiaolong Xu, Yue Wang, Kairan Wang. Sensitivity Analysis of Design Parameters for Envelope Structure of Near-Zero Energy Buildings Oriented by Energy Consumption. *Journal of Shenyang Jianzhu University* 2018;34(6): 1069-1077.
- [31] JOSEPH C. LAM, SAM C. M. HUI. Sensitivity analysis of energy performance of office buildings. *Building and Environment* 1996; 31:27–39.
- [32] Yelin Zhang, Xingxing Zhang, Pei Huang, Yongjun Sun. Global sensitivity analysis for key parameters identification of net-zero energy buildings for grid interaction optimization. *Applied Energy* 2020;279:115820.
- [33] Yusuf Yıldız, Zeynep Durmus, Arsan. Identification of the building parameters that influence heating and cooling energy loads for apartment buildings in hot-humid climates. *Energy* 2011; 36:4287-4296.

- [34] H. Breesch, A. Janssens. Performance evaluation of passive cooling in office buildings based on uncertainty and sensitivity analysis. *Solar Energy* 2010; 84:1453–1467.
- [35] D. Garcia Sancheza, B. Lacarrièrea, M. Musyb, B. Bourgesa. Application of sensitivity analysis in building energy simulations: Combining first- and second-order elementary effects methods. *Energy and Buildings* 2012.
- [36] VINCENZO CORRADO, HOUCEM EDDINE MECHRI. Uncertainty and Sensitivity Analysis for Building Energy Rating. *Building Physics* 2009; 6.
- [37] Michael Stendert DE WIT. Uncertainty predictions of thermal comfort in buildings. Technische Universiteit Delft 2001.
- [38] Ramkishore Singh, I.J. Lazarus, V.V.N. Kishore. Uncertainty and sensitivity analyses of energy and visual performances of office building with external venetian blind shading in hot-dry climate. *Applied Energy* 2016; 184:155-170.
- [39] Houcem Eddine Mechr, Alfonso Capozzoli, Vincenzo Corrado. USE of the ANOVA approach for sensitive building energy design. *Applied Energy* 2010; 87:3073-3083.
- [40] Xi Chen, Hongxing Yang, Weilong Zhang. Simulation-based approach to optimize passively designed buildings: A case study on a typical architectural form in hot and humid climates. *Renewable and Sustainable Energy Reviews* 2017; 06.018.
- [41] Byungyun Lee, Yoonjung Jang, Jungmann Choi. Multi-stage optimization and meta-model analysis with sequential parameter range adjustment for the low-energy house in Korea. *Energy & Buildings* 2020; 214:109873.
- [42] Xi Chen, Hongxing Yang, Ke Sun. Developing a meta-model for sensitivity analyses and prediction of building performance for passively designed high-rise residential buildings. *Applied Energy* 2016; 08.180.

- [43] Hangxin Li, Shengwei Wang, Howard Cheung. Sensitivity analysis of design parameters and optimal design for zero/low energy buildings in subtropical regions. *Applied Energy* 2018; 228:1280–1291.
- [44] Xi Chen, Hongxing Yang. A multi-stage optimization of passively designed high-rise residential buildings in multiple building operation scenarios. *Applied Energy* 2017; 206:541–557.
- [45] Clara Spitzza, Laurent Morab, Etienne Wurtzc, Arnaud Jay. Practical application of uncertainty analysis and sensitivity analysis on an experimental house. *Energy and Buildings* 2012. 55:459-470.
- [46] Song Yanga, Wei Tian, Eduard Cubic, QingXin Menga, YunLiang Liua, Lai Weia. Comparison of sensitivity analysis methods in building energy assessment. *Procedia Engineering* 2016; 146:174–181.
- [47] Delgarm N, Sajadi B, Azarbad K, et al. Sensitivity analysis of building energy performance: A simulation-based approach using OFAT and variance-based sensitivity analysis methods[J]. *Journal of Building Engineering*, 2018, 15: 181-193.
- [48] Zhengrong Li, Yuhui Hao, Dongkai Zhang, Cui Li. Study on design method of building thermal parameters of ultra-low-energy building in Shanghai. *IOP Conference Series: Earth and Environmental Science* 2019; 238:012060.
- [49] Sun Y. Sensitivity analysis of macro-parameters in the system design of net zero energy building[J]. *Energy and Buildings*, 2015, 86: 464-477.
- [50] Raji B, Tenpierik M J, Van Den Dobbelsteen A. An assessment of energy-saving solutions for the envelope design of high-rise buildings in temperate climates: A case study in the Netherlands[J]. *Energy and Buildings*, 2016, 124: 210-221.

- [51] Samuelson H, Claussnitzer S, Goyal A, et al. Parametric energy simulation in early design: High-rise residential buildings in urban contexts[J]. *Building and Environment*, 2016, 101: 19-31.
- [52] Menberg K, Heo Y, Choudhary R. Sensitivity analysis methods for building energy models: Comparing computational costs and extractable information[J]. *Energy and Buildings*, 2016, 133: 433-445.
- [53] Tian W, De Wilde P. Uncertainty and sensitivity analysis of building performance using probabilistic climate projections: A UK case study[J]. *Automation in construction*, 2011, 20(8): 1096-1109.
- [54] Yildiz Y, Korkmaz K, Özbalta T G, et al. An approach for developing sensitive design parameter guidelines to reduce the energy requirements of low-rise apartment buildings[J]. *Applied Energy*, 2012, 93: 337-347.
- [55] Tian W, Choudhary R. A probabilistic energy model for non-domestic building sectors applied to analysis of school buildings in greater London[J]. *Energy and Buildings*, 2012, 54: 1-11.
- [56] Kurnitski J, Saari A, Kalamees T, et al. Cost optimal and nearly zero (nZEB) energy performance calculations for residential buildings with REHVA definition for nZEB national implementation[J]. *Energy and Buildings*, 2011, 43(11): 3279-3288.
- [57] De Wilde P, Tian W. Identification of key factors for uncertainty in the prediction of the thermal performance of an office building under climate change[C]//*Building simulation*. Tsinghua Press, 2009, 2(3): 157-174.
- [58] Burhenne S, Jacob D, Henze G P. Uncertainty analysis in building simulation with Monte Carlo techniques[J]. *Proceedings of SIMBUILD*, 2010, 4(1): 419-426.

- [59] Dowd R M, Mourshed M. Low carbon buildings: Sensitivity of thermal properties of opaque envelope construction and glazing[J]. *Energy Procedia*, 2015, 75: 1284-1289.
- [60] Basinska M, Koczyk H, Szczechowiak E. Sensitivity analysis in determining the optimum energy for residential buildings in Polish conditions[J]. *Energy and Buildings*, 2015, 107: 307-318.
- [61] Mainini A G, Poli T, Zinzi M, et al. Metal mesh as shading devices and thermal response of an office building: parametric analysis[J]. *Energy Procedia*, 2015, 78: 103-109.
- [62] Daly D, Cooper P, Ma Z. Understanding the risks and uncertainties introduced by common assumptions in energy simulations for Australian commercial buildings[J]. *Energy and Buildings*, 2014, 75: 382-393.
- [63] Rasouli M, Ge G, Simonson C J, et al. Uncertainties in energy and economic performance of HVAC systems and energy recovery ventilators due to uncertainties in building and HVAC parameters[J]. *Applied Thermal Engineering*, 2013, 50(1): 732-742.
- [64] Hygh J S, DeCarolis J F, Hill D B, et al. Multivariate regression as an energy assessment tool in early building design[J]. *Building and environment*, 2012, 57: 165-175.
- [65] Mauro G M, Hamdy M, Vanoli G P, et al. A new methodology for investigating the cost-optimality of energy retrofitting a building category[J]. *Energy and Buildings*, 2015, 107: 456-478.
- [66] De Wilde P, Tian W. Predicting the performance of an office under climate change: A study of metrics, sensitivity and zonal resolution[J]. *Energy and Buildings*, 2010, 42(10): 1674-1684.

- [67] Eisenhower B, O'Neill Z, Fonoberov V A, et al. Uncertainty and sensitivity decomposition of building energy models[J]. *Journal of Building Performance Simulation*, 2012, 5(3): 171-184.
- [68] Lam T C, Ge H, Fazio P. Impact of curtain wall configurations on building energy performance in the perimeter zone for a cold climate[J]. *Energy Procedia*, 2015, 78: 352-357.
- [69] Shen H, Tzempelikos A. Sensitivity analysis on daylighting and energy performance of perimeter offices with automated shading[J]. *Building and environment*, 2013, 59: 303-314.
- [70] Ali-Toudert, F., & Böttcher, S. (2018). Urban microclimate prediction prior to dynamic building energy modelling using the TEB model as embedded component in TRNSYS. *Theoretical and Applied Climatology*, 134, 1413-1428.
- [71] Allegrini, J., & Carmeliet, J. (2018). Simulations of local heat islands in Zürich with coupled CFD and building energy models. *Urban climate*, 24, 340-359.
- [72] Mutani, G., & Fiermonte, F. (2016). Microclimate models for a sustainable and liveable urban planning. *Topics and Methods for Urban and Landscape Design: From the river to the project*, 183-209.
- [73] Mao, J., Fu, Y., Afshari, A., Armstrong, P. R., & Norford, L. K. (2018). Optimization-aided calibration of an urban microclimate model under uncertainty. *Building and Environment*, 143, 390-403.
- [74] Bueno, B., Roth, M., Norford, L., & Li, R. (2014). Computationally efficient prediction of canopy level urban air temperature at the neighbourhood scale. *Urban Climate*, 9, 35-53.

- [75] Bueno, B., Norford, L., Hidalgo, J., & Pigeon, G. (2013). The urban weather generator. *Journal of Building Performance Simulation*, 6(4), 269-281.
- [76] Mohammad, A. F., Zaki, S. A., Ali, M. S. M., Aya, H., Razak, A. A., Shirakashi, M., & Arai, N. (2015). Large eddy simulation of wind pressure distribution on heterogeneous buildings in idealised urban models. *Energy Procedia*, 78, 3055-3060.
- [77] Chow, T. T., Lin, Z., & Yang, X. Y. (2002). Placement of condensing units of split-type air-conditioners at low-rise residences. *Applied thermal engineering*, 22(13), 1431-1444.
- [78] Chen, L., Hang, J., Sandberg, M., Claesson, L., Di Sabatino, S., & Wigo, H. (2017). The impacts of building height variations and building packing densities on flow adjustment and city breathability in idealized urban models. *Building and Environment*, 118, 344-361.
- [79] Allegrini, J., Dorer, V., & Carmeliet, J. (2015). Influence of morphologies on the microclimate in urban neighbourhoods. *Journal of Wind Engineering and Industrial Aerodynamics*, 144, 108-117.
- [80] Middel, A., Häb, K., Brazel, A. J., Martin, C. A., & Guhathakurta, S. (2014). Impact of urban form and design on mid-afternoon microclimate in Phoenix Local Climate Zones. *Landscape and urban planning*, 122, 16-28.
- [81] Bourbia, F., & Boucheriba, F. (2010). Impact of street design on urban microclimate for semi arid climate (Constantine). *Renewable Energy*, 35(2), 343-347.
- [82] Merlier, L., Frayssinet, L., Johannes, K., & Kuznik, F. (2019, October). On the impact of local microclimate on building performance simulation. Part I: Prediction of building external conditions. In *Building Simulation* (Vol. 12, pp. 735-746). Tsinghua University Press.

- [83] Dimoudi, A., Kantzioura, A., Zoras, S., Pallas, C., & Kosmopoulos, P. (2013). Investigation of urban microclimate parameters in an urban center. *Energy and Buildings*, 64, 1-9.
- [84] Hang, J., & Li, Y. (2010). Ventilation strategy and air change rates in idealized high-rise compact urban areas. *Building and Environment*, 45(12), 2754-2767.
- [85] Ali-Toudert, F., & Mayer, H. (2006). Numerical study on the effects of aspect ratio and orientation of an urban street canyon on outdoor thermal comfort in hot and dry climate. *Building and environment*, 41(2), 94-108.
- [86] Yassin, M. F. (2013). Numerical modeling on air quality in an urban environment with changes of the aspect ratio and wind direction. *Environmental Science and Pollution Research*, 20, 3975-3988.
- [87] Theeuwes, N. E., Steeneveld, G. J., Ronda, R. J., Heusinkveld, B. G., Van Hove, L. W. A., & Holtslag, A. A. (2014). Seasonal dependence of the urban heat island on the street canyon aspect ratio. *Quarterly Journal of the Royal Meteorological Society*, 140(684), 2197-2210.
- [88] Mosteiro-Romero, M., Maiullari, D., Pijpers-van Esch, M., & Schlueter, A. (2020). An integrated microclimate-energy demand simulation method for the assessment of urban districts. *Frontiers in Built Environment*, 6, 553946.
- [89] Ignatius, M., Wong, N. H., & Jusuf, S. K. (2015). Urban microclimate analysis with consideration of local ambient temperature, external heat gain, urban ventilation, and outdoor thermal comfort in the tropics. *Sustainable Cities and Society*, 19, 121-135.
- [90] Guattari, C., Evangelisti, L., & Balaras, C. A. (2018). On the assessment of urban heat island phenomenon and its effects on building energy performance: A case study of Rome (Italy). *Energy and Buildings*, 158, 605-615.

- [91] Palme, M., Inostroza, L., Villacreses, G., Lobato-Cordero, A., & Carrasco, C. (2017). From urban climate to energy consumption. Enhancing building performance simulation by including the urban heat island effect. *Energy and buildings*, 145, 107-120.
- [92] Paolini, R., Zani, A., MeshkinKiya, M., Castaldo, V. L., Pisello, A. L., Antretter, F., ... & Cotana, F. (2017). The hygrothermal performance of residential buildings at urban and rural sites: Sensible and latent energy loads and indoor environmental conditions. *Energy and Buildings*, 152, 792-803.
- [93] Salvati, A., Roura, H. C., & Cecere, C. (2017). Assessing the urban heat island and its energy impact on residential buildings in Mediterranean climate: Barcelona case study. *Energy and Buildings*, 146, 38-54.
- [94] Cui, Y., Yan, D., Hong, T., & Ma, J. (2017). Temporal and spatial characteristics of the urban heat island in Beijing and the impact on building design and energy performance. *Energy*, 130, 286-297.
- [95] Allegrini, J., Dorer, V., & Carmeliet, J. (2012). Influence of the urban microclimate in street canyons on the energy demand for space cooling and heating of buildings. *Energy and Buildings*, 55, 823-832.
- [96] Shi, L., Luo, Z., Matthews, W., Wang, Z., Li, Y., & Liu, J. (2019). Impacts of urban microclimate on summertime sensible and latent energy demand for cooling in residential buildings of Hong Kong. *Energy*, 189, 116208.
- [97] Lee, G., & Jeong, Y. (2017). Impact of urban and building form and microclimate on the energy consumption of buildings-based on statistical analysis. *Journal of Asian Architecture and Building Engineering*, 16(3), 565-572.

- [98] Mao, J., Yang, J. H., Afshari, A., & Norford, L. K. (2017). Global sensitivity analysis of an urban microclimate system under uncertainty: Design and case study. *Building and environment*, 124, 153-170.
- [99] Liu, J., Heidarinejad, M., Nikkho, S. K., Mattise, N. W., & Srebric, J. (2019). Quantifying impacts of urban microclimate on a building energy consumption—a case study. *Sustainability*, 11(18), 4921.
- [100] Allen-Dumas, M. R., Sweet, L. T., & Brelsford, C. (2022). Determining Optimal Resolution for Urban Terrain Inputs to Microclimate Modeling. *Authorea Preprints*.
- [101] Lauzet, N. , Rodler, A. , Musy, M. , Azam, M. H. , Guernouti, S. , & Mauree, D. , et al. (2019). How building energy models take the local climate into account in an urban context - a review. *Renewable & Sustainable Energy Reviews*, 116(Dec.), 109390.1-109390.19.
- [102] Lac C, Chaboureau P, Masson V, Pinty P, Tulet P, Escobar J, Leriche M, Barthe C, Aouizerats B, Augros C, et al. Overview of the meso-nh model version 5.4 and its applications. *Geoscientific Model Development Discussions*; 2017. p. 1929–69
- [102] Mauree D, Blond N, Kohler M, Clappier A. On the coherence in the boundary layer: development of a canopy interface model. *Front Earth Sci* 2017;4:109.
- [104] Ding, C., & Lam, K. P. (2019). Data-driven model for cross ventilation potential in high-density cities based on coupled CFD simulation and machine learning. *Building and Environment*, 165, 106394.
- [105] Calzolari, G., & Liu, W. (2021). Deep learning to replace, improve, or aid CFD analysis in built environment applications: A review. *Building and Environment*, 206, 108315.

- [106] Wu, Y., Zhan, Q., Quan, S. J., Fan, Y., & Yang, Y. (2021). A surrogate-assisted optimization framework for microclimate-sensitive urban design practice. *Building and Environment*, 195, 107661.
- [107] Wu, Y., Zhan, Q., & Quan, S. J. (2021). Improving local pedestrian-level wind environment based on probabilistic assessment using Gaussian process regression. *Building and Environment*, 205, 108172.
- [108] Kastner, P., & Dogan, T. (2023). A GAN-based surrogate model for instantaneous urban wind flow prediction. *Building and Environment*, 110384.
- [109] Huang, C., Zhang, G., Yao, J., Wang, X., Calautit, J. K., Zhao, C., ... & Peng, X. (2022). Accelerated environmental performance-driven urban design with generative adversarial network. *Building and Environment*, 224, 109575.
- [110] Mokhtar, S., Sojka, A., & Davila, C. C. (2020, May). Conditional generative adversarial networks for pedestrian wind flow approximation. In *Proceedings of the 11th annual symposium on simulation for architecture and urban design* (pp. 1-8).
- [111] Weerasuriya, A. U., Zhang, X., Lu, B., Tse, K. T., & Liu, C. H. (2020). Optimizing lift-up design to maximize pedestrian wind and thermal comfort in 'hot-calm' and 'cold-windy' climates. *Sustainable Cities and Society*, 58, 102146.
- [112] Kim, B., Lee, D. E., Preethaa, K. S., Hu, G., Natarajan, Y., & Kwok, K. C. (2021). Predicting wind flow around buildings using deep learning. *Journal of Wind Engineering and Industrial Aerodynamics*, 219, 104820.
- [113] Musil, J., Knir, J., Vitsas, A., & Gallou, I. (2019). Towards sustainable architecture: 3d convolutional neural networks for computational fluid dynamics simulation and reverse design workflow. *arXiv preprint arXiv:1912.02125*.

- [114] Zhang, M., Zhang, X., Guo, S., Xu, X., Chen, J., & Wang, W. (2021). Urban micro-climate prediction through long short-term memory network with long-term monitoring for on-site building energy estimation. *Sustainable Cities and Society*, 74, 103227.
- [115] Kong, M., Yu, M., Liu, N., Gao, P., Wang, Y., & Zhang, J. (2017). Combined GIS, CFD and Neural Network Multi-Zone Model for Urban Planning and Building Simulation. In 15th International Conference of the International Building Performance Simulation Association, *Building Simulation 2017* (pp. 2392-2397). International Building Performance Simulation Association.
- [116] Tanaka, H., Matsuoka, Y., Kawakami, T., Azegami, Y., Yamamoto, M., Ohtake, K., & Sone, T. (2019). Optimization calculations and machine learning aimed at reduction of wind forces acting on tall buildings and mitigation of wind environment. *International journal of high-rise buildings*, 8(4), 291-302.
- [117] Li, H. , & Wang, S. . (2019). Coordinated optimal design of zero/low energy buildings and their energy systems based on multi-stage design optimization. *Energy*, 189.
- [118] Li, H. , Wang, S. , & Yan, J. . (2020). Coordinated robust optimal design of building envelope and energy systems for zero/low energy buildings considering uncertainties. *Applied Energy*, 265.
- [119] Li, Q., Zhang, L., Zhang, L., & Wu, X. (2021). Optimizing energy efficiency and thermal comfort in building green retrofit. *Energy*, 237, 121509.
- [120] Wang, Y. , & Wei, C. . (2020). Design optimization of office building envelope based on quantum genetic algorithm for energy conservation - sciencedirect. *Journal of Building Engineering*.

- [121] Bamdad, K. , Cholette, M. E. , Omrani, S. , & Bell, J. . (2020). Future energy-optimised buildings — addressing the impact of climate change on buildings. *Energy and Buildings*, 231(2), 110610.
- [122] Kiss, B., & Szalay, Z. (2020). Modular approach to multi-objective environmental optimization of buildings. *Automation in Construction*, 111, 103044.
- [123] Giouri, E. D. , Tenpierik, M. , & Turrin, M. . (2020). Zero energy potential of a high-rise office building in a mediterranean climate: using multi-objective optimization to understand the impact of design decisions towards zero-energy high-rise buildings. *Energy and buildings*(Feb.), 209.
- [124] Bui, D. K., Nguyen, T. N., Ghazlan, A., Ngo, N. T., & Ngo, T. D. (2020). Enhancing building energy efficiency by adaptive façade: A computational optimization approach. *Applied energy*, 265, 114797.
- [125] Malik, R. , Dua, S. , Shoran, P. , & Nain, A. . Enhancing Security and Resource Optimization in IoT Applications with Blockchain Inclusion. 2023 2nd International Conference on Futuristic Technologies (INCOFT). IEEE.
- [126] Sun, Z., Cao, Y., Wang, X., & Yu, J. (2021). Multi-objective optimization design for windows and shading configuration: considering energy consumption, thermal environment, visual performance and sound insulation effect. *International Journal of Energy and Environmental Engineering*, 12(4), 805-836.
- [127] Chen, K. W., Janssen, P., & Schlueter, A. (2018). Multi-objective optimisation of building form, envelope and cooling system for improved building energy performance. *Automation in construction*, 94, 449-457.

- [128] Jiang, M., & Araji, M. T. (2023). Multivariate optimization towards energy balance with geometric constraints of building design and urban space intensity. *Sustainable Energy Technologies and Assessments*, 57, 103124.
- [129] Feng, J., Luo, X., Gao, M., Abbas, A., Xu, Y. P., & Pouramini, S. (2021). Minimization of energy consumption by building shape optimization using an improved Manta-Ray Foraging Optimization algorithm. *Energy Reports*, 7, 1068-1078.
- [130] Rabani, M., Madessa, H. B., & Nord, N. (2021). Achieving zero-energy building performance with thermal and visual comfort enhancement through optimization of fenestration, envelope, shading device, and energy supply system. *Sustainable Energy Technologies and Assessments*, 44, 101020.
- [131] Ilbeigi, M., Ghomeishi, M., & Dehghanbanadaki, A. (2020). Prediction and optimization of energy consumption in an office building using artificial neural network and a genetic algorithm. *Sustainable Cities and Society*, 61, 102325.
- [132] Zhu, L., Wang, B., & Sun, Y. (2020). Multi-objective optimization for energy consumption, daylighting and thermal comfort performance of rural tourism buildings in north China. *Building and Environment*, 176, 106841.
- [133] Jalali, Z., Noorzai, E., & Heidari, S. (2020). Design and optimization of form and facade of an office building using the genetic algorithm. *Science and Technology for the Built Environment*, 26(2), 128-140.
- [134] Serjoscha Düring, Chronis, A. , & Koenig, R. . (2020). Optimizing Urban Systems: Integrated optimization of spatial configurations. *Symposium on Simulation for Architecture and Urban Design*.

- [135] Kaseb, Z., Hafezi, M., Tahbaz, M., & Delfani, S. (2020). A framework for pedestrian-level wind conditions improvement in urban areas: CFD simulation and optimization. *Building and Environment*, 184, 107191.
- [136] Zhang, J. , Cui, P. , & Song, H. . (2020). Impact of urban morphology on outdoor air temperature and microclimate optimization strategy base on pareto optimality in northeast china. *Building and Environment*, 180(1101), 107035.
- [137] Du, Y. , Mak, C. M. , & Li, Y. . (2019). A multi-stage optimization of pedestrian level wind environment and thermal comfort with lift-up design in ideal urban canyons. *Sustainable Cities and Society*, 46.
- [138] Wang, S. S. , Yi, Y. K. , & Liu, N. X. . (2021). Multi-objective optimization (moo) for high-rise residential buildings' layout centered on daylight, visual, and outdoor thermal metrics in china. *Building and Environment*(224), 108263.
- [139] Deb, K. , Pratap, A. , Agarwal, S. , & Meyarivan, T. . (2002). A fast and elitist multiobjective genetic algorithm: nsga-ii. *IEEE Transactions on Evolutionary Computation*, 6(2), 182-197.
- [140] Wang, R., Ren, C., Xu, Y., Lau, K. K. L., & Shi, Y. (2018). Mapping the local climate zones of urban areas by GIS-based and WUDAPT methods: A case study of Hong Kong. *Urban climate*, 24, 567-576.
- [141] Ng, E., & Cheng, V. (2012). Urban human thermal comfort in hot and humid Hong Kong. *Energy and Buildings*, 55, 51-65.
- [142] Lin, M., Hang, J., Li, Y., Luo, Z., & Sandberg, M. (2014). Quantitative ventilation assessments of idealized urban canopy layers with various urban layouts and the same building packing density. *Building and environment*, 79, 152-167.

- [143] Hershfield M. Building Envelope Thermal Bridging Guide, version 1.4[J]. 2020.
- [144] Design standard for energy efficiency of public buildings, GB 50189-2015.
- [145] Design code for heating ventilation and air conditioning of civil buildings, GB 50736-2012.
- [146] Technical standard for near zero energy buildings, GB/T 51350-2019.
- [147] Guglielmetti R, Macumber D, Long N. OpenStudio: an open source integrated analysis platform. In: Proceedings of building simulation 2011, Sydney, Australia, November 14–16, 2011.
- [148] Uniform standard for design of civil buildings, GB 50352-2019.
- [149] Hershfield M. Building Envelope Thermal Bridging Guide, version 1.4[J]. Vancouver, BC: Hydro Power Smart, 2020.
- [150] Theodosiou T G, Papadopoulos A M . The impact of thermal bridges on the energy demand of buildings with double brick wall constructions[J]. Energy & Buildings, 2008, 40(11):2083-2089.
- [151] Capozzoli A, Gorrino A, Corrado V. A building thermal bridges sensitivity analysis[J]. Applied Energy, 2013, 107: 229-243.
- [152] Inanici, M. N., & Demirbilek, F. N. (2000). Thermal performance optimization of building aspect ratio and south window size in five cities having different climatic characteristics of Turkey. Building and environment, 35(1), 41-52.
- [153] Back, Y., Kumar, P., Bach, P. M., Rauch, W., & Kleidorfer, M. (2023). Integrating CFD-GIS modelling to refine urban heat and thermal comfort assessment. Science of The Total Environment, 858, 159729.

- [154] Tominaga, Y., Yoshie, R., Mochida, A., Kataoka, H., Harimoto, K., & Nozu, T. (2005). Cross comparisons of CFD prediction for wind environment at pedestrian level around buildings. Part, 2, 2661-2670.
- [155] Tominaga, Y., Mochida, A., Yoshie, R., Kataoka, H., Nozu, T., Yoshikawa, M., & Shirasawa, T. (2008). AIJ guidelines for practical applications of CFD to pedestrian wind environment around buildings. *Journal of wind engineering and industrial aerodynamics*, 96(10-11), 1749-1761.
- [156] Potchter, O., Cohen, P., Lin, T. P., & Matzarakis, A. (2018). Outdoor human thermal perception in various climates: A comprehensive review of approaches, methods and quantification. *Science of the Total Environment*, 631, 390-406.
- [157] Franke, J., Hellsten, A., Schlünzen, H., & Carissimo, B. (2007). Best practice guideline for the CFD simulation of flows in the urban environment (Doctoral dissertation, COST European Cooperation in Science and Technology).
- [158] Martilli, A., Santiago, J. L., & Martín, F. (2007). Micrometeorological modelling in urban areas. *Física de la Tierra*, 133(19), 133-145.
- [159] Tominaga, Y., Mochida, A., Shirasawa, T., Yoshie, R., Kataoka, H., Harimoto, K., & Nozu, T. (2004). Cross comparisons of CFD results of wind environment at pedestrian level around a high-rise building and within a building complex. *Journal of Asian architecture and building engineering*, 3(1), 63-70.
- [160] Zhong, H., Wang, J., Jia, H., Mu, Y., & Lv, S. (2019). Vector field-based support vector regression for building energy consumption prediction. *Applied Energy*, 242, 403-414.
- [161] Zhang, L., Wen, J., Li, Y., Chen, J., Ye, Y., Fu, Y., & Livingood, W. (2021). A review of machine learning in building load prediction. *Applied Energy*, 285, 116452.

- [162] Chen, Y., Ye, Y., Liu, J., Zhang, L., Li, W., & Mohtaram, S. (2023). Machine learning approach to predict building thermal load considering feature variable Dimensions: an office building case study. *Buildings*, 13(2), 312.
- [163] Guo, J., Yun, S., Meng, Y., He, N., Ye, D., Zhao, Z., ... & Yang, L. (2023). Prediction of heating and cooling loads based on light gradient boosting machine algorithms. *Building and Environment*, 236, 110252.
- [164] Fan, C., Xiao, F., & Zhao, Y. (2017). A short-term building cooling load prediction method using deep learning algorithms. *Applied energy*, 195, 222-233.
- [165] Design standard for energy efficiency of residential buildings in hot summer and warm winter zone, JGJ 75-2012.
- [166] Helton JC, Davis FJ. Latin hypercube sampling and the propagation of uncertainty in analyses of complex systems. *Reliab Eng Syst Saf* 2003;81(1):23e69.
- [167] Mostafavi, F., Tahsildoost, M., & Zomorodian, Z. (2021). Energy efficiency and carbon emission in high-rise buildings: A review (2005-2020). *Building and Environment*, 206, 108329.
- [168] Wang, Y., Mauree, D., Sun, Q., Lin, H., Scartezzini, J. L., & Wennersten, R. (2020). A review of approaches to low-carbon transition of high-rise residential buildings in China. *Renewable and Sustainable Energy Reviews*, 131, 109990.
- [169] Ge, J., Wang, Y., Zhou, D., Gu, Z., & Meng, X. (2023). Building energy demand of urban blocks in Xi'an, China: Impacts of high-rises and vertical meteorological pattern. *Building and Environment*, 244, 110749.

- [170] Tang, Y., Sun, T., Luo, Z., Omidvar, H., Theeuwes, N., Xie, X., ... & Grimmond, S. (2021). Urban meteorological forcing data for building energy simulations. *Building and Environment*, 204, 108088.
- [171] Yu, H., Wang, M., Lin, X., Guo, H., Liu, H., Zhao, Y., ... & Jing, R. (2021). Prioritizing urban planning factors on community energy performance based on GIS-informed building energy modeling. *Energy and Buildings*, 249, 111191.
- [172] Liu, K., Xu, X., Zhang, R., Kong, L., Wang, W., & Deng, W. (2023). Impact of urban form on building energy consumption and solar energy potential: A case study of residential blocks in Jianhu, China. *Energy and Buildings*, 280, 112727.
- [173] Yoon, Y. B., Seo, B., Koh, B. B., & Cho, S. (2019). Performance analysis of a double-skin façade system installed at different floor levels of high-rise apartment building. *Journal of Building Engineering*, 26, 100900.
- [174] Du, J., & Pan, W. (2022). Cooling-related energy uses and adaptive behaviors in high-rise residential buildings in the subtropical climate: A case study in Hong Kong. *Building and Environment*, 223, 109456.
- [175] Huang, W., Shuai, B., Sun, Y., Wang, Y., & Antwi, E. (2018). Using entropy-TOPSIS method to evaluate urban rail transit system operation performance: The China case. *Transportation Research Part A: Policy and Practice*, 111, 292-303.
- [176] Huang, J. (2008, September). Combining entropy weight and TOPSIS method for information system selection. In *2008 IEEE conference on cybernetics and intelligent systems* (pp. 1281-1284). IEEE.